LEABHARLANN CHOLÁISTE NA TRÍONÓIDE, BAILE ÁTHA CLIATH | TRINITY COLLEGE LIBRARY DUBLIN
Ollscoil Átha Cliath | The University of Dublin

**Terms and Conditions of Use of Digitised Theses from Trinity College Library Dublin**

**Copyright statement**

All material supplied by Trinity College Library is protected by copyright (under the Copyright and Related Rights Act, 2000 as amended) and other relevant Intellectual Property Rights. By accessing and using a Digitised Thesis from Trinity College Library you acknowledge that all Intellectual Property Rights in any Works supplied are the sole and exclusive property of the copyright and/or other IPR holder. Specific copyright holders may not be explicitly identified. Use of materials from other sources within a thesis should not be construed as a claim over them.

A non-exclusive, non-transferable licence is hereby granted to those using or reproducing, in whole or in part, the material for valid purposes, providing the copyright owners are acknowledged using the normal conventions. Where specific permission to use material is required, this is identified and such permission must be sought from the copyright holder or agency cited.

**Liability statement**

By using a Digitised Thesis, I accept that Trinity College Dublin bears no legal responsibility for the accuracy, legality or comprehensiveness of materials contained within the thesis, and that Trinity College Dublin accepts no liability for indirect, consequential, or incidental, damages or losses arising from use of the thesis for whatever reason. Information located in a thesis may be subject to specific use constraints, details of which may not be explicitly described. It is the responsibility of potential and actual users to be aware of such constraints and to abide by them. By making use of material from a digitised thesis, you accept these copyright and disclaimer provisions. Where it is brought to the attention of Trinity College Library that there may be a breach of copyright or other restraint, it is the policy to withdraw or take down access to a thesis while the issue is being resolved.

**Access Agreement**

By using a Digitised Thesis from Trinity College Library you are bound by the following Terms & Conditions. Please read them carefully.

I have read and I understand the following statement: All material supplied via a Digitised Thesis from Trinity College Library is protected by copyright and other intellectual property rights, and duplication or sale of all or part of any of a thesis is not permitted, except that material may be duplicated by you for your research use or for educational purposes in electronic or print form providing the copyright owners are acknowledged using the normal conventions. You must obtain permission for any other use. Electronic or print copies may not be offered, whether for sale or otherwise to anyone. This copy has been supplied on the understanding that it is copyright material and that no quotation from the thesis may be published without proper acknowledgement.

# Magnetic field effects on the electrodeposition and electrodissolution of copper

by Gareth Hinds

A thesis submitted to
The University of Dublin
in application for the degree of
Doctor of Philosophy

Department of Physics
University of Dublin
Trinity College

September 2000

## Declaration

This thesis is submitted by the undersigned for examination for the degree of Doctor in Philosophy at the University of Dublin. It has not been submitted as an exercise for a degree at any other university.

This thesis, apart from the advice, assistance and joint effort mentioned in the acknowledgements and in the text, is entirely my own work.

I agree that the library may lend or copy this thesis freely on request.

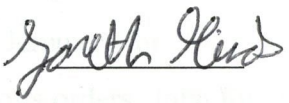

Gareth Hinds

## Acknowledgements

I would like to thank my supervisor Prof. J.M.D. Coey for his advice and assistance throughout this work. His work rate and commitment to his many research students has to be seen to be believed. If there is one thing that has rubbed off on me though, it is the true physicist's love for back of the envelope calculations. I would also like to thank my co-supervisor Dr Mike Lyons for his support, in particular for the use of his lab for three years. The Arches really was a fine place to work in and it will be sad to see it demolished.

I am grateful for the unstinting support of the technical staff of both the Physics and Chemistry departments. Dave, Paul and James for machining countless pieces at short notice. Jacquie, Joe, Ken, Rory, Chris, Tom and Jemmer for their help with malfunctioning electronics, stubborn computers and tedious orders. John for letting me use his digital camera all the time. Fred, Patsy, Brendan, John, Seamus, Martin and Eddie for their assistance with the chemicals. Niall and Colin in the EM unit for their expertise with the SEM images. My thanks are also due to the many unnamed technical staff of other departments, such as Mechanical and Electrical Engineering, who invariably helped me without hesitation when asked. I would also like to thank the secretarial staff for their help, in particular Corinne in Chemistry and Liz in Physics. On the experimental side of things, I would like to acknowledge the high field work carried out by J.M.D. Coey and F.E. Spada in Tallahasee.

The Arches gang deserve special mention for making the lab the unique working environment that it was. Tom 'Focus' Bannon, the fitness fanatic who could make anyone laugh at the drop of a hat. Dara, who could always be relied on for lasagne and chips in the Pav, when he wasn't mending something. Aileen, for her good humoured banter and strange affinity for piglets. Dave for his uncanny ability to create a perpetual motion machine from lollipop sticks and chewing gum (banana flavour). Many others have come and gone over the years - Andy, Edel, Trish, Pierre, Monica, Claire, Tania, Emmett, Gar and the two Gers. They all contributed to the tapestry that was the Arches.

I would also like to thank the members of Group D past and present for their friendship and support. The list is long but I'll give it a bash - Rui, Treasa, Janko, Katie, Venki, Cora, Jiang, Ciara, Mazhar, Laurent, James, Amanda, Rhian, Paul, Nora, Duncan, Xiao-lei, Fred, Jim, and Vassil. Thanks also to the summer students and fourth year students who have helped with various tasks, notably Donal, Cian, Emmanuel, Sandrine and Ryan.

Many housemates have passed through the doors of Carlisle Avenue in that time too. My thanks go to ABS, Alan (The Rock), Dao, Fionn, Gord, Kev (The Pebble), James, Ronan (The Cat), Garry, Jesus, Dave, Sean and Alex for providing much entertainment over the years. There'll always be a seat in McCloskeys for those that have left. Thanks to everyone I know for all those fun nights out - honourable mention goes to Psycho, Ash, Neal and ironically Matt (The Kiwi). The social juggernaut that is D.U.H.C. is also deserving of special praise. In addition, I would like to express my gratitude to the door staff of Leggs for their continued support and co-operation.

Finally I would like to thank my parents and family for their support and encouragement over the years.

**To Mum and Dad**

## Summary

The effect of a static magnetic field on the electrodeposition and electrodissolution of copper in acidified copper sulphate solution was investigated. The primary effect of the field was to increase the rate of mass transport in solution. Data from linear sweep voltammetry showed that the limiting current on both cathodic and anodic branches was dramatically increased by the field. The limiting current on each branch was found to vary as $B^{1/3}c^{4/3}$. The effect of the field on the cathodic limiting current was greatest at low pH. No significant effect of field orientation was observed. The magnitude of the field effect was significantly reduced in conditions of forced convection (rotating disk electrode), enhanced diffusion (microelectrode) and when the viscosity of the solution was increased by the addition of glycerol. This suggests that field-induced convection is responsible for the increase in the rate of mass transport.

No effect of the field on the diffusion coefficient of $Cu^{2+}$ was observed in either the complex impedance or chronoamperometric experiments. It was concluded that the concentration gradient must be increased by the field. The effect of a tangential fluid velocity on the thickness of the diffusion layer was determined from hydrodynamic theory and compared with the experimental data. Good agreement was obtained, suggesting that the field induced convection is due to the Lorentz force. The transition from laminar to turbulent flow in the presence of the field was studied, and a magnetic Reynolds number, $Re_m$, was proposed to characterise the field effect on the flow regime.

No effect of the field was observed on the heterogeneous electron transfer kinetics. The exchange current density was found to be 10 $A/m^2$ from Tafel plots and independently from impedance spectroscopy. The cathodic and anodic transfer coefficients were found to be 0.45 and 0.90 respectively. These kinetic parameters are in good agreement with the literature values and were unchanged in a field of 0.5 T. No effect of the field was found on the rest potential of the system.

The effect of the field on the morphology of electrodeposited copper was investigated using scanning electron microscopy. The samples deposited in a field of 0.5 T were considerably rougher than those in zero field. X-ray diffraction spectroscopy was used to characterise these samples and no effect of the field was observed on either the crystal structure or texture of the electrodeposited copper.

The growth pattern of two dimensional copper electrodeposits in a thin planar cell was strongly influenced by the magnitude and direction of an applied magnetic field. The deposits obtained with the field perpendicular to the plane of growth formed branching spirals, whose chirality was opposite when the field was reversed. Unidirectional stringy deposits were obtained when the field was applied in the plane of the cell. These results established the importance of competition between gravitational and magnetic forces in the growth modes of such deposits.

A comparison was made of the order of magnitude of the various magnetic forces acting in the solution. It was concluded that three of these forces were significant in most experimental conditions: the Lorentz force, the electrokinetic force and the field gradient force. These body forces are comparable in magnitude and are large enough to induce convection throughout the cell. The tangential fluid velocity sets up a hydrodynamic boundary layer at the electrode, which creates mixing in the diffusion layer, thus narrowing its width. This leads to an increase in the rate of mass transport, manifested by higher limiting currents in the presence of the field.

# Table of Contents


| | | |
|---|---|---|
| | Declaration | i |
| | Acknowledgements | ii |
| | Dedication | iv |
| | Summary | v |

**1 Introduction**

| | | |
|---|---|---|
| 1.1 | Electrochemistry | 2 |
| 1.2 | Kinetics of heterogeneous electron transfer | 5 |
| 1.3 | Mass transport processes | 10 |
| 1.4 | Hydrodynamics | 15 |
| 1.5 | Electrokinetic phenomena | 22 |
| 1.6 | Electrochemistry of copper | 24 |
| 1.7 | Magnetic field effects on electrochemical reactions | 27 |
| | References | 50 |

**2 Experimental Methods**

| | | |
|---|---|---|
| 2.1 | Electrochemical cell | 54 |
| 2.2 | Electrode construction and preparation | 57 |
| 2.3 | Potentiostat/Galvanostat | 58 |
| 2.4 | Rotating disk electrode | 61 |
| 2.5 | Microelectrodes | 63 |
| 2.6 | Application of a magnetic field | 64 |

**3 Magnetic field effects on the voltammetric behaviour of $Cu^{2+}/Cu$**

| | | |
|---|---|---|
| 3.1 | Linear sweep voltammetry | 66 |
| 3.2 | Magnetic field effects on mass transport | 68 |
| 3.3 | Magnetic field effects on electrode kinetics | 81 |
| 3.4 | Magnetic field effects in conditions of enhanced mass transport | 83 |
| 3.5 | Magnetic field effects on the rest potential | 86 |

## 4 Magnetic field effects on the diffusion of $Cu^{2+}$

4.1 Impedance spectroscopy 88

4.2 Magnetic field effects on the impedance response 93

4.3 Chronoamperometry 98

4.4 Magnetic field effects on the chronoamperometric response 101

References 103

## 5 Characterisation of magnetic field effects on Cu electrodeposition

5.1 Scanning electron microscopy 105

5.2 X-ray diffraction spectroscopy 107

5.3 Analysis of electrodeposited copper 109

5.4 Characterisation of the flow regime 113

## 6 Magnetic field effects on fractal electrodeposits

6.1 Fractal geometry 117

6.2 Magnetic field effects on fractal electrodeposits 119

References 126

## 7 Discussion and Future Work

7.1 Discussion 128

7.2 Future Work 147

References 149

# Chapter One

# Introduction

## 1.1 Electrochemistry

Electrochemistry, the study of the interconversion of chemical and electrical energy, has a pedigree stretching back to the late eighteenth century when Galvani noted that the electric discharge from a bolt of lightning stimulated the muscle reflexes of a dead frog. An electrochemical system typically consists of two electrodes immersed in an ionic solution (electrolyte) connected to each other by an external circuit. Such a system is known as an electrochemical cell and these may be divided into two categories. In a Galvanic cell, the energy of a spontaneous chemical reaction is converted into electrical energy. Batteries, fuel cells and corrosion processes are examples of Galvanic processes. In an electrolytic cell, on the other hand, chemical change is accomplished by the input of electrical energy. Electrolysis, electroplating and most electroanalytical techniques fall into this category. The ionic current flowing in an electrochemical cell is accompanied by charge transfer at each electrode. The electrode at which net reduction occurs is known as the cathode, while the electrode at which there is a net oxidation is termed the anode. A full treatment of a wide range of theoretical and experimental techniques is available in most standard electrochemical texts[1-4].

Much of the pioneering work in electrochemistry was carried out by Michael Faraday, who established empirical relationships between voltage, current, concentration, capacitance and conductivity. With the discovery of the electron (J.J. Thompson, 1893) and the development of chemical thermodynamics (G.N. Lewis, 1923), electrochemical techniques such as potentiometry and polarography gained importance in the characterisation of thermodynamic properties of solutions. In particular, the relationship between the cell potential and the Gibbs free energy enabled the determination of equilibrium constants for a multitude of chemical reactions from the measurement of relatively few standard reduction potentials. By the use of various transient methods, the mechanisms of electron transfer processes have been extensively studied via the application of transition state theory. Both the kinetics of the heterogeneous electron transfer process and homogeneous mass transport processes such as diffusion and convection may be quantitatively characterised.

The advent of powerful electronic instrumentation and improved data processing speed has had a significant impact on electrochemical techniques in the laboratory. In addition, numerical methods, made possible by the improved computational power of computers, have led to improvements in electrochemical theory and simulation. This has resulted in something of a renaissance in the field of electrochemistry over the last few decades. A wealth of information on both thermodynamic and kinetic processes is now available through modern electrochemical techniques.

A typical electrochemical reaction consists of several steps, namely diffusion of reactant species to the surface of the electrode, rearrangement of the ionic atmosphere, adsorption onto the electrode, electron transfer and finally diffusion of the product species away from the electrode. In the case when one of these steps is rate-determining, the dependence of the current on the applied potential is greatly simplified. For the case of a sequential electrochemical process involving the transfer of n electrons, the steady-state current density is given by:

$$j = \frac{nFk_c k_D c_0(O)}{k_c + k_D} - \frac{nFk_a k_D c_0(R)}{k_a + k_D} \qquad (1.1)$$

where F is the Faraday constant (96,500 C/mol), $k_c$ (m/s) is the rate constant for the cathodic (reduction) reaction, $k_a$ (m/s) is the rate constant for the anodic (oxidation) reaction, $k_D$ (m/s) is the diffusional rate constant and $c_0(O)$ and $c_0(R)$ are the surface concentrations ($mol/m^3$) of oxidised and reduced species. The first term on the right hand side of Eq. 1.1 is the cathodic (reduction) current and the second term is the anodic (oxidation) current. When the reaction is close to equilibrium both currents are comparable in magnitude and flow in opposite directions.

The equilibrium potential, $V_{eq}$, of an electrochemical cell, i.e. the potential at which the net current is zero, is known as the rest potential. The overpotential, $\eta$, is defined as the difference between the applied potential, V, and the equilibrium potential:

$$\eta = V - V_{eq} \tag{1.2}$$

The kinetics of the electron transfer, characterised by $k_c$ and $k_a$, are highly sensitive to the overpotential, whereas $k_D$ is independent of $\eta$. Hence, the magnitude of the applied potential determines whether the reaction is under activation (electrode kinetics) or mass transport (diffusional) control. Heterogeneous electrode kinetics are treated in Section 1.2, while mass transport is considered in Section 1.3.

Electrochemistry is rapidly becoming an important interdisciplinary area, with much to offer both biological and physical sciences.

## 1.2 Kinetics of heterogeneous electron transfer

The electron transfer process takes place in the interfacial region between the electrode and the electrolyte. Most of the potential drop occurs in a thin layer, typically around 1 nm, known as the electrical double layer. The double layer is a region of charge separation and behaves rather like a capacitor so that when a potential difference is applied across it, a charging current flows at short times. Several models of the structure of the double layer have been proposed. The most sophisticated incorporate both the rigid structure of the adsorbed ions at the electrode surface and the more diffuse structure further out into the solution.

At low overpotentials, the electrode kinetics are slower than the rate of mass transport ($k_c$, $k_a << k_D$) and Eq. 1.1 reduces to:

$$j = nF[k_c c_0(O) - k_a c_0(R)] \tag{1.3}$$

The reaction is under activation control since reactant species are arriving at the electrode faster than they can be reduced at the electrode. At equilibrium the forward and backward reactions take place at the same rate and the net current is zero. Therefore, an electrochemical reaction at equilibrium is an example of a dynamic equilibrium.

The dependence of the rate constants $k_c$ and $k_a$ on the overpotential may be determined using activated complex theory. Assuming an Arrhenius form for the dependence of the rate constants on the Gibbs free energy of activation, the following expressions are obtained for $k_c$ and $k_a$:

$$k_c = k_0 \exp[-\alpha_c nF(V - V^{0'}) / RT] \tag{1.4}$$

$$k_a = k_0 \exp[\alpha_a nF(V - V^{0'}) / RT] \tag{1.5}$$

where $k_0$ (m/s) is the standard electrochemical rate constant for the reaction, $V^{0'}$ (V) is the formal potential, R is the gas constant (8.314 $JK^{-1}mol^{-1}$) and $\alpha_c$ and $\alpha_a$ are the cathodic and anodic charge transfer coefficients. $k_0$ is equal to $k_c$ and $k_a$ at equilibrium, while the charge transfer coefficients are a measure of the symmetry of the activation energy barrier. Inserting the expressions for $k_c$ and $k_a$ into Eq. 1.3, we obtain the following equation:

$$j = nFk_0\{c_0(O)\exp[-\alpha_c nF(V - V^{0'}) / RT] - c_0(R)\exp[\alpha_a nF(V - V^{0'}) / RT]\} \tag{1.6}$$

The standard electrochemical rate constant, $k_0$, is a measure of the kinetic facility of the redox couple. Systems with large $k_0$ will reach equilibrium on a very short timescale while those with small $k_0$ will be sluggish. A wide range of values of $k_0$ exist, from rapid reactions with simple electron transfer such as the reduction of aromatic hydrocarbons ($k_0 \sim 0.1$ m/s) to complex multistep mechanisms involving significant molecular rearrangement ($k_0 \sim 10^{-11}$ m/s). It must be noted that the standard electrochemical rate constant is not a measure of the electron transfer itself, as this is an adiabatic process according to the Franck-Condon principle with a timescale of the order of $10^{-16}$ s. Rather it is a measure of the time taken for the reactant species to arrange themselves and their ionic atmospheres in a position for electron transfer to occur.

Eq. 1.6 completely describes the current-potential characteristic of a given electrochemical reaction. It, or a variation derived from it, may be used to determine kinetic parameters from data obtained using a wide range of experimental techniques.

At equilibrium, the net current is zero. Setting the cathodic and anodic currents equal in Eq. 1.6, we obtain:

$$\exp[nF(V_{eq} - V^{0'}) / RT] = c_0(O) / c_0(R) \tag{1.7}$$

Since the electrode is at equilibrium, the surface concentrations $c_0(O)$ and $c_0(R)$ are equal to those in the bulk solution, $c_\infty(O)$ and $c_\infty(R)$. Substituting the bulk values and rearranging yields the Nernst equation:

$$V_{eq} = V^{0'} + \frac{RT}{nF} \ln \frac{c_\infty(O)}{c_\infty(R)} \tag{1.8}$$

The Nernst equation describes how the equilibrium potential of an electrochemical system varies with the concentration of oxidised and reduced species in solution.

The exchange current density, $j_0$, is defined as the magnitude of either the cathodic or the anodic current density at equilibrium. Combining Eqs. 1.2, 1.6 and 1.7 gives:

$$j = j_0 \left[ \frac{c_0(O)}{c_\infty(O)} \exp\left( \frac{-\alpha_c nF\eta}{RT} \right) - \frac{c_0(R)}{c_\infty(R)} \exp\left( \frac{\alpha_a nF\eta}{RT} \right) \right] \tag{1.9}$$

Eq. 1.9 is known as the current density-overpotential equation. The first term on the right hand side is the cathodic current density as a function of $\eta$ and the second term gives the dependence of the anodic current density on $\eta$. If the solution is well stirred or the current is sufficiently low that surface concentrations do not drop below the bulk values, we obtain the Butler-Volmer equation:

$$j = j_0 \left[ \exp\left( \frac{-\alpha_c nF\eta}{RT} \right) - \exp\left( \frac{\alpha_a nF\eta}{RT} \right) \right] \tag{1.10}$$

The advantage of the Butler-Volmer equation over Eq. 1.6 is that it relates the current density to a readily measurable quantity, $\eta$, rather than the deviation from the formal potential, $V - V^{0'}$. As stated previously, close to equilibrium both cathodic and anodic currents are comparable in magnitude. However, the reaction may be driven in either direction by applying a sufficiently positive or negative overpotential to the electrode. At large negative overpotentials the anodic current becomes negligible and we have:

$$j = j_0 \exp \frac{-\alpha_c nF\eta}{RT} \tag{1.11}$$

Taking logarithms of both sides we obtain the Tafel relation:

$$\log j = \log j_0 - \frac{\alpha_c nF\eta}{2.3RT} \tag{1.12}$$

Similarly, when $\eta$ is large and positive, the cathodic current is negligible and then:

$$\log j = \log j_0 + \frac{\alpha_a nF\eta}{2.3RT} \tag{1.13}$$

Hence the parameters $j_0$, $\alpha_c$ and $\alpha_a$ may be determined from a plot of log j against $\eta$. Such a plot is known as a Tafel plot and is shown schematically in Fig. 1.1. Note that here n is the number of electrons transferred in the rate determining step. The exponential variation of a kinetic parameter (j) with a thermodynamic one ($\eta$) is common in physical chemistry. In a typical Tafel plot, deviations from linearity at low overpotentials are due to the contribution from the back reaction. At high overpotentials, mass transport effects cause a levelling off of the current response. These effects are considered in Section 1.3.

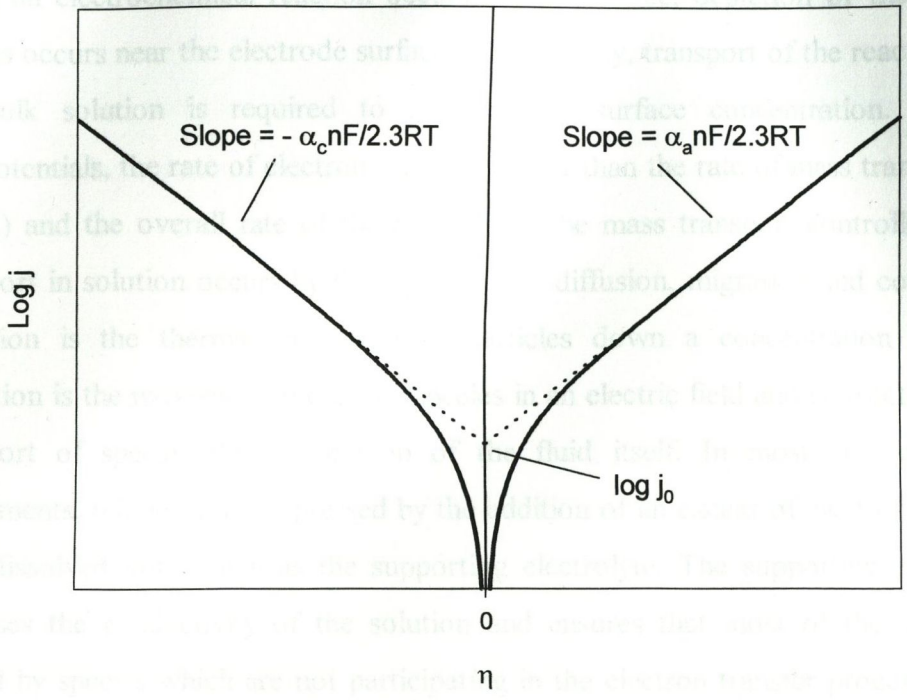


*Fig. 1.1: Tafel plots for both cathodic (left) and anodic (right) branches for $\alpha_c = \alpha_a = 0.5$.*

## 1.3 Mass transport processes

When an electrochemical reaction occurs at an electrode, depletion of the reactant species occurs near the electrode surface. Consequently, transport of the reactant from the bulk solution is required to replenish the surface concentration. At high overpotentials, the rate of electron transfer is faster than the rate of mass transport ($k_0 >> k_D$) and the overall rate of the reaction will be mass transport controlled. Mass transport in solution occurs by three processes - diffusion, migration and convection. Diffusion is the thermal movement of particles down a concentration gradient, migration is the movement of charged species in an electric field and convection is the transport of species through motion of the fluid itself. In most electrochemical experiments, migration is suppressed by the addition of an excess of electrochemically inert dissolved salt known as the supporting electrolyte. The supporting electrolyte increases the conductivity of the solution and ensures that most of the current is carried by species which are not participating in the electron transfer process. It also ensures that all of the potential drop occurs within the double layer. Systems under mass transport control may be divided into two categories - those under pure diffusion control (quiescent systems) and those where convection is significant (hydrodynamic systems). Even in quiescent systems, natural convection arising from density differences in the electrolyte may perturb the concentration gradients and hence steps are usually taken to render these effects negligible.

In a solution where the concentration, and therefore the electrochemical potential, $\bar{\mu}$ (J/mol), varies with position, the movement of ionic species may be related to an effective thermodynamic force per mole, $F_D$:

$$F_D = -\nabla\bar{\mu} \tag{1.14}$$

The concentration dependence of the electrochemical potential, neglecting activity coefficients, is given by:

$$\bar{\mu} = \bar{\mu}^0 + RT \ln c \tag{1.15}$$

where $\bar{\mu}^0$ is the standard electrochemical potential (J/mol). Combining Eqs. 1.14 and 1.15 and neglecting migrational effects we obtain:

$$F_D = -\frac{RT}{c} \nabla c \tag{1.16}$$

This force per mole may be converted into a force per unit volume by multiplying by the concentration.

The movement of ionic species in solution is described by Fick's first law as follows:

$$J = -D\nabla c - \frac{zc_\infty F}{RT} \nabla V \tag{1.17}$$

where J is the number flux of species, D is the diffusion coefficient of the species ($m^2/s$), $\nabla c$ is the concentration gradient, z is the charge on the ion and $\nabla V$ is the potential gradient. The first term on the right hand side is the flux due to diffusion while the second term is that due to migration. The flux due to migration is usually rendered negligible by the addition of an excess of supporting electrolyte. The number flux of species is related to the drift speed, s, by:

$$J = sc_\infty \tag{1.18}$$

Combining Eqs. 1.16-1.18 yields:

$$s = -\frac{D}{RT} F_D \tag{1.19}$$

Once the drift speed and the effective driving force are known, the diffusion coefficient may be calculated. One case for which both these are known is that of an ion of charge ze moving in an electric field, E, where we have:

$$s = \mu E \tag{1.20}$$

$$F_D = zeE \tag{1.21}$$

where $\mu$ is the mobility of the ion ($m^2V^{-1}s^{-1}$). Substitution of these relations into Eq. 1.19 yields the Einstein relation:

$$D = \frac{\mu RT}{zF} \tag{1.22}$$

The Einstein relation shows that the diffusion coefficient is proportional to both ionic mobility and temperature, and inversely proportional to the charge on the ion. Diffusion coefficients in aqueous solution typically vary between $10^{-10}$ and $10^{-9}$ $m^2/s$.

Fick's second law expresses the variation in concentration with time as a result of diffusion and in the absence of migration:

$$\frac{\partial c}{\partial t} = D\nabla^2 c \tag{1.23}$$

The solution of this equation under the appropriate boundary conditions gives the variation of flux, and hence of the diffusion-limited current, with time. For a reduction process at a uniformly accessible planar electrode the current density, j, is given by:

$$j = -nFD\nabla c \tag{1.24}$$

The concentration gradient is nonlinear and tends to zero at large distances from the electrode surface. However, it is useful to define a diffusion layer of thickness $\delta$ over which the concentration gradient varies in a linear manner. The value of $\delta$ is obtained by extrapolation of the concentration gradient at the electrode surface until the bulk concentration is reached as shown in Fig. 1.2. Hence we obtain for the current density:

$$j = -\frac{nFD(c_\infty - c_0)}{\delta} \tag{1.25}$$

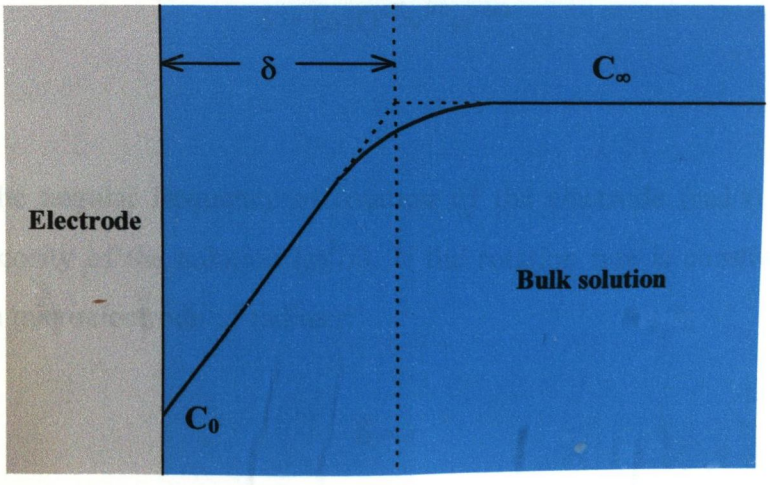


*Fig 1.2: Illustration of the definition of the diffusion layer thickness, δ.*

At sufficiently high overpotentials, the surface concentration of reactant species, $c_0$, will become infinitesimal and the concentration gradient will reach a maximum. The current density under these conditions is known as the limiting current density and is given by:

$$j_L = -\frac{nFDc_\infty}{\delta} \tag{1.26}$$

This corresponds to a situation in which all reactant species reaching the electrode are instantaneously reduced. In quiescent solution, solution of Eq. 1.23 shows that the thickness of the diffusion layer increases with $t^{1/2}$ as depletion of reactant species spreads into the solution. Hence, at a given potential, the current density will fall off with time as the concentration gradient decreases. Eventually, natural convection will set in and a steady state will be reached. However, the thickness of the diffusion layer may be controlled in hydrodynamic systems, where forced convection maintains the bulk concentration at a fixed distance from the electrode surface, or at a microelectrode, where $\delta$ is independent of time. At a rotating disk electrode, the diffusion layer thickness is given by[2]:

$$\delta = 1.61 D^{1/3} \nu^{1/6} \omega^{-1/2} \tag{1.27}$$

where $\omega$ is the angular frequency of rotation of the electrode (rad/s) and $\nu$ is the kinematic viscosity of the solution ($m^2/s$). If the rotation rate is constant, $\delta$ is fixed. Similarly, at a microelectrode of radius r:

$$\delta \approx r \tag{1.28}$$

which is also independent of time.

## 1.4 Hydrodynamics

Hydrodynamics is the study of the effect of fluid motion on both physical and chemical processes in solution. A comprehensive review of this interdisciplinary area was published by Levich[5] in 1962. In this section we consider the velocity and concentration profiles close to a flat plate, at which an electrochemical reaction is occuring, and past which the solution is flowing at a main stream velocity, U. In a hydrodynamic system, i.e. when both convection and diffusion are present in a fluid, Fick's first law becomes:

$$J = cv - D\nabla c \tag{1.29}$$

where v is the velocity of the fluid. The first term on the right hand side of Eq. 1.29 is the flux due to convection, the second is that due to diffusion. Fick's second law is then:

$$\frac{\partial c}{\partial t} = -v\nabla c + D\nabla^2 c \tag{1.30}$$

which is known as the convective-diffusion equation. The solution to Eq. 1.30 requires a knowledge of the velocity profile in the fluid, which is obtained by solving the Navier-Stokes and continuity equations:

$$\frac{d\vec{v}}{dt} + \vec{v}\cdot\nabla\vec{v} = -\frac{\vec{\nabla}P}{\rho} + \nu\nabla^2\vec{v} + \vec{F} \tag{1.31}$$

$$\vec{\nabla}\cdot\vec{v} = 0 \tag{1.32}$$

The Navier-Stokes equation (Eq. 1.31) expresses Newton's second law for an incompressible fluid element. The left hand side of the equation is the acceleration of the fluid element and the right hand side is the sum of the external volume forces on it. The first term on the right hand side is the force due to the pressure gradient, $\vec{\nabla}P$, through the system. The second term accounts for the effect of viscous forces and only applies when one part of the fluid moves relative to another. Here $\nu$ is the kinematic viscosity of the fluid ($m^2/s$). Momentum is transferred from faster moving layers of fluid to slower moving layers. The third term, $\vec{F}$, refers to any other external volume forces acting on the fluid element, e.g. gravitational, electrical, magnetic. In general, the differential equations in the Navier-Stokes equation are nonlinear and analytical solutions do not exist. Hence numerical methods must be employed.

Dimensional analysis and similarity theory have been widely employed to hydrodynamic systems for the same reasons. The most important dimensionless variable characterising the flow of a viscous fluid is the Reynolds number, Re:

$$\mathrm{Re} = \frac{UL}{\nu} \tag{1.33}$$

where U is a characteristic fluid velocity and L is a characteristic length. For the steady flow of an incompressible fluid, the flow regime is entirely determined by the value of Re. In practice, flow at large Reynolds numbers is usually observed. Below a certain threshold value, $\mathrm{Re}_{crit}$, the flow is laminar; above $\mathrm{Re}_{crit}$ the flow becomes turbulent. For a flat plate, $\mathrm{Re}_{crit} \sim 1500$.

The flow velocity must become zero at the surface of a solid body immersed in a fluid. This is known as the 'no slip' condition. Hence there is a region immediately adjacent to the solid surface where the flow velocity changes abruptly from zero to its value in the bulk stream. This region is known as the hydrodynamic boundary layer, and is depicted in Fig. 1.3. The retardation of fluid motion in the boundary layer is due to viscous forces alone. The concept of viscosity in convective flow is analogous to that

of the diffusion coefficient for diffusive motion. Whereas the diffusion coefficient, D, is the proportionality factor between the flux of material and the concentration gradient, the kinematic viscosity, $\nu$, is the proportionality factor between the flux of momentum and the velocity gradient. Although the boundary layer occupies a very small volume, its properties dominate the hydrodynamic behaviour of the system.

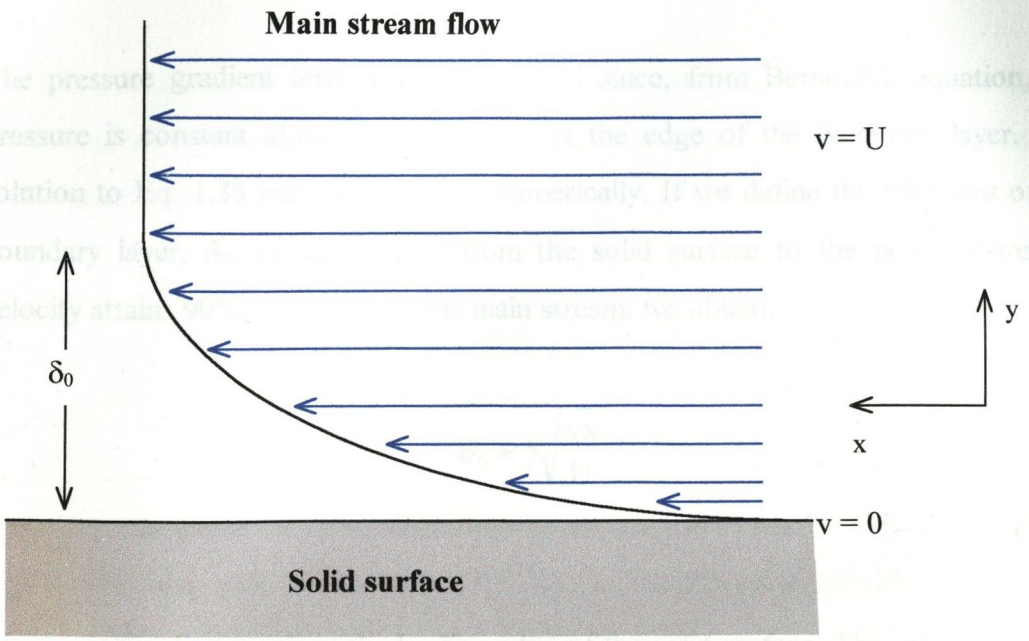


*Fig. 1.3: Variation of tangential fluid velocity in the hydrodynamic boundary layer.*

The fluid flow next to a solid surface may thus be divided into two distinct regions - the bulk flow and the boundary layer. In the bulk solution, the flow is inviscid and the viscosity term may be omitted from the Navier-Stokes equation. This simplification leads to the Euler equation, whose solution is known as Bernoulli's equation:

$$\tfrac{1}{2}\rho v^2 + P + \rho g h = \text{const.} \tag{1.34}$$

Within the boundary layer, the velocity gradient normal to the surface (y-direction) is large compared to the tangential (x-direction) velocity gradient and the Navier-Stokes equation may be written:

$$v_x \frac{\partial v_x}{\partial x} + v_y \frac{\partial v_x}{\partial y} = \nu \frac{\partial^2 v_x}{\partial y^2} \tag{1.35}$$

The pressure gradient term has been omitted since, from Bernoulli's equation, the pressure is constant along the x-direction at the edge of the boundary layer. The solution to Eq. 1.35 may be computed numerically. If we define the thickness of the boundary layer, $\delta_0$, as the distance from the solid surface to the point where the velocity attains 90% of its value in the main stream, we obtain:

$$\delta_0 \approx 5\sqrt{\frac{\nu x}{U}} \tag{1.36}$$

where x is the distance from the leading edge of the solid surface. The velocity profiles in the x and y directions are then:

$$v_x \approx \frac{Uy}{\delta_0} \tag{1.37}$$

$$v_y \approx \frac{\nu y^2}{\delta_0^3} \tag{1.38}$$

These equations are valid only when the thickness of the boundary layer is small compared to the dimensions of the solid surface, i.e. when $\delta_0 << L$. This inequality is satisfied at large Reynolds numbers.

Once the velocity profile in the boundary layer is known, the convective-diffusion equation may be solved in order to determine the material flux toward the surface. Under steady-state conditions in two dimensions, Eq. 1.30 may be rewritten:

$$v_x \frac{\partial c}{\partial x} + v_y \frac{\partial c}{\partial y} = D\left(\frac{\partial^2 c}{\partial x^2} + \frac{\partial^2 c}{\partial y^2}\right) \tag{1.39}$$

The left hand side of Eq. 1.39 represents the convective transport in the fluid, while the right hand side represents that due to diffusion. A useful dimensionless number for characterising convective diffusion systems is the Peclet number, defined as:

$$Pe = \frac{UL}{D} \tag{1.40}$$

The Peclet number is the ratio of transport by convection to that by diffusion in a fluid. It plays the same role in convective diffusion as the Reynolds number does in fluid flow. Diffusion predominates at low Peclet numbers, while convection becomes significant at high Peclet numbers. The crossover value is Pe = 1. From Eq. 1.40, it can be seen that diffusion only becomes important at low fluid velocities and on short length scales, so that in most hydrodynamic systems Pe >> 1. One important exception is within the diffusion layer near an electrode surface, where the concentration gradient is large and the fluid velocity is retarded by viscous forces.

The ratio of the Peclet number to the Reynolds number is known as the Prandtl number, Pr.

$$Pr = \frac{\nu}{D} \tag{1.41}$$

The Prandtl number is solely a property of the fluid and is the ratio of momentum transfer to mass transfer in the fluid. In aqueous solutions, $\nu \sim 10^{-6}$ $m^2/s$ and $D \sim 10^{-9}$ $m^2/s$, so that $Pr \sim 1000$. Therefore we can expect velocity gradients in aqueous solution to vary over greater distances than concentration gradients. The high value of the Prandtl number in aqueous solution means that, even for low Reynolds numbers, the Peclet number is greater than unity and convection is the dominant transport mechanism in hydrodynamic systems.

The solution to the convective-diffusive equation is obtained in much the same way as that of the Navier-Stokes equation. Two distinct regions are identified - the bulk solution where the concentration is constant and the diffusion layer over which the concentration varies from zero at the electrode surface to its bulk value at a distance $\delta$ from the electrode. In the bulk solution, convection dominates and the diffusive term on the right hand side of Eq. 1.39 can be neglected. The solution to the resulting equation is that the concentration must be constant. Within the diffusion layer, however, Eq. 1.39 may be rewritten:

$$v_x \frac{\partial c}{\partial x} + v_y \frac{\partial c}{\partial y} = D \frac{\partial^2 c}{\partial y^2} \tag{1.42}$$

The diffusive term in the x-direction has been omitted since the concentration gradient in the y-direction is much larger than that in the x-direction. Note that Eq. 1.42 is similar in form to Eq. 1.35 for the case of momentum transfer. Again, an exact solution is only possible for systems where the configuration is particularly simple. Substituting for $v_x$ and $v_y$ using Eqs. 1.37 and 1.38, we arrive at the following expression for the thickness of the diffusion layer:

$$\delta = \frac{\delta_0}{Pr^{1/3}} \tag{1.43}$$

Hence the thickness of the diffusion layer in aqueous solution is one tenth that of the hydrodynamic boundary layer. Substituting for $\delta_0$ from Eq. 1.36:

$$\delta \approx D^{1/3}\nu^{1/6}\sqrt{\frac{x}{U}} \tag{1.44}$$

The thickness of the diffusion layer is thus inversely proportional to the square root of the main stream fluid velocity and proportional to the square root of the distance from the leading edge of the solid surface. It also depends on the kinematic viscosity of the fluid and the diffusion coefficient of the reactant species. The limiting current density may then be calculated from the diffusion layer thickness using Eq. 1.26.

Very few hydrodynamic systems admit analytical solutions for the limiting current density. One of these, however, is the rotating disk electrode, for which the limiting current density is given by:

$$j_L = 0.620nFD^{2/3}\nu^{-1/6}\omega^{1/2}c_\infty \tag{1.45}$$

which is independent of both electrode radius and time (if the rotation rate, $\omega$, is constant). The rotating disk electrode is thus an extremely useful tool for investigating kinetic phenomena, since at high rotation rates mass transport effects are significantly reduced.

## 1.5 Electrokinetic phenomena

Electrokinetic phenomena occur when two phases on either side of an electrified interface are moving relative to one another. An electric field applied parallel to the interface induces relative motion and, conversely, relative motion induces an electric field[2]. These effects may be categorised according to whether the solid or the liquid phase is the mobile phase. In colloidal systems the solid phase is the mobile phase. Colloidal particles may be forced to move under the influence of an applied electric field (electrophoresis), while the motion of colloids due to the force of gravity induces a potential difference called the sedimentation potential. In electrochemical systems the liquid phase is generally the mobile phase. An electric field applied parallel to the interface induces movement of the solution phase. This phenomenon is known as electro-osmosis. Conversely, when the liquid phase is forced to flow parallel to the interface, a potential difference known as the streaming potential is induced.

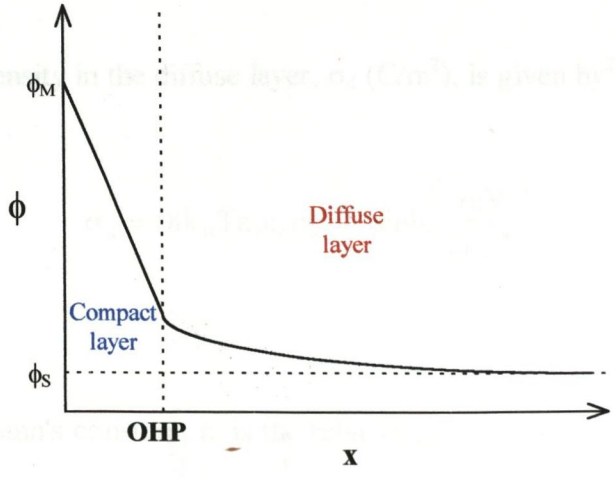


*Fig. 1.4: Variation of potential across the electrical double layer.*

The variation of potential across the electrical double layer is shown in Fig. 1.4. A compact layer of rigidly held ions exists close to the electrode followed by a diffuse layer extending into the bulk solution. The potential varies linearly across the compact

layer and approximately exponentially in the diffuse layer, where the ions are under the combined influence of ordering electrical forces and disordering thermal forces. The boundary between the two layers is known as the outer Helmholtz plane (OHP). The higher the electrolyte concentration, the less the importance of the diffuse layer as the potential drop is more confined to the compact layer. A shear plane exists, not necessarily at the outer Helmholtz plane, beyond which the ions are free to move as they are not rigidly held by the electrostatic force. The potential of this plane is known as the zeta or electrokinetic potential, $\xi$. The electrokinetic effects are manifested in the diffuse layer beyond this plane.

The electrokinetic phenomenon of most relevance to this work is electro-osmosis. An electric field, $E_{\|}$, applied parallel to the electrode surface produces an electrostatic force, $F_E$ ($N/m^2$), in the diffuse layer of magnitude:

$$F_E = \sigma_d E_{\|} \tag{1.46}$$

where the charge density in the diffuse layer, $\sigma_d$ ($C/m^2$), is given by[2]:

$$\sigma_d = (8k_B T \varepsilon_r \varepsilon_0 n_\infty)^{1/2} \sinh\left(\frac{zeV}{2k_B T}\right) \tag{1.47}$$

where $k_B$ is Boltzmann's constant, $\varepsilon_r$ is the relative permittivity of the solvent, $\varepsilon_0$ is the permittivity of free space and $n_\infty$ is the numerical concentration of the ionic species.

## 1.6 Electrochemistry of copper

Copper is a transition metal with a $3d^{10}\ 4s^1$ configuration. It has two valence electrons which can be removed to form the cations $Cu^+$ and $Cu^{2+}$. $Cu^+$ cannot exist in aqueous solution due to the disproportionation reaction:

$$2Cu^+(aq) \rightarrow Cu^{2+}(aq) + Cu(s)$$

which is extremely rapid and goes to completion. Salts such as $CuSO_4$ dissociate in aqueous solution to form the ionic species $Cu^{2+}$ and $SO_4^{2-}$, which act as charge carriers under the influence of an applied electric field. When two copper electrodes are immersed in such a solution and a voltage is applied between them, as shown in Fig. 1.5, an electrochemical redox reaction is initiated. Oxidation of metallic copper takes place at the positively charged electrode - the anode, while reduction of copper ions in solution takes place at the negatively charged electrode - the cathode.

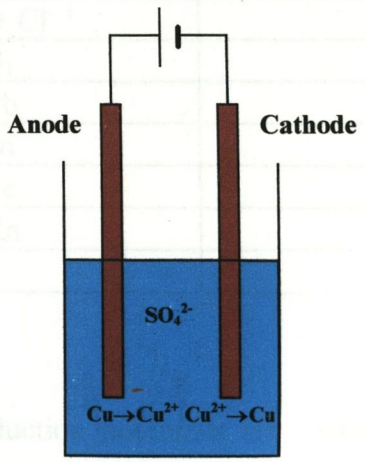


*Fig. 1.5: Schematic diagram of a simple copper electrolysis cell.*

Anode: $Cu(s) \rightarrow Cu^{2+}(aq) + 2e^-$

Cathode: $Cu^{2+}(aq) + 2e^- \rightarrow Cu(s)$

The anodic process is known as electrodissolution and the cathodic process is termed electrodeposition. The potential at which these processes are at equilibrium is determined by thermodynamic parameters (see Section 1.2) and differs widely from metal to metal. The electrochemical series is a list of such standard reduction potentials from the most strongly oxidising (high positive potentials) to the most strongly reducing (low negative potentials). A selection of representative standard reduction potentials, including that of copper, is shown in Table 1.1.

*Table 1.1: Standard reduction potentials at 25 °C and unit activity.*

| **Reduction reaction** | **Potential (V)** |
|---|---|
| $F_2 + 2e^- \rightarrow 2F^-$ | + 2.87 |
| $Au^{3+} + 3e^- \rightarrow Au$ | + 1.52 |
| $Ag^+ + e^- \rightarrow Ag$ | + 0.80 |
| $Cu^{2+} + 2e^- \rightarrow Cu$ | + 0.34 |
| $AgCl + e^- \rightarrow Ag + Cl^-$ | + 0.22 |
| $2H^+ + 2e^- \rightarrow H_2$ | 0 |
| $Pb^{2+} + 2e^- \rightarrow Pb$ | - 0.13 |
| $Ni^{2+} + 2e^- \rightarrow Ni$ | - 0.26 |
| $Fe^{2+} + 2e^- \rightarrow Fe$ | - 0.44 |
| $Zn^{2+} + 2e^- \rightarrow Zn$ | - 0.76 |
| $Li^+ + e- \rightarrow Li$ | - 3.04 |

By definition, standard reduction potentials are measured relative to the hydrogen electrode (0 V). From purely thermodynamic considerations, substances in the electrochemical series will be reduced by those below them in the series, e.g. zinc will reduce copper. However, even if a reaction is thermodynamically favourable, it may not proceed at an appreciable rate if the kinetics of the reaction are slow. Copper is a relatively noble metal and thus has a more positive reduction potential than most metals. Since it lies above hydrogen in the electrochemical series, it will not dissolve in acid solution unless the solution contains oxidising anions.

Electroplating of copper is an important technological process. Electrolysis is used on an industrial scale to separate pure metals from their ores. All of the copper used in the electronics industry is produced in this way. Apart from silver, copper has the highest conductivity of any other metal. Its malleability and ductility make it ideal for large scale production in electronic applications. Recently, electrodeposition of copper has superseded sputtering in the fabrication of interconnnects in the semiconductor industry[6].

## 1.7 Magnetic field effects on electrochemical reactions

Mention of the effect of a static magnetic field on an electrochemical process dates from as early as the work of Faraday[7]. However the last decade has seen research in this area intensify as much interest focuses both on understanding the physical mechanisms involved and on using a magnetic field as an additional control variable in electrochemical systems. Magnetoelectrolysis is the term used for the effect of an applied magnetic field on heterogeneous electrochemical processes at an electrode/solution interface. In recent years, various effects have been reported in the literature under a wide range of conditions. Notable reviews of the subject are those by Fahidy[8] and Tacken and Janssen[9].

Most reports in the literature have dealt with the enhancement in the rate of mass transport in the presence of a magnetic field. The dependence of the limiting current density, $j_L$, on the applied field, B, is usually expressed in the form:

$$j_L = j_L^0 + aB^m \tag{1.48}$$

where $j_L^0$ is the limiting current density in zero field and a and m are regression parameters. A range of values for the exponent m, ranging from 0.1 to 2, have been reported by various authors. The parameter a may be either positive or negative, depending on the relative orientation of the electrode and the applied field. The experimental data may be treated by dimensional analysis and classical hydrodynamic theory. The effect of the field on the kinetics of electron transfer is a topic of more controversy, with contradictory reports abounding in the literature. The main problem is the difficulty of ensuring that a system is under pure activation control. Most practical systems operate under diffusion control and mass transport effects may obscure any magnetic field effects on kinetic phenomena.

It is evident even from a cursory glance through the literature that much of the work in the area of magnetoelectrochemistry over the last few decades has been conducted by

a small number of research groups. Notably, Fahidy (University of Ontario), Aogaki (NRLMS, Saitama), White (University of Utah), Olivier (CNRS, Reims) and Mogi (Tohoku University) have all published extensively in the field.

In 1972, Mohanta and Fahidy[10] reported that the electrodeposition of copper from acidified copper sulphate solution was enhanced by the application of a uniform magnetic field. The cathodic limiting current in a 0.05 M solution increased by 30% in a field of 0.7 T. The dependence of the limiting current density on the applied field was fitted to Eq. 1.48 with m = 1.64. Fahidy[11] then examined several hydrodynamic models in an attempt to explain these results. He found that the calculated diffusion layer thickness was of the same order of magnitude (~ 0.2 mm) in each of the models, although the flow regime, characterised by the Reynolds number, was not always the same. He predicted that the diffusion layer thickness should decrease as $B^{-m}$, and from the experimental limiting current densities deduced m ~ 1.4.

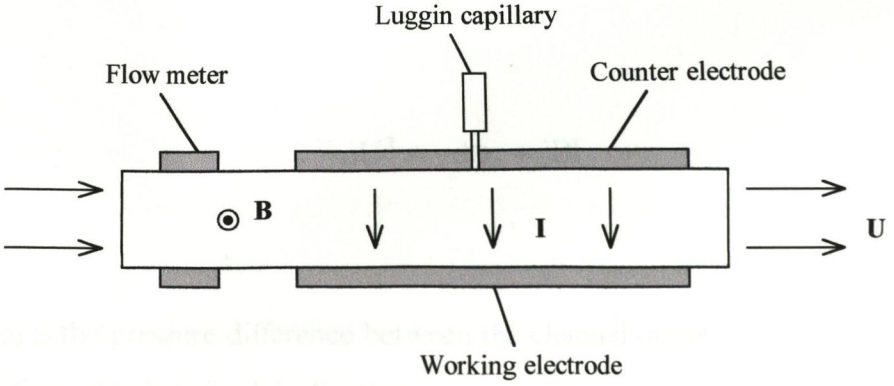


*Fig. 1.6: Side elevation of the channel electrode cell used by Aogaki et al[12].*

As mentioned in Section 1.4, due to the nonlinear nature of the Navier-Stokes equation, analytical solutions are in general not obtainable. However, in 1975, Aogaki et al[12] derived an analytical solution for the limiting current density in a rectangular channel cell, where the geometry was well defined and certain valid approximations were possible. The cell, illustrated in Fig. 1.6, consisted of two copper electrodes, of

length l, embedded in the walls of a short channel of rectangular cross-section. The dimensions of the channel were of the order of a few mm. The cell was designed so that the fluid flow could not develop vortices but rather a streamline flow like that shown in Fig. 1.3.

The Lorentz body force, $\vec{j} \times \vec{B}$, was incorporated into the Navier-Stokes equation to obtain:

$$\frac{d\vec{v}}{dt} + \vec{v}\nabla\vec{v} = -\frac{\vec{\nabla}P}{\rho} + \nu\nabla^2\vec{v} + \frac{1}{\rho}\vec{j} \times \vec{B} \tag{1.49}$$

The flow in the main channel was considered inviscid so the viscous term on the right hand side of Eq. 1.49 could be neglected. Under steady-state conditions, the first term on the left hand side may also be omitted. Integrating the resulting expression leads to the relationship between the main flow velocity, the current density and the applied field.

$$\tfrac{1}{2}\rho U^2 = -\Delta p_0 + jBl \tag{1.50}$$

where $\Delta p_0$ is the pressure difference between the channel outlet and a point far into the bulk solution. As described in Section 1.4, the presence of a tangential velocity U causes an increase in the diffusional flux to the electrode (Eq. 1.44) thereby increasing the current density. This in turn increases U (Eq. 1.50) so that a positive feedback is established, limited only by viscous forces in the boundary layers of the channel. Aogaki et al calculated that the steady-state limiting current density varies as:

$$j_L = Hc_\infty{}^{4/3}B^{1/3} - 0.333\frac{\Delta p_0}{Bl} \tag{1.51}$$

where H is a constant which is a function of n, D, $\nu$, $\rho$ and the dimensions of the electrodes. The dependence of the limiting current on $c_\infty^{4/3}$ and $B^{1/3}$ was confirmed by experiment.

The same authors extended their treatment to a longer channel where the boundary layer thicknesses become comparable to the channel dimensions[13]. Under these conditions the flow in the main stream may no longer be considered inviscid and the limiting current density was found to vary as:

$$j_L = Kc_\infty^{3/2}B^{1/2} \tag{1.52}$$

where K is a constant which depends on n, D, $\nu$, $\rho$ and the dimensions of the electrodes. The authors suggested that such a cell could be used for electrochemical voltammetric experiments under forced convection in much the same way as a rotating disk electrode, pointing out that the advantage of their system is that there are no moving parts.

One of the first attempts to quantify the effect of a magnetic field on an electrochemical process under activation control was published by Kelly[14] in 1977. The rate of corrosion of titanium electrodes in flowing electrolyte ($H_2SO_4$) was enhanced by the application of a static magnetic field. The active state anodic current was increased by a factor of 2.5 in fields of up to 2.1 T. The change in interfacial potential was shown to be proportional to the applied field. These results were explained in terms of the Lorentz force on the charged components of the flowing electrolyte.

In 1978, Mohanta and Fahidy[15] reported that the application of a non-uniform field could produce comparable enhancements in the rate of mass transport to that obtained in a uniform field. A comparable enhancement in limiting current was observed in non-uniform fields whose average value was about one tenth of the uniform field strength required.

In 1981, Hubbard and Wolynes[16] calculated the electrohydrodynamic forces on a moving ion due to the polarisation of water molecules under the influence of an applied magnetic field. The resultant force due to the effects of changing local polarisation in the vicinity of the moving ion was found to be:

$$F = \frac{-7}{24}\frac{(\varepsilon - 1)}{\varepsilon} \qquad (1.53)$$

which is about 30 % of the Lorentz force and acts in the opposite direction.

In 1984, Iwakura et al[17] studied the effect of an applied magnetic field on the cathodic and anodic limiting currents corresponding to the reduction and oxidation of ferricyanide ions at a Pt electrode. In both cases, the limiting current rose sharply at first and then steadily with increasing field. When the field was reversed, the limiting current was decreased in fields of up to 0.1 T, above which it increased with increasing field. The results were justified in terms of competition between the convective force arising from density differences in solution between reactants and products and the Lorentz force. The two forces appeared to be comparable in low fields but in high fields the magnetic force became dominant. The theoretical current enhancement factor dependence on magnetic field was plotted based on the limiting current arising from the relative magnitude and orientation of these two forces and good agreement with the experimental data was obtained. Further study revealed that a downward convection was always present irrespective of applied field since the density of the product $Fe(CN)_6^{4-}$ is higher than that of the reactant $Fe(CN)_6^{3-}$. This idea was put forward to account for the variation in experimental data with different electrode orientations and field directions.

At the same time, Aogaki and Fueki[18] proposed a magnetohydrodynamic generator-detector electrode for application in voltammetric experiments. Based on their flow cell described above, the system consisted of two pairs of electrodes embedded in the walls of a rectangular channel. Intermediates formed at the generator pair of electrodes were swept downstream by the magnetohydrodynamic flow to the detector pair where

a current was measured. The system is analogous to the ring-disk electrode system commonly used in the study of electrochemical intermediates. Unfortunately, the magnetic field applied to the cell (0.5 T) was not large enough to induce a sufficiently fast flow (0.03 m/s). This meant that lifetimes below about 10 ms were not detectable by the system. The authors pointed out that with a superconducting magnet delivering a field of 10 T to the cell, they would expect to be able to measure lifetimes of the order of 0.1 ms.

Voltammetric studies carried out by Noninski[19] in 1986 showed that the copper deposition overpotential in acidifed copper sulphate solution was reduced by a factor of two in a field of 1.2 T. Measurement of the deposition overpotential as a function of distance between the Luggin capillary tip and the electrode surface suggested that the field effects are felt in the bulk solution rather than at the electrode/electrolyte interface. The decrease in Ohmic resistance across the solution close to the cathode was ascribed to electrolyte concentration changes under the action of the Lorentz force.

In 1990, Aaboubi et al[20] found that the limiting current density for both the reduction and oxidation of a 0.1 M ferro-ferricyanide couple in 1 M KCl varied as $B^{1/3}c_{\infty}^{4/3}$, as predicted by Aogaki. The frequency response of the system to a sinusoidal magnetic field perturbation was analysed and was compared to the electrohydrodynamical impedance obtained through the modulation of the angular frequency of a rotating disk. It was noted that the impedance response was the same as that for a convective diffusion system, except for the depression observed in the Bode plot, which was ascribed to the non-uniformity of the diffusion layer over the electrode surface. A magnetohydrodynamic velocity gradient, $\alpha$, was introduced, which was experimentally determined to be proportional to $c_{\infty}B$. Since the limiting current density can be shown to vary as $c_{\infty}\alpha^{1/3}$, the overall dependence was confirmed to be $B^{1/3}c_{\infty}^{4/3}$.

In 1991, Fahidy[21] put forward the idea of a magnetoelectrolytic reactor where the magnetic field is generated in a solenoid surrounding the system by the same current that drives the electrolysis. He proposed that such a reactor could operate on an

industrial scale. Taking into account most of the important design parameters, he computed the optimal currents which would minimise the costs of running such a reactor. He concluded that a magnetoelectrolytic reactor could operate at a lower optimal current than a conventional electrolyser, with specific cost ratios of less than 7.5 kWh/kg.

The effect of a magnetic field on the electrodeposition and electrodissolution of copper in acidified copper sulphate solution at low overpotentials was investigated by Chopart et al[22] in 1991. The steady state current was found to increase with applied field but no effect on the either the cathodic or the anodic transfer coefficient was found. A small change in exchange current density was observed in the field, but this was ascribed to an increase in the active surface area of the electrode. Although there was no change in the Tafel slopes, the overpotential range of the Tafel region was observed to increase when the field was applied. The authors concluded that magnetoelectrochemistry would thus be a useful tool for the elucidation of kinetic parameters as there are no limitations of working electrode or cell geometry.

In 1993, Waskaas[23] showed that the diffusion rate of a paramagnetic solution through an inert membrane was significantly enhanced by the application of a magnetic field perpendicular to the membrane. The experiment consisted of a permeable membrane separating two compartments, one containing a solution of nickel(II) chloride, the other distilled water. It was claimed that the reluctance gradient created by mass transfer through the membrane was deemed to be responsible for the magnetomotive force between the two compartments. Results showed that the rate of diffusion in unstirred solutions depended both on the initial concentration of $NiCl_2$ (and hence on the magnetic susceptibility), and on the square of the magnetic flux density. An increase of 68 % in the diffusion rate was observed in a 1 M solution at 0.82 T. A theoretical model based on the processes of diffusion, free convection and magnetic field induced migration was proposed which provided quantitative agreement with the experimental data. The effect did not persist beyond about 6 minutes of exposure to the field, consistent with the diffusion equation which predicts a decrease in the concentration gradient with respect to time. No magnetic field effect was observed in stirred solutions.

Magnetic field effects on the anodic dissolution of copper into aqueous NaCl/KSCN solution were investigated by Gu et al[24] in 1993. The application of a magnetic field was found to modify the oscillatory behaviour of the anodic current during electrodissolution. The spontaneous periodic oscillations in anodic current at a copper electrode near the Flade potential are due to a feedback reaction cycle of active dissolution, passivation and reactivation. They established the experimental conditions in which the interaction of the field with the anodic potential determines the existence domain of the current oscillations. Both the induction time and the period of oscillation were increased by the application of the field. By applying fractional Brownian motion theory to the current-time transients, two general trends were identified. Firstly, at a given anode potential the degree of disorder increased with increasing magnetic field, and secondly, in a given field the degree of disorder decreased with increasing anode polarisation even though the opposite was the case in zero field.

In 1994, Aogaki et al[25] used his channel electrode cell[12] to determine the effect of magnetic fields of up to 13 T on the electron transfer process during the electrodeposition of copper in acidified copper sulphate solution. No effect of the field was observed on the cathodic Tafel slope, but the exchange current density was drastically reduced (by up to a factor of 4) in the field. The field dependence was found to be $B^{1/3}$ when the reaction was mass transport controlled and $B^{1/4}$ when the reaction is under mixed mass transport and activation control. A hysteresis effect of the field on the electron transfer process was identified. It was suggested that the change in crystal growth mode due to field-induced convection led to a reduction of active growth sites thus decreasing the electron transfer rate.

In 1994, Mori et al[26] investigated the effect of a static magnetic field on the rate of mass transfer during the electroreduction of ferricyanide ions in sodium hydroxide solution. By measuring the limiting current at a platinum electrode oriented at various angles to the applied field, the variation of mass transfer coefficient was determined. The rate of mass transfer was increased by up to a factor of two in a field of 0.3 T. The experimental data were in good correlation with a dimensionless regression equation which included a dimensionless term called the magneto-diffusion factor to account for the magnetic field effect.

The effect of a magnetic field on the pattern formation of two-dimensional metal electrodeposits was investigated by Mogi et al[27,28] in 1994. Such deposits may be grown from ionic solutions in a thin planar cell with a central cathode and a ring anode. The fractal patterns obtained are sensitive to the electrolyte concentration and the applied voltage[29,30]. Using both electroless deposition (Ag and Pb reduced by Zn) and electrodeposition (Zn), the authors found that the growth mode was modified from diffusion-limited aggregation (DLA) in zero field to mixed diffusion/activation control due to the field-induced convection, which changed the growth direction of the branches in fields up to 0.1 T. Above this value, the convection became stronger and the thickness of the diffusion layer was reduced, leading to the formation of more compact patterns. Dendritic growth was suppressed in higher fields, which was attributed to a disturbance of the surface diffusion process by convection, preventing growth units from adhering to steps or kinks.

In 1995, Lee et al[31] studied the voltammetric response of Au and Pt microelectrodes in highly concentrated organic solutions as a function of both field magnitude and orientation. The main advantage of working with microelectrodes is that the effects of convective flow are significantly reduced when the electrode dimensions are comparable to the diffusion layer thickness. Thus it may be possible to observe magnetic field effects that would otherwise be swamped by the effect of the Lorentz force. The limiting current density arising from the electroreduction of nitrobenzene was observed to depend linearly on B at low fields. The dependence of the current enhancement on the angle, $\theta$, between the field direction and the normal to the electrode was sinusoidal, with maxima of 100% at 90° and 270° and minima of -15% at 0° and 180°, in a field of 0.7 T. The authors explained these results in terms of an indirect effect of the field on the diffusional flux of the neutral nitrobenzene molecule as follows. The nitrobenzene molecule (NB) is reduced at the electrode to form the radical anion $NB^-$, which then diffuses away from the surface. When the field is oriented at 90° or 270°, the Lorentz force on the $NB^-$ ions will move them parallel to the electrode surface, decreasing the near surface solution viscosity. This results in an increase in the diffusional transport of NB to the electrode surface. When the field is oriented at 0° or 180°, the radial component of the flux of $NB^-$ will experience a

torsional force, resulting in a cyclotron motion of the ions as they leave the surface. This increases the residence time of the ions near the surface and the resultant increase in the near surface solution viscosity lowers the observed current.

The effect of a magnetic field on the reaction kinetics of electroless nickel deposition on alumina powder was investigated by Lee et al[32] in 1995. Using sodium hypophosphite as a reducing agent and with mechanical agitation to ensure the reaction was under activation control, both the frequency factor and the activation energy were found to decrease in the field. It was suggested that the magnetic field influenced the rephasing of singlet-phased and triplet-phased radical pairs of adsorbed $Ni^{+}$ and H, thus accelerating their recombination. This is one of the few reports in the electrochemical literature which considers the possibility of such a mechanism influencing the kinetics of a heterogeneous reaction.

In 1995, a magnetic field effect on the growth morphology of thallium oxide crystals on a Ti electrode was observed by Kudo et al[33]. X-ray diffraction and SEM showed that the films deposited both in the absence and presence of the field were highly oriented columnar $Tl_2O_3$ - however the effect of the field was to smooth and round the edges of the cube-shaped crystals. This effect was observed in fields ranging from 1.5 - 15 T applied perpendicular to the faradaic current and disappeared in parallel fields. It was suggested that since the reaction was under kinetic control, the magnetohydrodynamic convection parallel to the electrode surface was disturbing surface diffusion rather than mass transport in the diffusion layer.

In 1995, the effect of magnetic field on free convective ion transport was investigated in depth by Kim and Fahidy[34]. The effect of relative field orientation with respect to the direction of free convection was found to be stronger for the $CuSO_4/H_2SO_4$ system than for $K_4Fe(CN)_6/K_3Fe(CN)_6/KOH$ system. This was presumed to be due to weaker free convective forces in the latter system. Mass transfer at the cathode rather than the anode was confirmed to be rate-determining.

The effect of magnetic field on the photoelectrochemical response of a porphyrin-viologen linked modified electrode was investigated by Yonemura et al[35] in 1996. The

increase of anodic photocurrent with field was observed to saturate at about 15 % in fields over 0.3 T. A reaction mechanism was proposed whereby decay of triplet radical pairs photogenerated at the electrode surface was suppressed by the field, leading to an increase in the rate of electron transfer at the interface.

In 1996, Wang et al[36] reported an effect of an applied magnetic field on the anodic dissolution of iron in sulphuric acid solution. In addition to shifting the potential range in which the electrode switched between the active and passive states, the effect of the field was to decrease the period of anodic current oscillations. This was ascribed to an increase in the rate of transport of $H^+$ which causes the local pH fluctuations driving the oscillatory behaviour. When glycerol was added to the solution in order to increase the viscosity the effect was to counteract the influence of the field on mass transport.

The first detailed description of the effect of a static magnetic field on the steady-state voltammetric response at a microelectrode appeared in 1996[37]. Ragsdale et al studied the electroreduction of acetophenone (AP) at Pt and Au microdisk electrodes ($r < 6$ μm) and found that the limiting current could be significantly enhanced or diminished by fields in the range 0.05 T - 1 T. It was established that the current enhancement was proportional to the square of the zero field limiting current, $I_0^2$, which was a strong function of AP concentration and electrode radius. The maximum enhancement in limiting current was observed when the magnetic field was applied parallel to the surface of the electrode. A mechanism was proposed whereby convective flow, generated by the effect of the Lorentz force on the divergent flux of reduced product species $AP^-$, led to an enhancement in mass transport of the neutral species AP.

In 1996, Mogi et al[38] examined the effect of an applied field on the growth of electopolymerised polypyrrole films. They found that the open ramified pattern of the deposit in zero field changed to a dense closed one in a field of 0.5 T. This was believed to be due to the large diamagnetic susceptibility of the aromatic ring perpendicular to the plane of the ring which tends to orient the deposited chains in the presence of a magnetic field. Related effects were observed on the rate of dopant exchange and the redox behaviour of the deposited films.

Mogi et al[39] also showed in 1996 that the application of a magnetic field was found to modify the oscillatory behaviour of the anodic current during the electrodissolution of zinc. The period of oscillation increased from 13.5 seconds in zero field to 31.5 seconds in 1.7 T, while in fields of over 2 T, the oscillation disappeared. The oscillations occur near the transition region between the active and passive states. Rapid dissolution of zinc creates a local reduction in pH which leads to passivation of the electrode (zinc oxide formation). Diffusion of $OH^-$ towards the electrode then increases the local pH causing dissolution of ZnO and reactivating the electrode. From the shape of the current oscillations it was inferred that the magnetic field influences only the active state of the electrode as the current flowing in the passive state is too small. The enhancement in the faradaic dissolution current disturbs the formation of the ZnO layer. In higher fields, this convective effect prevents passivation of the electrode completely.

A numerical solution to the nonlinear convective diffusion problem was devised by Kim and Fahidy[40] in 1996. A staggered grid structure was used to map the velocity and concentration profiles of the electrolyte and the effect of an external magnetic field was represented by additional terms in the ionic flux and momentum equations. In agreement with experimental data, the current density was found to vary according to Eq. 1.48. The authors also applied a low-order ARX approximation to establish discrete time transfer function models for free convective magnetoelectrolysis. They found that three-pole/two-zero configurations provided the optimum compromise between mathematical complexity and experimental correlation.

In 1997, Shannon et al[41] used confocal scanning laser microscopy to examine the surface morphology of electrodeposited nickel. The application of a magnetic field during the electrodeposition process led to a more uniform deposit. The surface uniformity, characterised by the slope (SCF) of the linear portion of the cumulative frequency curve associated with the depth distribution, was observed to increase with increasing magnetic flux density in a horizontal field. When the deposit was made in a vertical field however, a maximum was observed in the SCF ratio in a field of 0.1 T, followed by a minimum at 0.2 T and a subsequent increase in uniformity with

increasing field. These results were explained in terms of competition between gravitational and magnetic forces in a metastable hydrodynamic condition.

In 1997, Ragsdale et al[42] reported the effect of a magnetic field on the limiting current arising from the reduction of nitrobenzene at a vertical Pt microelectrode. The field was applied horizontally at an angle $\varphi$ to the normal of the electrode. A considerable enhancement in limiting current was observed for $\varphi = 90°$ and 270° whereas a small decrease occurred when $\varphi = 0°$ or 180°. It was suggested that convective solution flow near the electrode was initiated by the magnetic force on the electroreduced nitrobenzene ion due to the viscous drag from the solvent and electrolyte ions. This magnetohydrodynamic convection would either increase or decrease the transport rate of the reactant species to the electrode, depending on the direction of the applied field. An analytical expression was developed to express the dependence of the magnetic force per unit volume, F, on the magnitude and direction of the field.

$$F = \frac{I_L |B| (R - r_0) \sin \varphi}{2} \qquad (1.54)$$

where $I_L$ is the limiting current in the absence of field, $r_0$ is the electrode radius and R is a characteristic length over which the magnetic force is acting. Although the choice of R is somewhat arbitrary it leads to a good order of magnitude estimate of the forces responsible for the observed effects. Bearing in mind that the magnetic force falls off as $1/r^2$, R was chosen as the distance at which F has decreased to 1% of its value at the electrode surface, i.e. $10r_0$. The model provided good agreement with the experimental data although it did not predict the slight decrease of the limiting current when the field was applied at angles of 0° and 180°. The authors postulated that the circular solution flow created at these angles reduces the rate of mass transport due to natural convection. A threshold magnetic force of 20 pN for the onset of convection was calculated, above which F increased linearly with field.

In 1997, O'Brien and Santhanam[43] showed that a nonuniform induced magnetic field is created when a magnetic field is applied to an electrolytic cell consisting of two

horizontal parallel electrodes. The depletion of copper ions in the diffusion layer near the cathode and the corresponding increase in copper ion concentration in the anode diffusion layer leads to a difference in paramagnetic susceptibilities between the two regions. A nonuniform induced magnetic field which varies with current density is created and drives the slow rotation of the electrolyte. Laser interferometry was used to monitor the electrolyte concentration between the two electrodes. It was shown the that direction of rotation was opposite for paramagnetic ($Cu^{2+}$) and diamagnetic ($Zn^{2+}$) ions.

The voltammetric response of a microelectrode in a magnetic field was compared to that of a rotating microelectrode by Lee et al[44] in 1997. The effect of an applied field on the voltammetric response corresponding to the reduction of nitrobenzene at Au and Pt microelectrodes was qualitatively similar to that produced by rotating the electrode. The enhancement of limiting current in a field of 0.8 T was found to be equivalent to that obtained by rotating the electrode at about 50 rad/s. The increase in mass transfer coefficient due to the magnetic field induced convective effect was observed to be several orders of magnitude larger than that at a macroscopic electrode, which was ascribed to the considerably larger current density and hence magnetic force per unit volume at a microelectrode. The difference between the pattern of convection obtained by applying a magnetic field and that obtained by rotating the electrode was also noted. Since the flux of electroreduced nitrobenzene ions is radially outward from the electrode, the magnetic force is at all points oriented parallel to the electrode surface (neglecting edge effects). In addition, since the current density is approximately inversely proportional to the distance from the electrode, the magnetic force also falls off as the inverse of distance. This results in a localisation of the magnetic field induced convective effects to the depletion layer. This form of convection is in contrast to that observed at a rotating electrode, where the solution is sucked up towards the electrode and spreads out radially in all directions. Two further observations were made. Firstly, the increase in reaction overpotential in the presence of a magnetic field, manifested in a shift in half-wave potential, was ascribed to the convective transport of charge compensating counterions away from the depletion region, which reduced the driving force for electron transfer. Secondly, the enhancement in limiting current, $|I_B - I_0|$, was

found to be linearly dependent on the magnetic force per unit length at the electrode surface, $I_0B$, above a threshold field required to initiate convection.

In 1997, Cai et al[45] showed that the conductivity of electropolymerised polyaniline films deposited on a Pt electrode was dramatically increased by the application of a magnetic field during the growth process. The upper value of the conductivity for the polyaniline film was increased by a factor of three in a field of 0.7 T applied parallel to the electrode surface. The films exhibited significant anisotropy in conductivity, with only a 30 % increase in conductivity perpendicular to the field direction. The increase in conductivity was ascribed to magnetic orientation and stretching effects of the applied field, leading to a more ordered and compact film with a higher degree of crystallinity, which was confirmed by X-ray diffraction. It would appear that the anisotropy observed in the conductivity was due to the orientation of the aniline radical cation in the field which was also responsible for the increased polaron delocalisation in the film. When rare earth cations were used as charge-compensating dopants, the rate of polymerisation was increased in a field of 0.5 T, while the conductivity of the deposited film was increased by an order of magnitude. The degree of polymer alignment was greater the higher the magnetic moment of the paramagnetic rare earth cation used.

A magnetic field driven electrochemical cell consisting of two iron electrodes in oxygen saturated sodium chloride solution was designed by Shinohara et al[46] in 1998. Oxidation of iron by dissolved oxygen in solution occurs at the thermodynamically determined corrosion potential but since identical electrodes are used the emf is zero in the absence of magnetic field. For an equilibrium process, the potential change is not expected to exceed 0.1 mV in fields of the order of 10 T, but when the electrode is far from equilibrium the magnetic field effect on the metal dissolution rate becomes significant. The field effect on an equilibrium copper/copper sulphate cell was compared with that on the iron/oxygen cell. While the emf of the copper/copper sulphate cell remained at around 0.1 mV in fields up to 6.5 T, the emf of the iron/oxygen cell was observed to increase steadily with applied field up to a value of 8 mV in 6.5 T. This was attributed to an increase in the rate of corrosion of iron in the field. The authors pointed out that although the reaction rate for the cell was too slow

for practical applications, the fabrication of high power cells remains a possibility with the right choice of materials.

In 1998, Ragsdale et al[47] demonstrated that in addition to the Lorentz force, a gradient magnetic force arising from the electrogeneration of paramagnetic species in a nonuniform magnetic field can produce comparable effects on the rate of mass transport. They showed that when a neutral diamagnetic molecule such as nitrobenzene (S = 0) is reduced to form a radical anion (S = 1/2), a thin layer of solution close to the cathode is formed with a gradient in the volume magnetic susceptibility, $\chi$. In the presence of an applied magnetic field, a nonuniform internal field is induced so that a gradient force $F_B$ is generated in the diffusion layer.

$$F_B = \frac{\chi}{\mu_0}(B \cdot \nabla B) \tag{1.55}$$

where $\mu$ is the magnetic permeability of the diffusion layer. This force drives convection in the cell and leads to similar enhancements in limiting current to those observed under the influence of the Lorentz force. The increase in limiting current was observed to be proportional to $F_B$. The relative magnitudes of the two forces were found to be independent of solution conditions to a zero-order approximation. When the magnetic field is applied parallel to the electrode surface the two forces are comparable in magnitude, whereas $F_L$ is negligibly small in comparison to $F_B$ when the field is perpendicular to the electrode surface. The authors suggested that electrochemical reactions could be controlled by varying the susceptibilities of the redox species and the uniformity of the applied field.

A semiempirical relationship between the limiting current and the various parameters, including magnetic field, which control mass transport in solution was established by Leventis et al[48] in 1998. Using a range of solvents and compounds to examine the effect, the limiting current, $I_L$, was found to vary according to:

$$I_L = (4310)n^{f+1}FA^{3/4}B^{1/3}D\nu^{-1/4}c_\infty^{4/3} \quad (1.56)$$

where $f > 0$. The authors noted that the magnetic field effect on convection must result from magnetic forces on all ions, including those produced by ionisation of the supporting electrolyte. They suggested that the supporting electrolyte may play a significant role in the momentum transfer to solvent molecules.

In 1998, Devos et al[49,50] investigated an electrochemical reaction under purely kinetic control, the electrodeposition of nickel on titanium from a Watts bath. The application of a magnetic field led to preferential formation of the <211> texture over the <100> orientation. The quality of the <211> texture increased with the intensity of the applied magnetic field. The magnitude of the field effect on the current density increased from a reduction of a few percent with no organic inhibitor present to 25 % reduction in the presence of the organic inhibitor 2-butyne-1,4-diol. Rather than a direct effect on the electron transfer process at the electrode/electrolyte interface, the authors suggested that the field acts indirectly on nickel electrodeposition through its effect on mass transport of inhibiting species and hydrogen evolution. The magnetic field also produced a dramatic change in the appearance of bubble tracks on the nickel surface, which arise as a consequence of hydrogen evolution. In quiescent solution and zero field the tracks were spherical but in the presence of forced convection due to the Lorentz force, the tracks formed with long tails normal to the direction of the applied field. SEM images showed that these tails were narrow depressions in the nickel which were accompanied by an overthickness at the opposite side of the bubble pit. These observations were explained in terms of a turbulent drag in the wake of the bubble in the magnetohydrodynamically induced convective flow of electrolyte which enhances transport of inhibiting species to the electrode surface. Electrochemical impedance measurements showed that the magnetic field had no effect on the charge transfer coefficient at the interface.

In 1998, Mizuseki et al[51] used a Monte Carlo model to simulate crystal growth from solution under diffusion-limited aggregation (DLA). The effect of the Lorentz force

was incorporated as a random walk with different transition probabilities in each direction. The results obtained were qualitatively similar to those observed experimentally by Mogi et al[27,28].

Nakabayashi et al[52] reported in 1998 that during electrodeposition of silver-antimony alloy, long-range spatial patterns were formed on the surface of a copper electrode. The patterns consisted of small spiral waves and wide bands rather like wind formations in sand. When a magnetic field was applied during the electrodeposition, the propagation direction of the bands was altered. Results suggested that the formation of these patterns was strongly linked to the electrolyte flow close to the surface of the electrode. The authors proposed that the preferential deposition rate of antimony around clusters of previously deposited antimony, coupled to the electrolyte flow, produced the observed patterns. The effect of the field was then to change the convective flow, thus altering the pattern formation. The process was termed flow-induced electrochemical instability.

An interaction mechanism for the effect of a magnetic field on electrochemical processes occuring at a ferromagnetic electrode immersed in a paramagnetic solution was proposed by Waskaas and Kharkats[53] in 1999. The open circuit potential of the $Fe^{3+}/Fe^{2+}$ system was shifted to more positive values by the application of the field, while those of $Ni^{2+}/Ni$ and $Co^{2+}/Co$ were shifted to more negative values. This effect could only be observed with ferromagnetic electrodes. The field effect was attributed to transport of all ions in solution due to a gradient in the magnetic susceptibility in the solution close to the electrode surface. The direction of this ionic flux was away from the electrode surface, resulting in a change in the rate of reaction at the electrode. The authors proposed that the pertinent magnetic driving force, $F_P$, to be included in the Navier-Stokes equation should then be:

$$F_P = \frac{B^2 \chi_m}{2\mu_0} \nabla c \qquad (1.57)$$

where $\mu_0$ is the permeability of free space and $\chi_m$ is the paramagnetic molar susceptibility. Considering the case of corrosion of an iron electrode in a solution of $CoSO_4$, the limiting corrosion current was found to vary as $B^2$ in low fields and linearly with B at high fields. The authors termed this effect the magnetoconvective effect and suggested that its magnitude is greater than the effect of the Lorentz force under these conditions.

The effect of a magnetic field on the corrosion of copper in nitric acid was investigated by Shinohara and Aogaki[54] in 1999. They reported that the corrosion rate in 3 M nitric acid was reduced by a factor of three in a field of 10 T. However, the field caused an acceleration in the corrosion rate at low nitrate concentrations. The localised processes of oxidation of copper and reduction of the nitrate ion give rise to circulating currents flowing on the scale of a few microns. The authors postulated that the Lorentz force on these currents gives rise to a micro-magnetohydrodynamic effect, which produces convection on this scale. Depending on whether the local anodic or cathodic process is rate-determining, the corrosion rate may be accelerated or reduced.

Leventis and Gao[55] reported in 1999 that the limiting current resulting from the reduction of various organic compounds at a Au electrode was proportional to $n^{3/2}$. They were thus able to present the following modified version of Eq. 1.56 for the limiting current at an electrode whose surface is oriented parallel to an applied field:

$$I_L = (431)n^{3/2}FA^{3/4}B^{1/3}D\nu^{-1/4}c_\infty^{4/3} \qquad (1.58)$$

The nonlinearity in n was ascribed to a feedback mechanism whereby, larger faradaic currents give rise to more vigorous stirring in the field, which in turn increases the diffusion limited current. The authors considered their empirical analysis complete and found it unlikely that any further variables were contained in the numerical constant of Eq. 1.58.

In 1999, Kishioka et al[56] used steady state voltammetry with a microdisk electrode to study the magnetic field effect on the dissolution rate of atmospheric oxygen in water. The concentration of dissolved oxygen in aqueous solution with tetraetylammonium perchlorate as supporting electrolyte was obtained by measuring the limiting current arising from the 4-electron reduction of oxygen. The rate of dissolution was observed to increase steadily with increasing field. The effect of the Lorentz force on the solution convection was believed to be responsible for this effect. For magnetic fields above 4 T, this increase in dissolution rate became more dramatic as field-induced convection of the air above the solution occurred. This was confirmed when a cotton pad was placed above the cell to eliminate convection of the air and the effect was removed.

In 1999, Grant et al[57] described how the magnetisation of a ferromagnetic electrode could be used to focus the flux of paramagnetic molecules towards the electrode surface. The non-uniform field close to the electrode surface generates a gradient magnetic force given by Eq. 1.55. Paramagnetic ions will be drawn into this field, while diamagnetic ions will be repelled. The reduction of nitrobenzene at Pt, Fe and Ni microelectrodes was investigated using cyclic voltammetry. Whereas a 110% increase in limiting current was observed at a Pt microelectrode in a field of 1 T, reductions of 48% and 43% in $I_L$ were observed at the Fe and Ni electrodes respectively. Video micrographs showed that the flux of the red nitrobenzene radical anion was tightly focused at the Fe and Ni electrodes, in contrast to the vortex flow pattern observed at the Pt electrode. From the suppression of the vortex flow pattern at the ferromagnetic electrodes, the authors inferred that at these dimensions the magnitude of the field gradient force is larger than that of the Lorentz force.

Results obtained using a magnetic impedance method[20] for the characterisation of electrochemical processes were presented by Devos et al[58] in 1999. The authors claimed that magnetic transfer function measurements on zinc and nickel electrodeposition showed that the effect of magnetic fields on surface processes such as adsorption, which determine texture and morphology, originate from the influence of magnetohydrodynamic convection on the flux of inhibiting species.

In 1999, Bodea et al[59] reported the effect of a magnetic field on the pattern formation of iron electrodeposits in a thin planar cell with a central copper cathode and a copper ring anode. The application of a field of 0.2 T in the plane of the cell resulted in a change of morphology from radial to rectangular, with one edge of the rectangle parallel to the field. No such effect was observed for zinc electrodeposits. The explanation put forward is that the observed aggregate results from a minimisation of the magnetic dipolar energy under the constraints of the crystalline anisotropy. The rectangular shape could then result from slight growth differences parallel and perpendicular to the field. The authors draw a parallel between the morphology symmetry breaking in the field and the symmetry breaking associated with an order-disorder phase transition.

In 2000, Devos et al[60] used impedance spectroscopy to evaluate the magnetic field effect on the kinetics of several different electrochemical systems. Three different types of system were investigated - those under mass transport control, those under activation control and mixed control systems. In all three types of system, the charge transfer coefficients were unaffected by fields of up to 1 T. The only weak magnetic field effects observed were ascribed either to changes in the electrode area during electrodeposition or electrodissolution, or indirect effects of magnetohydrodynamic convection.

Olivier et al[61] recently showed that the effect of a magnetic field on the limiting current is equivalent to that produced by the application of a tangential electric field, $E_{\parallel}$, close to the electrode surface. Such an electric field may be created by the use of a non-equipotential working electrode or by the application of a magnetic field parallel to the electrode surface. An electrokinetic force, $F_E$:

$$F_E = \sigma_d E_{\parallel} \qquad (1.59)$$

on the charge density, $\sigma_d$ ($C/m^2$), in the diffuse double layer induces a tangential convection which is transmitted to the bulk solution via viscous forces. The authors proposed that this force could account for the experimentally observed field effects.

The general features of the various data reported in the literature are summarised in Table 1.2.

In summary, research into magnetic field effects on electrochemical reactions has diversified over the last few years. While earlier reports generally focused on the magnetohydrodynamic convection induced by the Lorentz force, the field effects are now being studied in more detail under a wider range of conditions, and several new ideas have emerged, notably the magnetic gradient forces and the electrokinetic force. The use of microelectrodes and impedance spectroscopy has opened up new areas of interest in these effects. The effect of the field on the electrode kinetics is still a matter of debate, while effects on morphology have not been investigated in any great depth. The aim of this work was to examine in detail the effect of a magnetic field on a well known electrochemical system ($Cu^{2+}/Cu$) in order to shed further light on the phenomenon.

*Table 1.2: Summary of magnetic field effects in the literature.*

| Property | Field effect | Explanation | References |
|---|---|---|---|
| Mass transport | Limiting current at conventional electrode increased | Lorentz force | 11, 13, 17, 20, 22, 48 |
| | | Paramagnetic force | 43 |
| | | Gradient force | 10, 15 |
| | | Electrokinetic force | 61 |
| | Limiting current at microelectrode increased / decreased | Lorentz force<br>Gradient force | 31, 37, 42<br>47, 57 |
| | Limiting current varies as $B^{1/3}c^{4/3}$ | Lorentz force | 13, 20, 48 |
| Electron transfer kinetics | Exchange current density increased | Lorentz force<br>Singlet / triplet recombination | 14<br>32 |
| | Exchange current density decreased | Change in crystal growth | 25 |
| | Exchange current density unchanged | None | 22 |
| | Charge transfer coefficients unchanged | None | 22, 25 |
| Morphology | Crystal growth mode changed | Lorentz force | 33 |
| | Surface morphology altered | Lorentz force | 41, 49, 50 |
| | Fractal growth patterns modified | Lorentz force | 27, 28 |
| Chemical equilibrium | Rest potential increased / decreased | Paramagnetic force | 53 |
| | Rest potential unchanged | None | 8, 9 |

## References


1 A.J. Bard and L.R. Faulkner, *Electrochemical Methods, Fundamentals and Applications*, John Wiley & Sons, New York, 1980.

2 C.M.A. Brett and A.M.O. Brett, *Electrochemistry, Principles, Methods, and Applications*, Oxford University Press, Oxford, 1993.

3 D.T. Sawyer, A. Sobkowiak and J.L. Roberts Jr., *Electrochemistry for Chemists*, John Wiley & Sons, New York, 1995.

4 C.H. Hamann, A. Hamnett and W. Vielstich, *Electrochemistry*, Wiley-VCH, Weinheim, 1998.

5 V.G. Levich, *Physicochemical Hydrodynamics*, Prentice-Hall, Englewood Cliffs, N.J., 1962.

6 P.C. Andricacos, C. Uzoh, J.O. Dukovic, J. Horkans and H. Deligianni, IBM J. Res. Develop., **42**, 567 (1999).

7 M. Faraday, *Diary*, Bell & Sons, Vol. IV 288, pp. 7706-21, 1933.

8 T.Z. Fahidy, J. Appl. Electrochem., **13**, 553 (1983).

9 R.A. Tacken and L.J.J. Janssen, J. Appl. Electrochem., **25**, 1 (1995).

10 S. Mohanta and T.Z. Fahidy, Can. J. Chem. Engng., **50**, 248 (1972).

11 T.Z. Fahidy, Electrochim. Acta, **18**, 607 (1973).

12 R. Aogaki, K. Fueki and T. Mukaibo, Denki Kagaku, **43**, 504 (1975).

13 R. Aogaki, K. Fueki and T. Mukaibo, Denki Kagaku, **43**, 509 (1975).

14 E. Kelly, J. Electrochem. Soc., **124**, 987 (1977).

15 S. Mohanta and T.Z. Fahidy, J. Appl. Electrochem., **8**, 265 (1978).

16 J. Hubbard and P. Wolynes, J. Chem. Phys., **75**, 3051 (1981).

17 C. Iwakura, T. Edamoto and H. Tamura, Denki Kagaku, **52**, 596;654 (1984).

18 R. Aogaki and K. Fueki, J. Electrochem. Soc.,**131**, 1295 (1984).

19 V. Noninski and C. Noninski, Elek. Obra. Mat., **6**, 50 (1986).

20 O. Aaboubi, J.-P. Chopart, J. Douglade, A. Olivier, C. Gabrielli and B. Tribollet, J. Electrochem. Soc., **137**, 1796 (1990).

21 T.Z. Fahidy, Electrochim. Acta, **36**, 1907 (1991).

22 J.-P. Chopart, J. Douglade, P. Fricoteaux and A. Olivier, Electrochim. Acta, **36**, 459 (1991).

[23] M. Waskaas, J. Phys. Chem., **97**, 6470 (1993).

[24] Z.H. Gu, J. Chen, A. Olivier and T.Z. Fahidy, J. Electrochem. Soc., **140**, 408 (1993).

[25] R. Aogaki, T. Negishi, M. Yamato, E. Ito and I. Mogi, Physica B, **201**, 611 (1994).

[26] S. Mori, K. Satoh and A. Tanimoto, Electrochim. Acta, **39**, 2789 (1994).

[27] I. Mogi, M. Kamiko, S. Okubo and G. Kido, Physica B, **201**, 606 (1994).

[28] I. Mogi and M. Kamiko, J. Cryst. Gr., **166**, 276 (1996).

[29] M. Matsushita, M. Sano, Y. Hayakawa, H. Honjo and Y. Sawada, Phys. Rev. Lett., **53**, 286 (1984).

[30] D. Grier, E. Ben-Jacob, R. Clarke and L.M. Sander, Phys. Rev. Lett., **56**, 1264 (1986).

[31] J. Lee, X. Gao, L.D.A. Hardy and H.S. White, J. Electrochem. Soc., **142**, L90 (1995).

[32] C.-C. Lee and T.-C. Chou, Electrochim. Acta, **40**, 965 (1995).

[33] S. Kudo and I. Mogi, Denki Kagaku, **63**, 238 (1995).

[34] K. Kim and T.Z. Fahidy, J. Electrochem. Soc., **142**, 4196 (1995).

[35] H. Yonemura, K. Ohishi and T. Matsuo, Chem. Lett., 661 (1996).

[36] C. Wang, S. Chen and X. Yu, J. Electrochem. Soc., **143**, L283 (1996); C. Wang, S. Chen and H. Ma, J. Electrochem. Soc., **145**, 2214 (1998); C. Wang and S. Chen, Electrochim. Acta, **43**, 2225 (1998).

[37] S.R. Ragsdale, J. Lee, X. Gao and H.S. White, J. Phys. Chem., **100**, 5913 (1996).

[38] I. Mogi, Chem. Lett., 53;419 (1996).

[39] I. Mogi, H. Kikuya, K. Watanabe, S. Awaji and M. Motokawa, Chem. Lett., 673 (1996).

[40] K. Kim and T.Z. Fahidy, Appl. Math. Modelling, **10**, 379 (1996).

[41] J.C. Shannon, Z.H. Gu and T.Z. Fahidy, J. Electrochem. Soc., **144**, L314 (1997).

[42] S.R. Ragsdale, J. Lee and H. White, Anal. Chem., **69**, 2070 (1997).

[43] R.N. O'Brien and K.S.V. Santhanam, J. Appl. Electrochem., **27**, 573 (1997).

[44] J. Lee, S.R. Ragsdale, X. Gao and H.S. White, J. Electroanal. Chem., **422**, 169

(1997).

[45] L. Cai, S. Yao and S. Zhou, Synthetic Metals, **88**, 205 (1997).

[46] K. Shinohara and R. Aogaki, Chem. Lett., 1223 (1998).

[47] S.R. Ragsdale, K.M. Grant and H.S. White, J. Am. Chem. Soc., **120**, 13461 (1998).

[48] N. Leventis, M. Chen, X. Gao, M. Canalas and P. Zhang, J. Phys. Chem. B, **102**, 3512 (1998).

[49] O. Devos, A. Olivier, J. Chopart, O. Aaboudi and G. Maurin, J. Electrochem. Soc., **145**, 401 (1998).

[50] O. Devos, O. Aaboudi, J-P. Chopart, E. Merienne, A. Olivier and J. Amblard, J. Electrochem. Soc., **145**, (1998).

[51] H. Mizuseki, K. Tanaka, K. Kikuchi, K. Ohno and Y. Kawazoe, Comp. Mat. Sci., **10**, 46 (1998).

[52] S. Nakabayashi, I. Kratsev, R. Aogaki and K. Inokuma, Chem. Phys. Lett., **294**, 204 (1998).

[53] M. Waskaas and Y.I. Kharkats, J. Phys. Chem. B, **103**, 4876 (1999).

[54] K. Shinohara and R. Aogaki, Electrochemistry, **67**, 126 (1999).

[55] N. Leventis and X. Gao, J. Phys. Chem. B, **103**, 5832 (1999).

[56] S.Y. Kishioka and R. Aogaki, Chem. Lett., 91 (1999).

[57] K.M. Grant, J.W. Hemmert and H.S. White, Electrochem. Comm., **1**, 319 (1999).

[58] O. Devos, O. Aaboubi, J.-P. Chopart, E. Merienne and O. Olivier, Electrochemistry, **67**, 180 (1999).

[59] S. Bodea, L. Vignon, R. Ballou and P. Molho, Phys. Rev. Lett., **83**, 2612 (1999).

[60] O. Devos, O. Aaboubi, J.-P. Chopart, A. Olivier, C. Gabrielli and B. Tribollet, J. Phys. Chem. A, **104**, 1544 (2000).

[61] A. Olivier, J.-P. Chopart, J. Amblard, E. Merienne and O. Aaboubi, Models in Chemistry, **137**, 213 (2000).

# Chapter Two

# Experimental Methods

## 2.1 Electrochemical cell

A standard three electrode electrochemical cell was used in all of the electrochemical experiments in this work. A schematic diagram of such a cell is shown in Fig. 2.1.

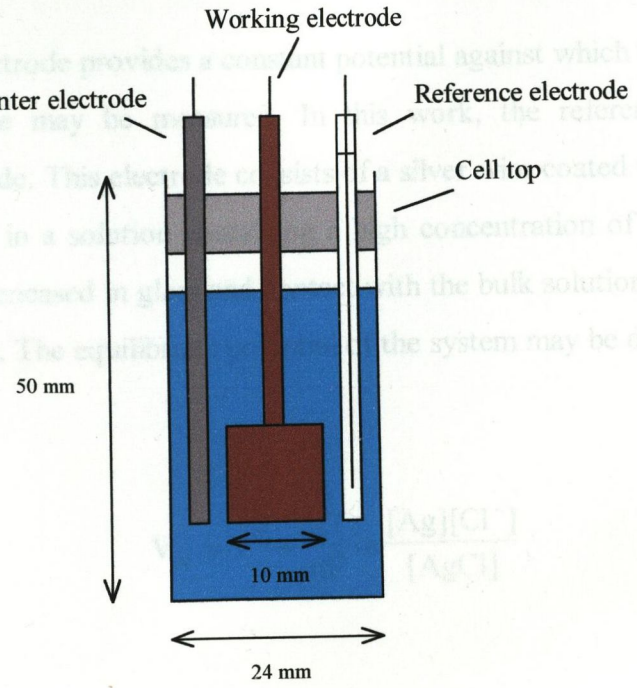


*Fig. 2.1: Schematic diagram of a three electrode electrochemical cell.*

The working electrode defines the interface under investigation and may act either as a cathode or an anode depending on the applied overpotential. The choice of electrode material for a particular application depends on a number of factors. In general, the electrode should not react chemically with the solvent or the supporting electrolyte within the potential range of the experiment. In addition, if the material is too porous, the electrode may become contaminated. Inert metals such as platinum, silver and gold are commonly used in electrochemical experiments. One advantage of working with metallic electrodes is that their high conductivity results in negligible background currents. Other advantages include ease of construction and polishing of such

electrodes. Another commonly used electrode is the glassy carbon electrode. Glassy carbon is formed by heating phenol/formaldehyde polymers or polyacrylonitrile between 1000°C and 3000°C under pressure. Due to its hardness and fragility, electrode construction is difficult, but it may be polished to a mirror finish and electrodeposited layers may be readily removed for analysis. Copper, platinum and glassy carbon were used as working electrodes in this work.

The reference electrode provides a constant potential against which the potential of the working electrode may be measured. In this work, the reference electrode was silver/silver chloride. This electrode consists of a silver wire coated with a porous layer of silver chloride in a solution containing a high concentration of chloride ions. The entire solution is encased in glass and contact with the bulk solution is made through a porous Vycor frit. The equilibrium potential of the system may be determined from the Nernst equation:

$$V_{eq} = V^{0'} + \frac{RT}{nF} \ln \frac{[Ag][Cl^-]}{[AgCl]} \qquad (2.1)$$

Both [Ag] and [AgCl] are unity, since they are pure solids, hence the equilibrium potential depends only on the chloride ion concentration. If this is constant, a reliable reference potential will be maintained. Two different reference electrodes were used during the course of this work - Ag/AgCl (saturated KCl) and Ag/AgCl (3 M NaCl). Both exhibited good stability in the potential range employed. The standard reduction potential of the Ag/AgCl electrode relative to the redox couple $Cu^{2+}/Cu$ is - 0.12 V (Table 1.1).

The counter, or auxiliary, electrode is used to pass current through the cell in order to avoid any polarisation of the reference electrode which might affect the stability of its potential. The surface area of the counter electrode should be greater than that of the working electrode to ensure that the potential distribution is uniform at the working electrode. Counter electrodes used in this work were copper, platinum and graphite.

The electrolyte in all the experiments described in this work was copper (II) sulphate. Solutions of various concentrations were prepared in triply distilled water using anhydrous $CuSO_4$ (98.5 %). The supporting electrolyte was either $H_2SO_4$ or $Na_2SO_4$. These solutions were prepared in triply distilled water from standard concentrated $H_2SO_4$ (95 %) or anhydrous $Na_2SO_4$ (98 %). The pH was adjusted by the addition of $H_2SO_4$. Glycerol (98 %) was used to increase the viscosity of the electrolyte. All solutions were air saturated and no precautions were taken to remove dissolved oxygen.

## 2.2 Electrode construction and preparation

Copper working electrodes were constructed from 1.5 mm copper plate by two different methods. In the first method, a copper wire was spot welded to the back of a rectangular piece of copper plate, typically of dimensions 1 cm x 1 cm. The back and sides of the electrode and the wire were then encased in epoxy, leaving the working area of the electrode exposed. In the second method, a small hole was drilled near the edge of the plate and a copper wire was inserted and soldered in place before sealing in epoxy.

Before each experiment the Cu electrodes were prepared by polishing with fine grain sandpaper, rinsing with 2 M $H_2SO_4$ and then with triply distilled water. This process was then repeated and the electrodes were left to equilibrate in the solution in which the electrochemical experiment was to take place.

The platinum and glassy carbon working electrodes were manufactured by BAS. Each electrode consisted of a metal cylinder embedded in an insulating Kel-F sheath with electrical contact made through a brass rod. The disk diameters were 3 mm (glassy carbon) and 2 mm (Pt).

These electrodes were prepared by polishing with 0.3 μm alumina to a mirror finish before rinsing with triply distilled water. The electrodes were then placed in an ultrasonic bath to remove any particles of abrasive from the polishing process. Finally, they were left to equilibrate in the solution in which the electrochemical experiment was to take place.

## 2.3 Potentiostat/Galvanostat

With the improvement in the quality and performance of electronic components, electrochemical instrumentation has developed considerably in recent years, allowing far greater accuracy and precision in both the control and measurement of electrochemical parameters, as well as lower electrical noise levels and the capability of measuring much smaller currents. An instrument that controls the working electrode potential while measuring the current response is known as a potentiostat. Conversely, an instrument that controls the current passed by the working electrode while measuring the potential is called a galvanostat. At present, both analogue and digital instrumentation are used for these purposes, although with the development of more powerful microprocessors, digital instrumentation is beginning to supersede analogue.

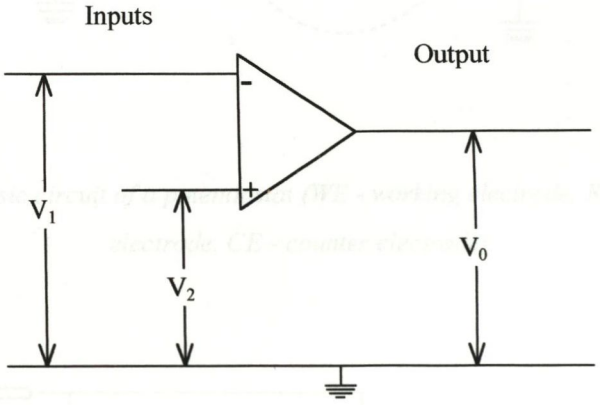


*Fig. 2.2: Operational amplifier (OA).*

The basis of analogue instrumentation is the operational amplifier (OA), a versatile integrated circuit with two inputs and one output (Fig. 2.2). An ideal OA has infinite input impedance, zero current consumption and infinite gain. Real OAs have input impedances of 1 MΩ and upwards, current consumption in the nA to pA range and gains between $10^4$ and $10^8$. By introducing various forms of feedback from output to input it is possible to perform a variety of functions using an OA. Simple potentiostat

and galvanostat circuits are shown in Fig. 2.3 and Fig. 2.4 respectively. Under galvanostatic control, a reference electrode is not required unless the potential has to be measured. Note that these circuits require a finite time to settle after a voltage step, of the order of 100 μs, which may be important for transient techniques. In most potentiostats the working electrode is grounded and the potential at the counter and reference electrodes is varied. However, it is possible for the working electrode to function with a floating voltage if required for a particular application.

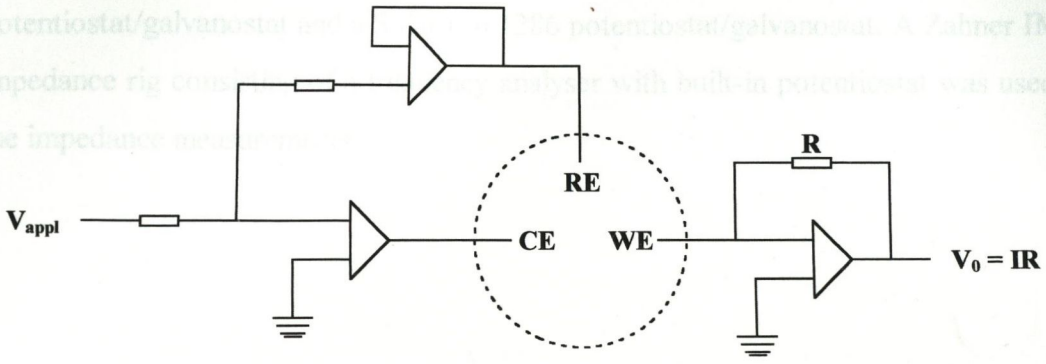


*Fig. 2.3: Basic circuit of a potentiostat (WE - working electrode, RE - reference electrode, CE - counter electrode).*

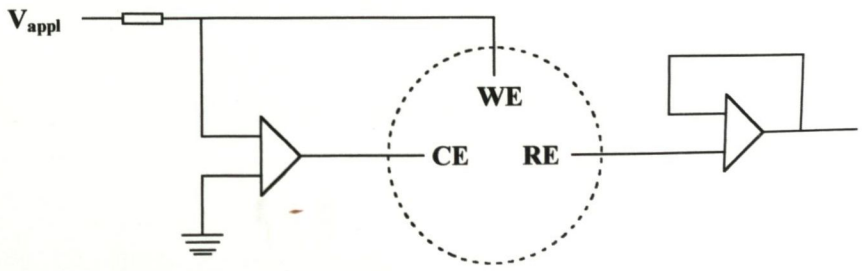


*Fig. 2.4: Basic circuit of a galvanostat (WE - working electrode, RE - reference electrode, CE - counter electrode).*

Analogue instruments may either record their data on an X-Y plotter or via an ADC to a computer hard drive. Most modern instruments are digitally controlled, either by

their own microprocessor or externally by a PC. Since digital instruments operate at discrete rather than continuous points, any change in the applied potential will be in steps. Thus a linear sweep will appear as a staircase instead of a continuous ramp. This is not such a problem for modern 32-bit microprocessors, which can make the step increment so small that there is no practical difference between the analogue and digital signals.

Four different instruments were used to control the electrochemical experiments in this work - a BAS CV-50W potentiostat, a BAS 100B potentiostat, an EG&G Model 273 potentiostat/galvanostat and a Solartron 1286 potentiostat/galvanostat. A Zahner IM-6 impedance rig consisting of a frequency analyser with built-in potentiostat was used in the impedance measurements.

## 2.4 Rotating disk electrode

The rotating disk electrode consists of a metallic electrode, encased in an insulating sheath, which may be rotated about its own axis in a fluid. Electrical contact is made via brushes in the shaft of the electrode body. The velocity profile at such an electrode is well defined, so that solution of the convective diffusion equation is made possible. Essentially the fluid is flung radially outwards by the centrifugal force and fresh solution is sucked up from below to produce the flow pattern shown in Fig. 2.5.

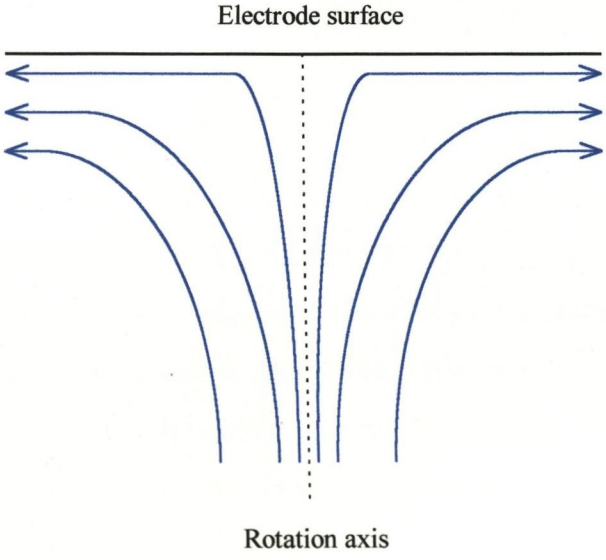


*Fig. 2.5: Streamlines at a rotating disk electrode.*

The rotating disk electrode is an example of a hydrodynamic system, where the rate of mass transport may be significantly increased by forced convection. It is commonly used to determine kinetic parameters as mass transport effects may be neglected at high rotation rates (> 1000 rpm).

The system used in this work was a BAS RDE-1 Rotating Disk Electrode, capable of rotating at up to 10,000 rpm. The glassy carbon electrode itself (diameter 3 mm) could be removed from the rotating shaft for either polishing or analysis. A silver/silver

chloride reference electrode and a platinum counter electrode were used with this system.

## 2.5 Microelectrodes

A microelectrode may be defined as an electrode with dimensions of the order of a few microns. Microelectrodes exhibit high current densities and low total currents and their small surface area means that their capacitance is many times lower than that of conventional electrodes. However, it is the diffusional behaviour at a microelectrode that makes it especially useful for most electrochemical applications, especially transient techniques. At an electrode of any size, under conditions of planar diffusion, the thickness of the diffusion layer increases with time according to:

$$\delta = \sqrt{\pi Dt} \tag{2.2}$$

If the diffusion layer thickness becomes comparable to the dimensions of the electrode, spherical diffusion will set in. Under these conditions the volume of solution from which the electroactive material is being drawn will be extremely large in proportion to the active area of the electrode and a steady-state current will result. At conventional electrodes, natural convection disturbs the planar diffusion long before the steady-state is reached. However, at a microelectrode the steady-state is reached very quickly. For example, according to Eq. 2.2, a 10 μm microelectrode in an electrolyte with $D = 10^{-9}$ $m^2/s$ will exhibit a steady-state response after about 30 ms. The high rate of diffusion in the steady-state results in higher sensitivities and means that effects of natural and even forced convection may be negligible.

Platinum microelectrodes of various dimensions were used in this work. These were manufactured by BAS and consisted of fine Pt wires, of diameter 7 - 32 μm, sealed in glass and ground to a disk surface. These electrodes were prepared in the same way as the conventional platinum and glassy carbon electrodes. However, the voltammetric experiments using these microelectrodes were carried out in a Faraday cage in order to eliminate electrical noise as the observed currents were below 1 μA in magnitude. A BAS PA-1 Pre-Amplifier was used to amplify the current to a measurable level.

## 2.6 Application of a magnetic field

The magnetic field was applied to the working electrode by placing the entire cell in the bore of a permanent magnet. The magnetic field was applied parallel to the electrode surface unless otherwise stated. Two different sources of magnetic field were employed in this work - a Magnetic Solutions HC-500-54 Halbach cylinder and a Magnetic Solutions MM-1000-48 Multimag. The Halbach cylinder was a $Nd_2Fe_{17}B$ magnet with a fixed static field of 0.5 T transverse to the bore. The bore diameter was 54 mm. The Multimag system consisted of two nested Halbach cylinders which could be rotated relative to one another by stepper motors to produce a variable static field in the range 0 - 1 T. The bore diameter of the Multimag was 48 mm. The field could be oriented in any azimuthal direction relative to the cell. The field homogeneity was below 1% in 1 cm parallel to the bore and the maximum field gradient in the volume occupied by the cell was 2 T/m. The high field experiments were carried out by F.E. Spada and J.M.D. Coey at the National High Magnetic Field Laboratory in Tallahassee, Florida. In these experiments a superconducting magnet was used to apply axial fields of up to 6 T to the cell, mounted in its 60 mm bore. Some data were also collected in a 2 T electromagnet.

# Chapter Three

## Magnetic field effects on the voltammetric behaviour of $Cu^{2+}/Cu$

## 3.1 Linear sweep voltammetry

Linear sweep voltammetry is a well established and versatile electrochemical technique. The potential of the working electrode in an electrolytic cell is varied at a fixed rate from an initial value to a final value and the current response is measured. The resulting I-V plot is known as a voltammogram. A great deal of electrochemical information may be gleaned from analysis of such plots. A typical voltammogram for a copper working electrode in acidified copper sulphate solution is shown in Fig. 3.1.

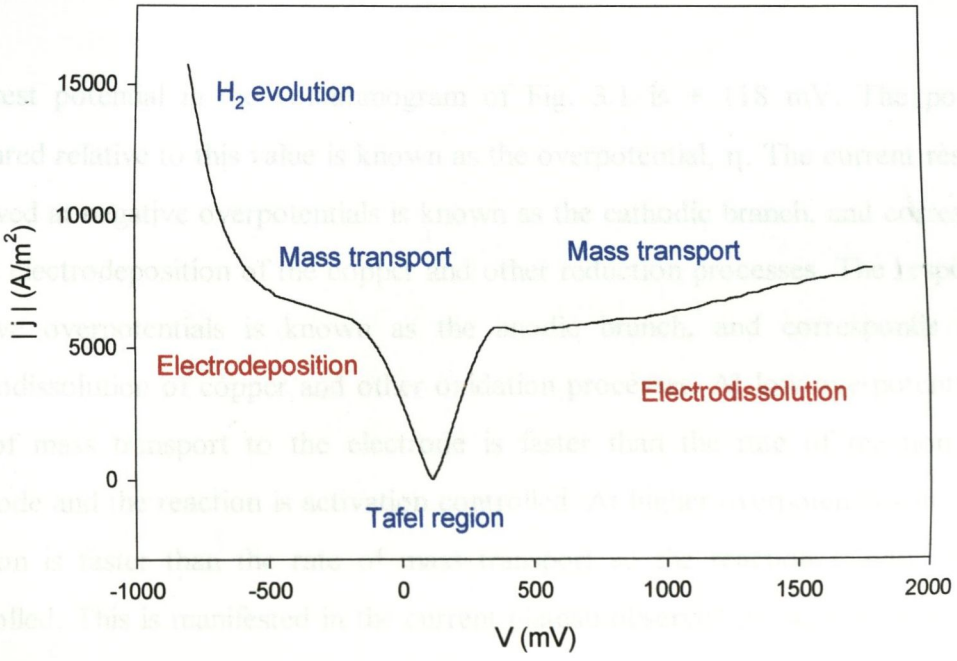


*Fig. 3.1: Voltammogram for the electrolysis of copper in acidified copper sulphate solution (vs Ag/AgCl). $[Cu^{2+}] = 0.75$ M and pH = 0.5.*

The rest potential of the system is the potential at which the current is zero. Here both anodic and cathodic reactions are taking place at the working electrode at equal rates. The rest potential is determined experimentally by measuring the open circuit potential of the cell. All potentials in this work are measured relative to the silver/silver chloride electrode. The difference between the standard reduction potentials of $Cu^{2+}/Cu$ and

that of AgCl/Ag,$Cl^-$ is, from Table 1.1, 0.34 V - 0.22 V = + 120 mV. When the $Cu^{2+}$ concentration is 1 M, the rest potential, $V_{eq}$, should be close to this value. The Nernst equation (Eq. 1.8) describes how the rest potential varies with concentration. For the $Cu^{2+}$/Cu system, this corresponds to:

$$V_{eq} = V^{0'} + (13mV)\ln[Cu^{2+}] \tag{3.1}$$

At lower concentrations, the rest potential becomes more negative. According to Eq. 3.1, the rest potential for a 0.005 M solution of $CuSO_4$ decreases to + 52 mV with respect to silver/silver chloride.

The rest potential in the voltammogram of Fig. 3.1 is + 118 mV. The potential measured relative to this value is known as the overpotential, $\eta$. The current response observed at negative overpotentials is known as the cathodic branch, and corresponds to the electrodeposition of the copper and other reduction processes. The response at positive overpotentials is known as the anodic branch, and corresponds to the electrodissolution of copper and other oxidation processes. At low overpotentials the rate of mass transport to the electrode is faster than the rate of reaction at the electrode and the reaction is activation controlled. At higher overpotentials the rate of reaction is faster than the rate of mass transport so the reaction is now diffusion controlled. This is manifested in the current plateau observed on both branches of the voltammogram. In aqueous solution, hydrogen evolution due to the reduction of either water molecules or hydronium ions occurs at more negative overpotentials. This appears on the voltammogram as a sharp increase in current on the end of the cathodic branch.

In this work, anodic currents are considered positive and cathodic currents negative, in line with the European convention. It should be noted that this is opposite in polarity to the U.S. convention. Hence care must always be taken when examining data from other sources, although it is usually clear from the context which convention is in use.

## 3.2 Magnetic field effects on mass transport

The effect of a static magnetic field on the electrochemical behaviour of the redox couple $Cu^{2+}/Cu$ was investigated using linear sweep voltammetry. The effect of fields in the range 0 - 1 T on the voltammogram for a copper working electrode in 0.75 M $CuSO_4$ at pH 0.5 is shown in Fig. 3.2. In each case, the potential was swept from the rest potential to - 500 mV at a sweep rate of 20 mV/s.

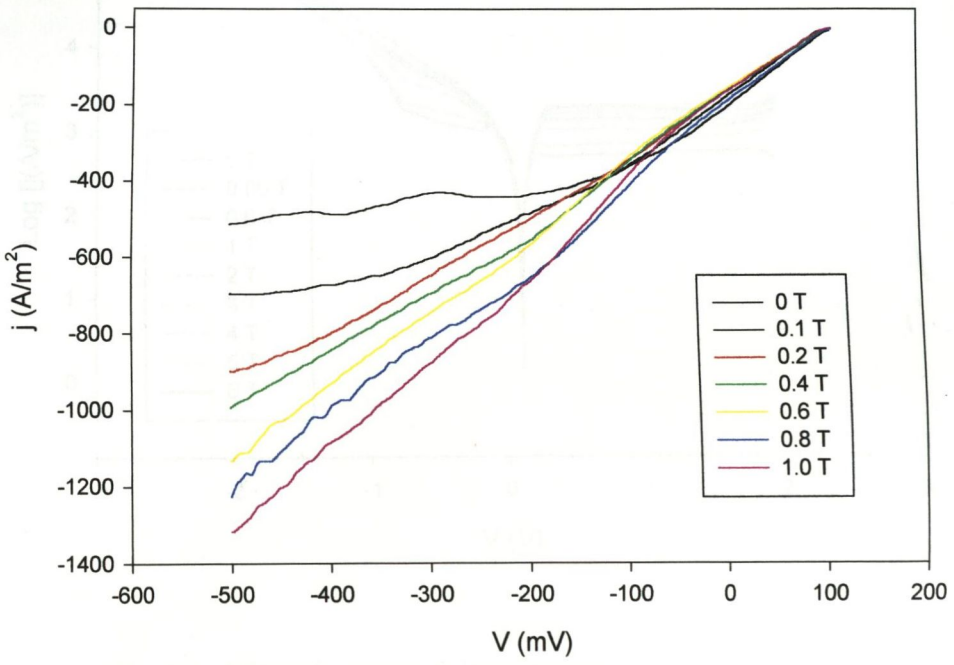


*Fig. 3.2: Effect of magnetic field on the voltammogram for a copper working electrode in 0.75 M $CuSO_4$ (pH = 1.0).*

The effect of the magnetic field on the magnitude of the current density is small in the kinetically controlled region close to the rest potential. However, the diffusion controlled limiting current density is dramatically increased by the application of the field. The current density observed at a potential of - 500 mV increases from 510 $A/m^2$ in zero field to 1320 $A/m^2$ in a field of 1 T. The largest effects on current enhancement are observed for fields in the range 0.1 - 0.2 T.

Experiments in higher fields carried out by F.E. Spada and J.M.D. Coey at the NHMFL in Tallahassee extended the range of study of the effects of the field magnitude on the current response. Data obtained for 0.75 M $CuSO_4$ at pH 0.5 are shown in Fig. 3.3. The potential was swept from + 2 V to - 2 V at a sweep rate of 10 mV/s in each case.

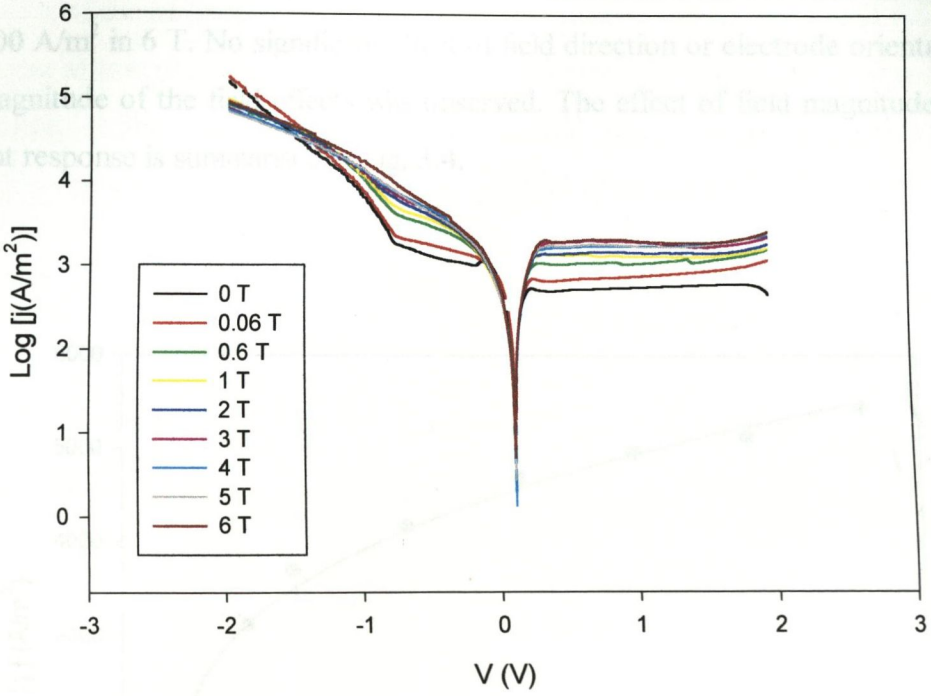


*Fig. 3.3: Effect of magnetic field on the voltammogram for a copper working electrode in 0.75 M $CuSO_4$ (pH =0.5).*

Two distinct regimes may be identified on each branch in Fig. 3.3 - the activation regime close to the rest potential and the mass transport regime, characterised by the current plateau. A third regime is identifiable on the cathodic branch, that of hydrogen evolution (below - 800 mV). No effect of the field is immediately obvious in the activation regime. However, this in itself is not sufficient evidence since mass transport effects may obscure kinetic effects even at relatively low overpotentials. The crossing of the curves in the hydrogen evolution regime indicates that in higher fields the hydrogen evolution reaction is somehow suppressed. However, the effect of the field is

most pronounced in the mass transport regime. On the cathodic branch, the current density at - 500 mV increases by a factor of 4, from 1300 $A/m^2$ in zero field to 5400 $A/m^2$ in a field of 6 T. In fact, such is the enhancement of mass transport in the field that a limiting current is not reached on the cathodic branch before hydrogen evolution sets in. The currents flowing in the anodic branch are smaller than those on the cathodic branch by a factor of 2 to 3. In contrast to the cathodic branch, a limiting current is observed on the anodic branch in all fields. Similar magnetic field effects are observed here - the current density at + 1.5 V is increased from 600 $A/m^2$ in zero field to 1900 $A/m^2$ in 6 T. No significant effect of field direction or electrode orientation on the magnitude of the field effects was observed. The effect of field magnitude on the current response is summarised in Fig. 3.4.

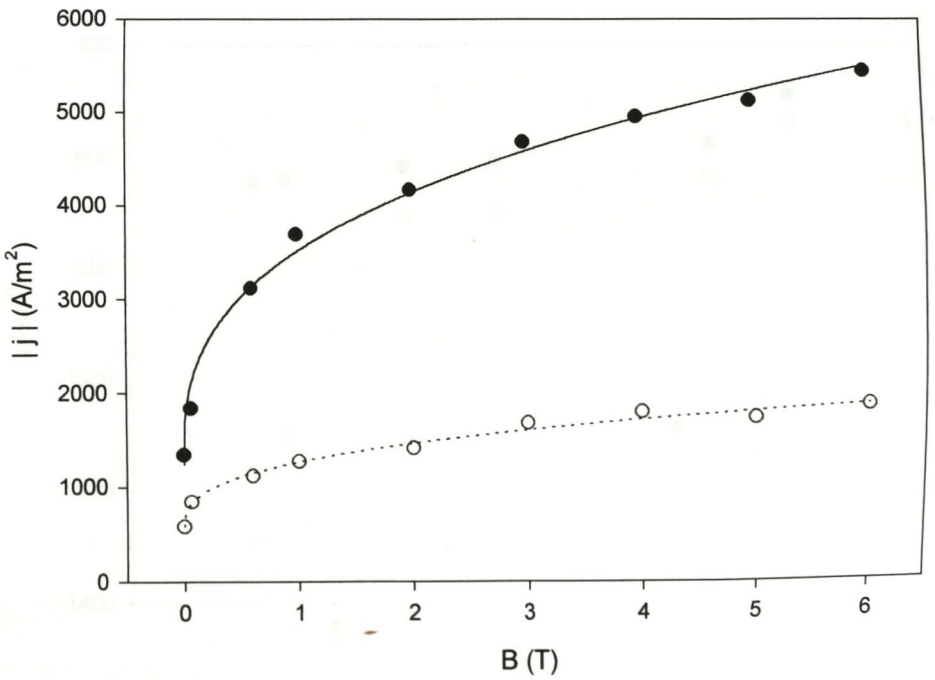


*Fig. 3.4: Effect of magnetic field on the limiting current density at - 500 mV for both cathodic (•) and anodic (o) branches for 0.75 M $CuSO_4$ (pH = 0.5). The data are fitted to Eq. 3.2.*

The effect begins to saturate in the larger fields of 5 - 6 T. The data are fitted to:

$$j = j_0 + aB^m \qquad (3.2)$$

where for the cathodic branch $j_0 = 1200 \pm 100$ A/m$^2$ , a = $2300 \pm 200$ A/m$^2$ and m = $0.35 \pm 0.03$, and for the anodic branch $j_0 = 600 \pm 50$ A/m$^2$, a = $680 \pm 70$ A/m$^2$ and m = $0.36 \pm 0.04$.

The effect of the magnetic field on the deposition rate of copper was found to be more significant at low pH. The pH was adjusted by varying the concentration of supporting electrolyte, $H_2SO_4$. Fig. 3.5 shows how the field effect on the deposition current density at - 500 mV varies with pH for a copper working electrode in 0.75 M $CuSO_4$.

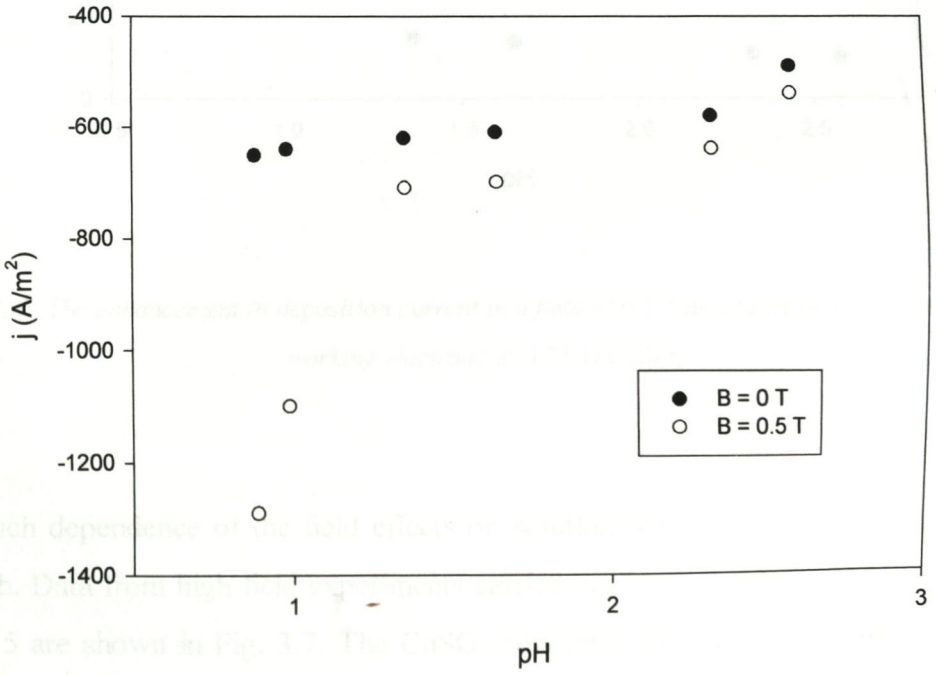


*Fig. 3.5: Effect of pH on the deposition current density at - 500 mV for a copper working electrode in 0.75 M $CuSO_4$.*

The enhancement in the deposition current is plotted as a function of pH in Fig. 3.6. The extent of current enhancement is typically 10 to 15 % over the pH range 1.5 to

2.5, but as the solution becomes more acidic a marked increase in current enhancement is observed. At pH 0.7 the current enhancement is 117 % in a field of 0.5 T.

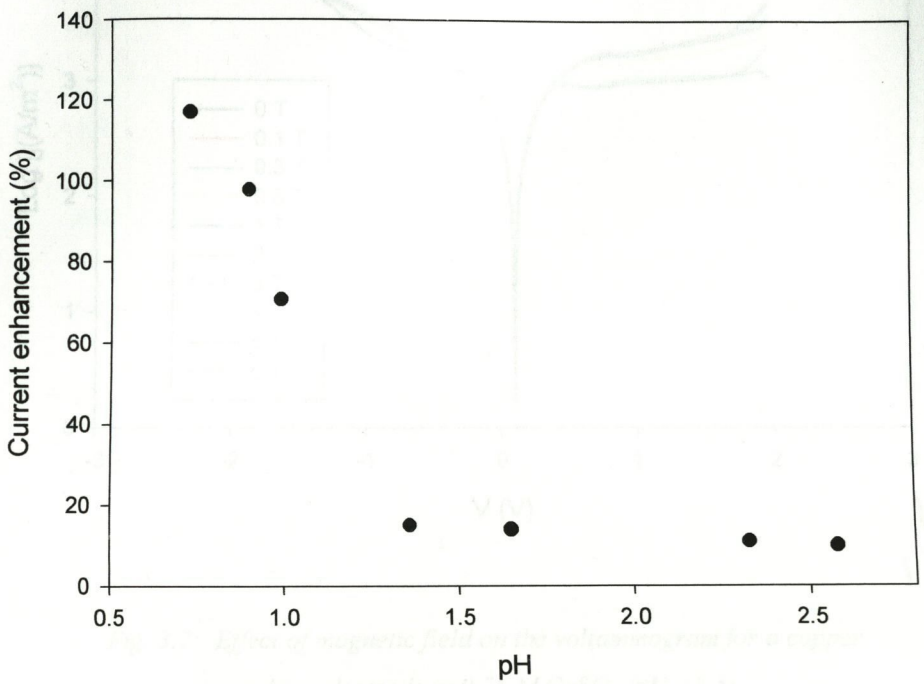


*Fig. 3.6: The enhancement in deposition current in a field of 0.5 T as a function of pH for a copper working electrode in 0.75 M $CuSO_4$.*

No such dependence of the field effects on solution pH was observed on the anodic branch. Data from high field experiments carried out by F. Spada and J.M.D. Coey at pH 3.5 are shown in Fig. 3.7. The $CuSO_4$ concentration was 0.75 M and the sweep rate was 10 mV/s.

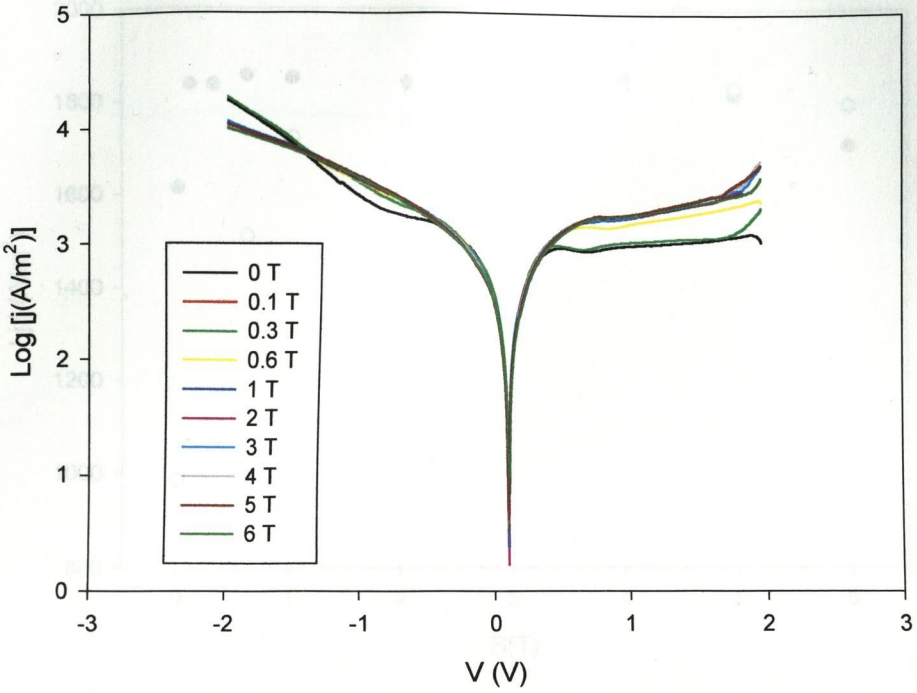


*Fig. 3.7: Effect of magnetic field on the voltammogram for a copper working electrode in 0.75 M $CuSO_4$ (pH =3.5).*

The effect of the field on the anodic branch is clearly more pronounced than that on the cathodic branch at pH 3.5. The effect on the anodic branch is comparable to that at pH 0.5. These effects are summarised in Fig. 3.8. Again, the crossing of the curves in the hydrogen evolution regime is noted, together with the lack of any obvious effect in the activation regime.

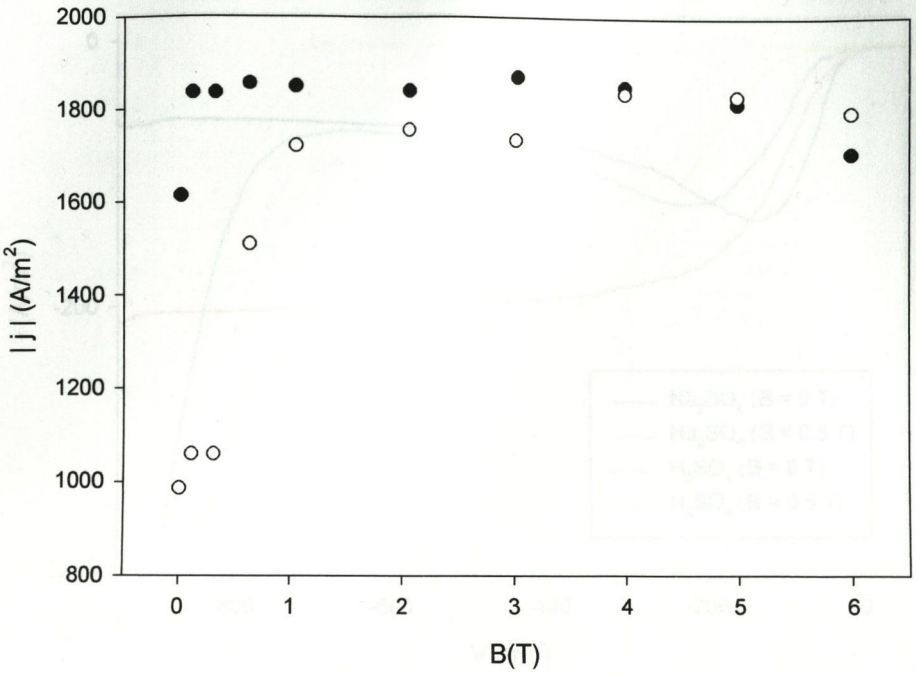


*Fig. 3.8: Effect of magnetic field on the limiting current density for both cathodic (•) and anodic (o) branches for 0.75 M $CuSO_4$ (pH = 3.5).*

On the anodic branch, the limiting current density at + 1.5 V increases from 990 A/m$^2$ in zero field to 1800 A/m$^2$ in a field of 6 T. On the cathodic branch, the current density at - 500 mV increases from 1610 A/m$^2$ in zero field to 1870 A/m$^2$ in a field of 3 T. Note that in higher fields the current enhancement actually falls off with increasing field.

The effect of using $Na_2SO_4$ instead of $H_2SO_4$ as the supporting electrolyte is demonstrated in Fig. 3.9. A similar enhancement in deposition current is obtained for a glassy carbon working electrode in 0.1 M $CuSO_4$ with 1 M concentrations of each species. Note that for $Na_2SO_4$, the hydrogen evolution reaction does not occur in this potential range.

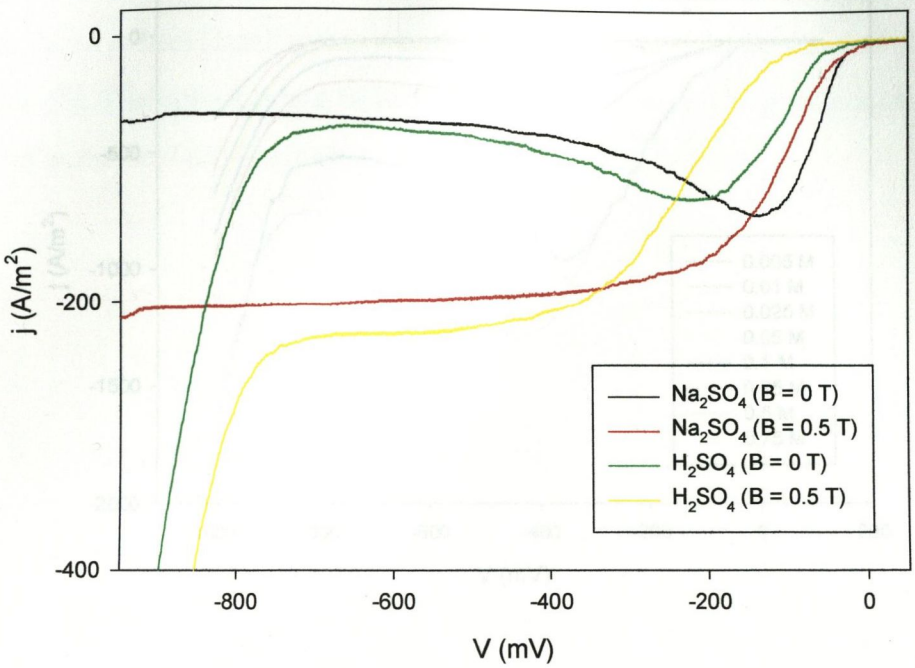


*Fig. 3.9: Effect of supporting electrolyte (1 M) on the voltammogram for a glassy carbon working electrode in 0.1 M $CuSO_4$, with and without an applied field of 0.5 T.*

The $Cu^{2+}$ concentration dependence of the magnetic field effect on electrodeposition at constant pH was investigated using linear sweep voltammetry. The voltammograms obtained at various concentrations in zero field are shown in Fig. 3.10 and those obtained in a field of 0.5 T are shown in Fig. 3.11. The working electrode was glassy carbon and the sweep rate was 20 mV/s.

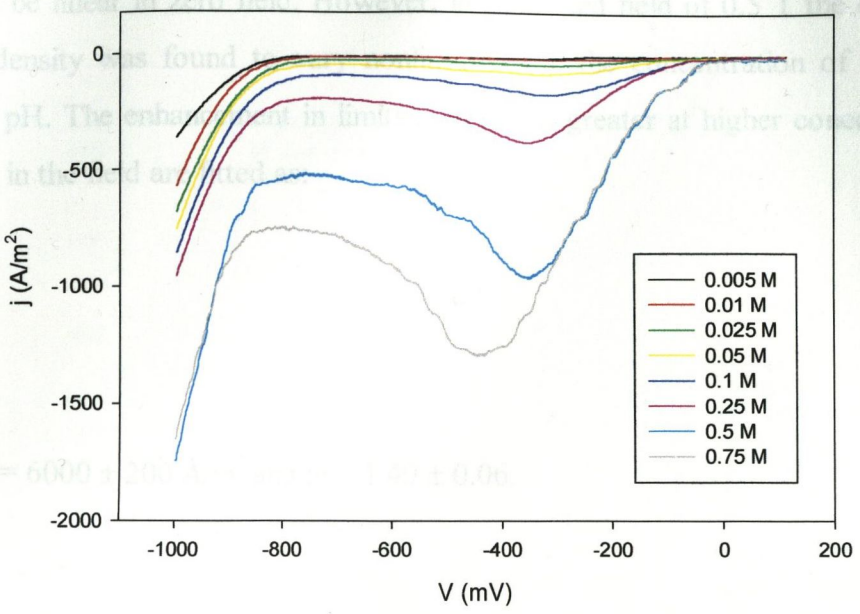


*Fig. 3.10: Effect of $Cu^{2+}$ concentration on the voltammogram for a glassy carbon working electrode in $CuSO_4$ solution (pH = 0.4) in the absence of field.*

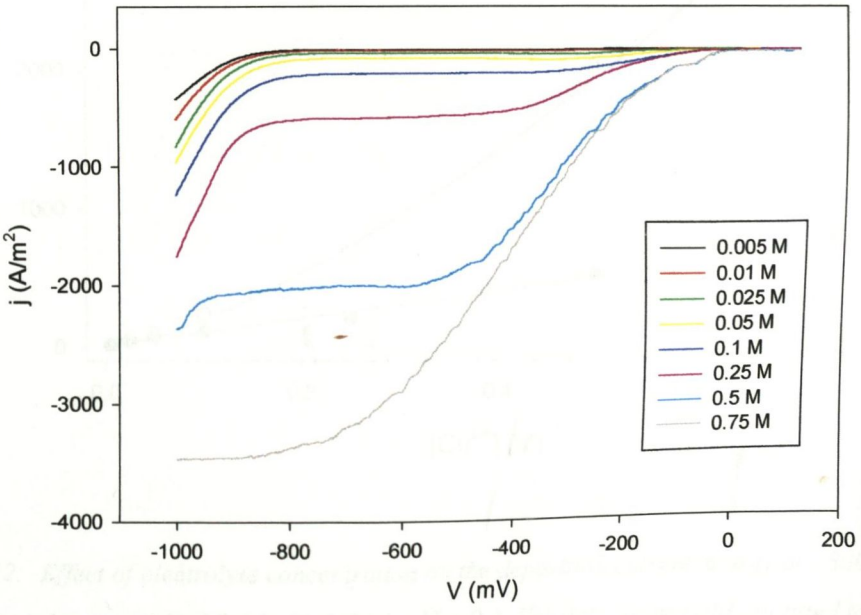


*Fig. 3.11: Effect of $Cu^{2+}$ concentration on the voltammogram for a glassy carbon working electrode in $CuSO_4$ solution (pH = 0.4) in a field of 0.5 T.*

The variation in the current density at - 800 mV as a function of electrolyte concentration is displayed in Fig. 3.12. As expected, the concentration dependence was found to be linear in zero field. However, in an applied field of 0.5 T the deposition current density was found to vary nonlinearly with the concentration of $CuSO_4$ at constant pH. The enhancement in limiting current is greater at higher concentrations. The data in the field are fitted as:

$$j = \alpha c^m \tag{3.3}$$

where $\alpha = 6000 \pm 200$ A/m$^2$ and $m = 1.40 \pm 0.06$.

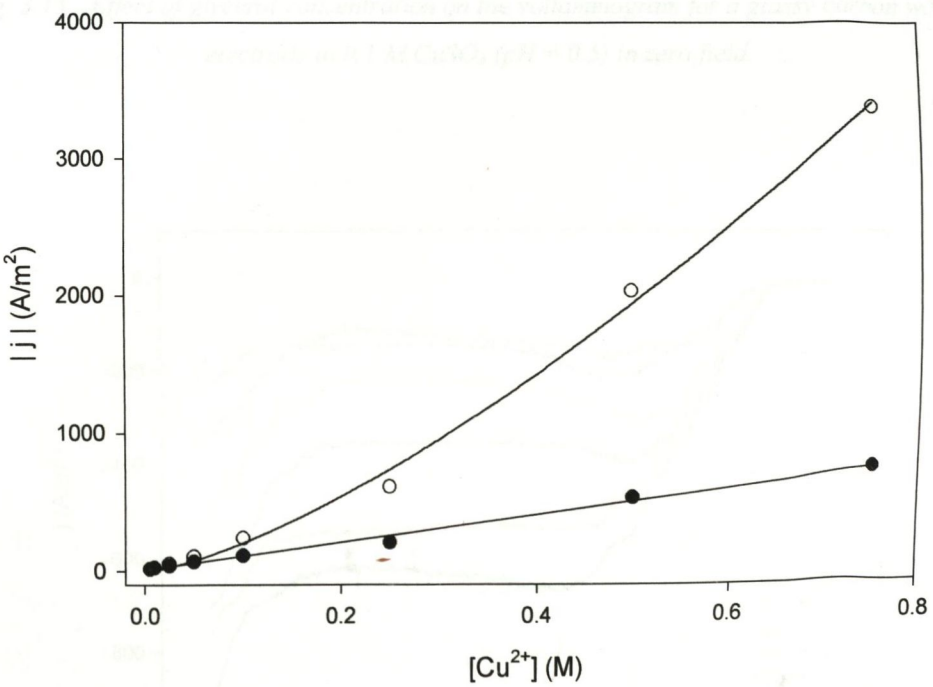


*Figure 3.12: Effect of electrolyte concentration on the deposition current density at - 800 mV in zero field (•) and in an applied field of 0.5 T (o). pH = 0.4. The data in the field are fitted to Eq. 3.3.*

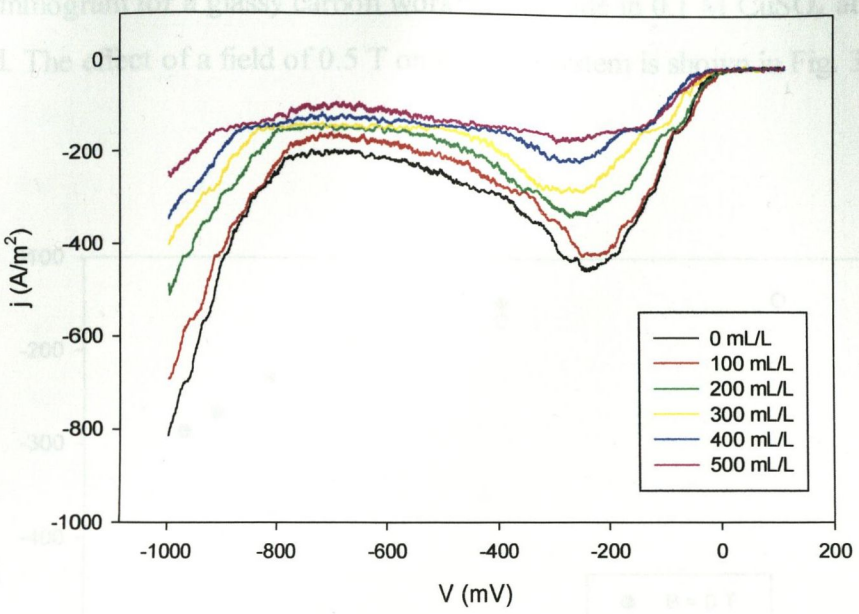


*Fig. 3.13: Effect of glycerol concentration on the voltammogram for a glassy carbon working electrode in 0.1 M $CuSO_4$ (pH = 0.5) in zero field.*

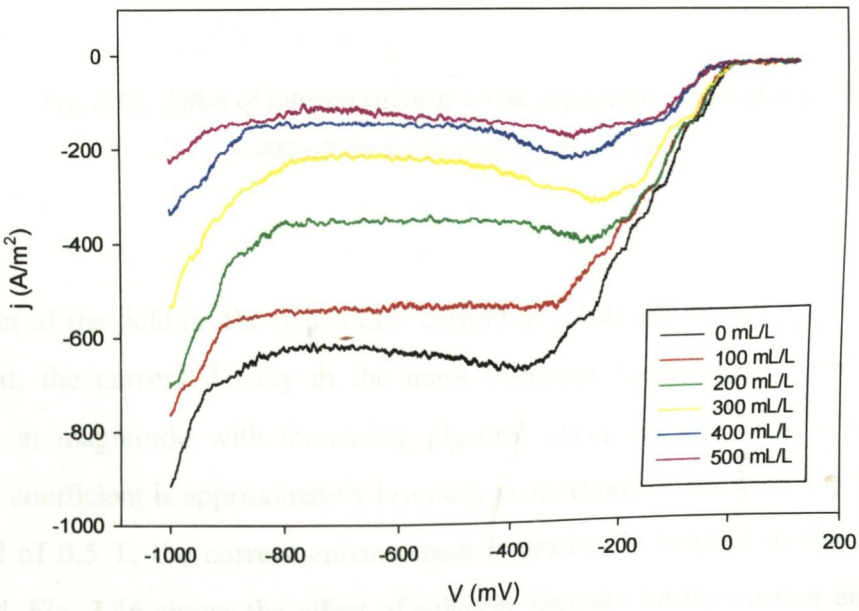


*Fig. 3.14: Effect of glycerol concentration on the voltammogram for a glassy carbon working electrode in 0.1 M $CuSO_4$ (pH = 0.5) in a field of 0.5 T.*

The effect of increasing the solution viscosity was investigated by the addition of glycerol in varying concentrations. Fig. 3.13 shows the effect of solution viscosity on the voltammogram for a glassy carbon working electrode in 0.1 M $CuSO_4$ at pH 0.5 in zero field. The effect of a field of 0.5 T on the same system is shown in Fig. 3.14.

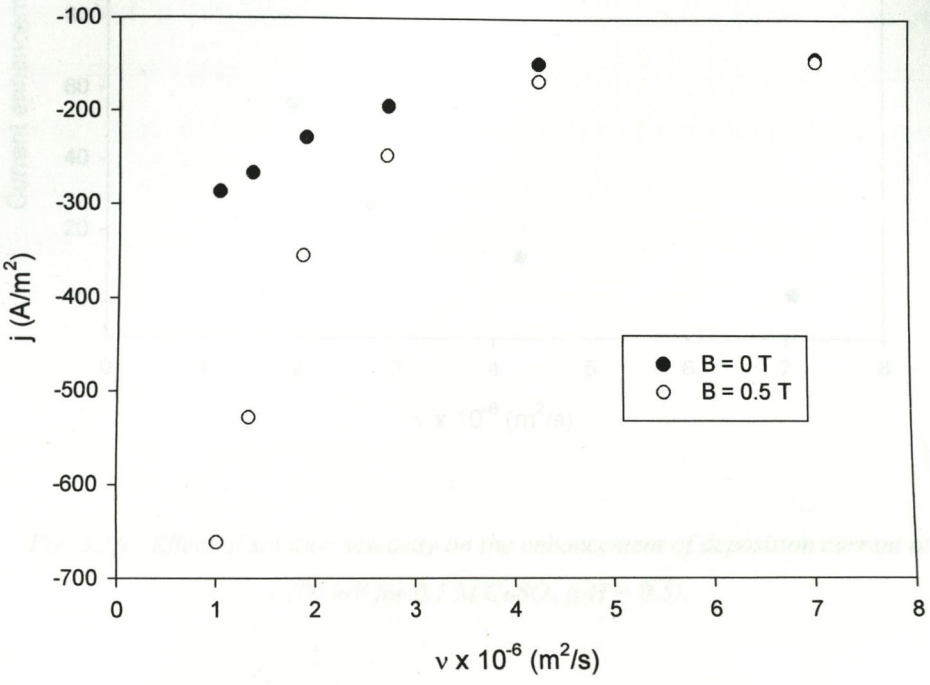


*Fig. 3.15: Effect of solution viscosity on the deposition current density at - 400 mV for 0.1 M $CuSO_4$ (pH = 0.5).*

The effect of the field on the deposition current at - 400 mV is shown in Fig. 3.15. In zero field, the current density in the mass transport limited regime shows a clear decrease in magnitude with increasing glycerol concentration. This is because the diffusion coefficient is approximately inversely proportional to the viscosity. Moreover, in a field of 0.5 T, the current enhancement is drastically reduced as the viscosity is increased. Fig. 3.16 shows the effect of solution viscosity on the current enhancement observed in a 0.5 T field. The current enhancement is reduced from 131 % in the absence of glycerol to just 2 % when the concentration of glycerol is 500 mL/L, corresponding to a solution viscosity of 7 x $10^{-6}$ $m^2/s$.

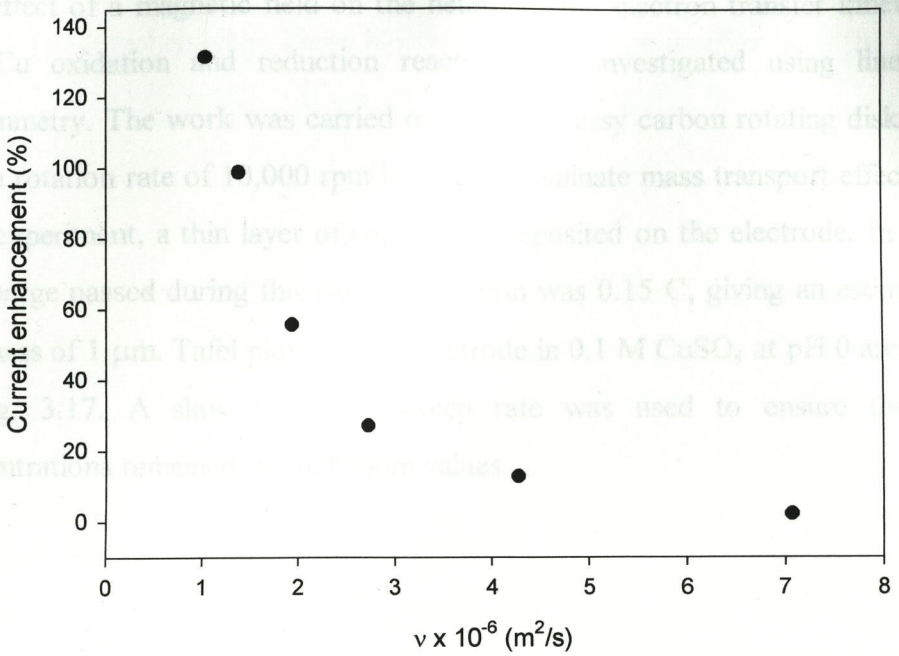


*Fig. 3.16: Effect of solution viscosity on the enhancement of deposition current at - 400 mV for 0.1 M $CuSO_4$ (pH = 0.5).*

## 3.3 Magnetic field effects on electrode kinetics

The effect of a magnetic field on the heterogeneous electron transfer kinetics of the $Cu^{2+}/Cu$ oxidation and reduction reactions was investigated using linear sweep voltammetry. The work was carried out using a glassy carbon rotating disk electrode with a rotation rate of 10,000 rpm in order to eliminate mass transport effects. Before each experiment, a thin layer of copper was deposited on the electrode. In each case the charge passed during this electrodeposition was 0.15 C, giving an estimated layer thickness of 1 μm. Tafel plots for this electrode in 0.1 M $CuSO_4$ at pH 0 are presented in Fig. 3.17. A slow (1 mV/s) sweep rate was used to ensure that surface concentrations remained at equilibrium values.

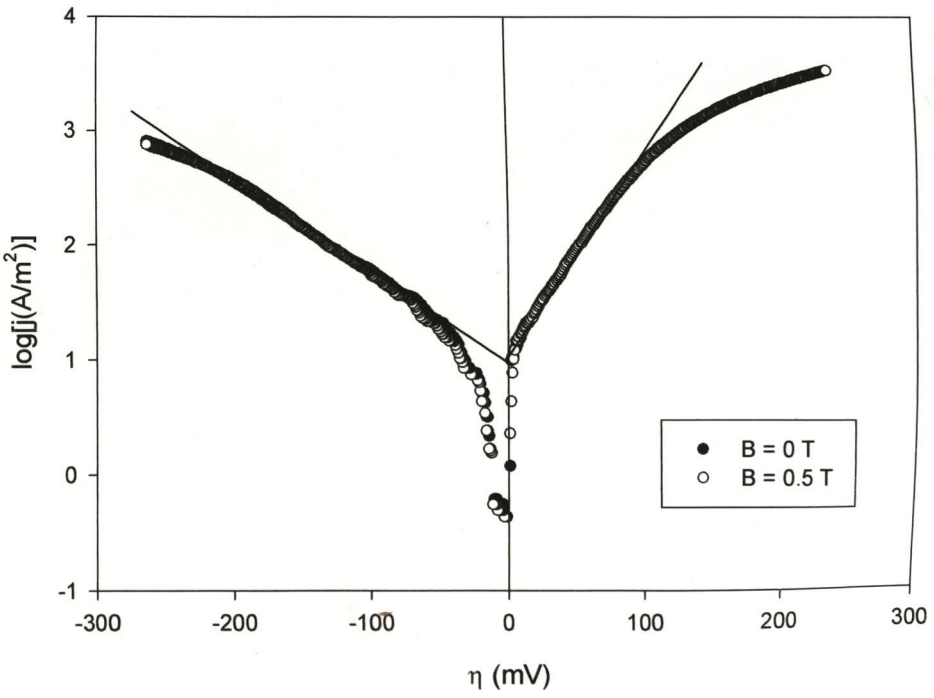


*Fig. 3.17: Tafel plots at a copper modified rotating disk electrode in 0.2 M $CuSO_4$ (pH = 0.5). Rotation rate is 10,000 rpm.*

Good Tafel behaviour was observed on both cathodic and anodic branches. The exchange current density was found to be 10 $A/m^2$ for each branch. From Eqs. 1.12 and 1.13, the cathodic and anodic charge transfer coefficients were calculated to be 0.45 and 0.90 respectively. These kinetic parameters were unaffected by the field.

## 3.4 Magnetic field effects in conditions of enhanced mass transport

The effect of a static magnetic field on the electrodeposition of copper under conditions of enhanced mass transport was examined using linear sweep voltammetry. The first system was one with a high rate of convection, the rotating disk electrode, and the second was one with a high rate of diffusion, the microelectrode.

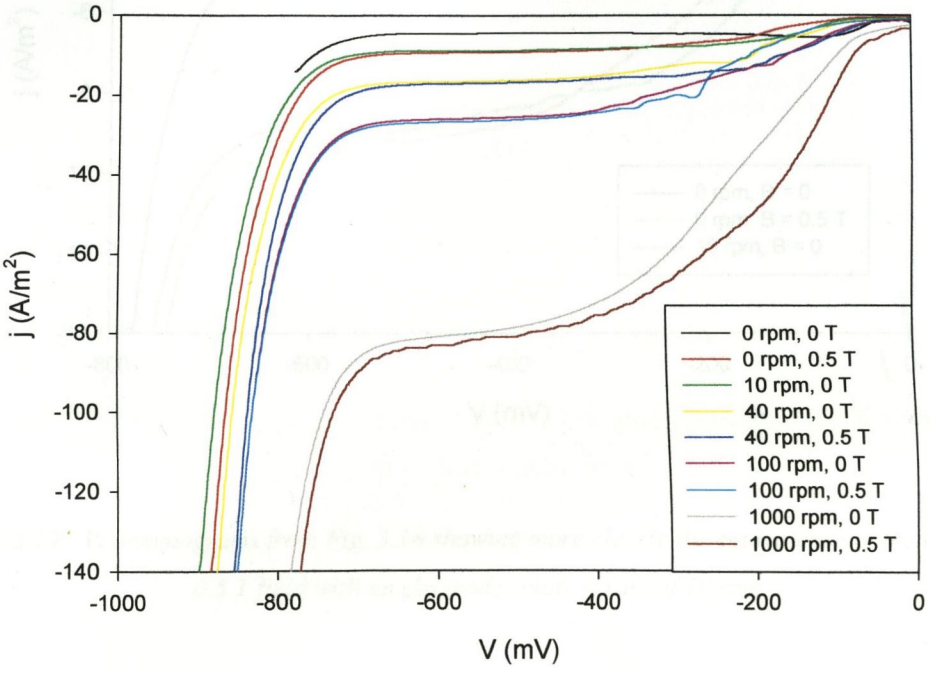


*Fig. 3.18: Effect of rotation rate and magnetic field on the voltammogram for a glassy carbon rotating disk electrode in 0.01 M $CuSO_4$ (pH = 1.0).*

The effect of a magnetic field on mass transport in a regime of forced convection was investigated using a glassy carbon rotating disk electrode. Fig. 3.18 shows the effect of an applied field of 0.5 T on the voltammograms obtained at several different rotation rates in 0.01 M $CuSO_4$ (pH = 1.0). The limiting current density with a stationary electrode in the absence of an applied field is 4.5 $A/m^2$. When a magnetic field of 0.5 T is applied to the cell, the limiting current density increases to 9.4 $A/m^2$. The effect of the field on the quiescent solution is quantitatively equivalent to a rotation rate of 10

rpm (Fig. 3.19). Enhancements of just 2 to 3 % were observed on the limiting currents at each rotation rate.

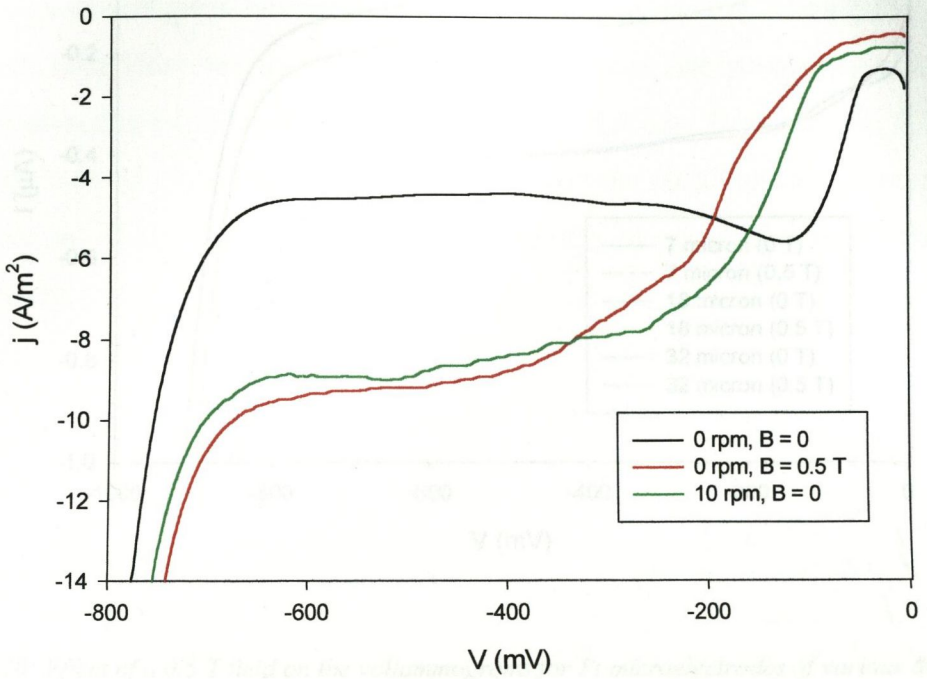


*Figure 3.19: Voltammograms from Fig. 3.18 showing more clearly the equivalence of the effect of a 0.5 T field with an electrode rotation rate of 10 rpm.*

The effect of a magnetic field on the voltammograms for Pt microelectrodes of various dimensions in 0.05 M $CuSO_4$ at pH 0.5 is shown in Fig. 3.20. The deposition current at - 500 mV was increased by only 1 to 2 % by the application of a 0.5 T magnetic field.

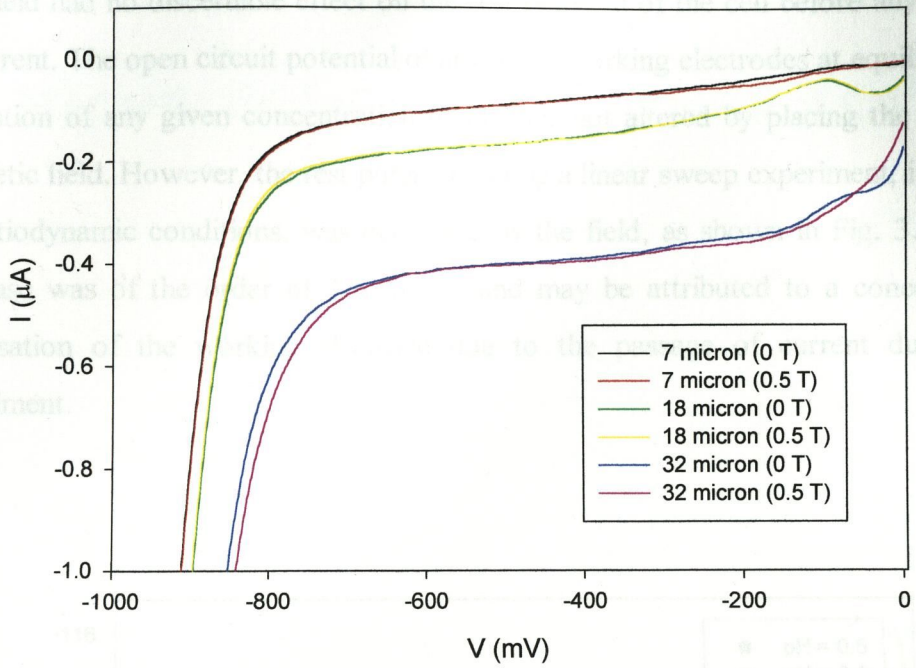


*Fig. 3.20: Effect of a 0.5 T field on the voltammograms for Pt microelectrodes of various dimensions in 0.05 M $CuSO_4$ (pH = 0.5).*

## 3.5 Magnetic field effects on the rest potential

The field had no discernible effect on the rest potential of the cell before any passage of current. The open circuit potential of any of the working electrodes at equilibrium in a solution of any given concentration or pH was not altered by placing the cell in a magnetic field. However, the rest potential during a linear sweep experiment, i.e. under potentiodynamic conditions, was decreased by the field, as shown in Fig. 3.21. This decrease was of the order of 2 to 3 mV and may be attributed to a concentration polarisation of the working electrode due to the passage of current during the experiment.

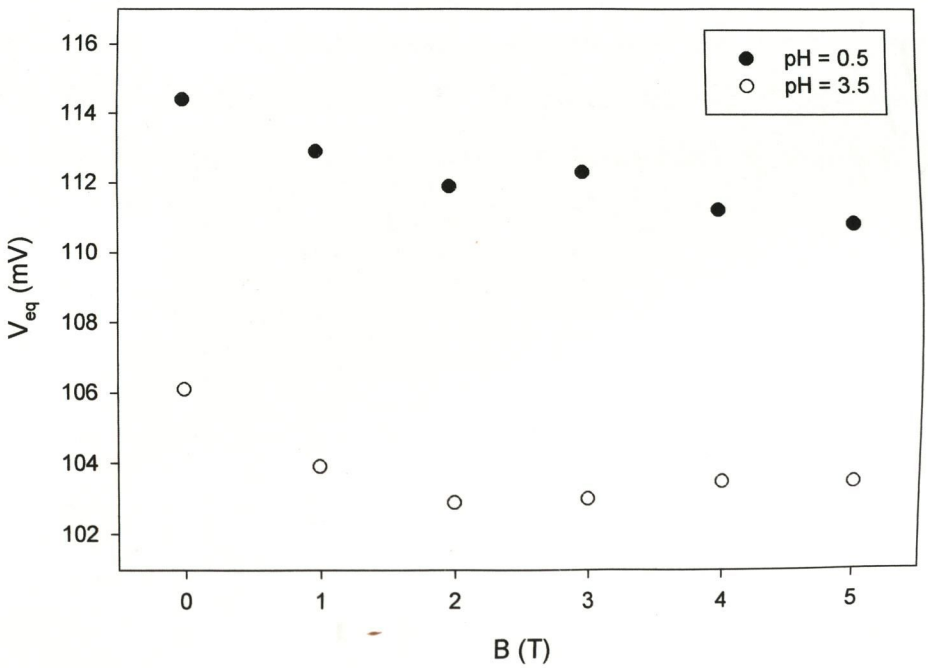


*Fig. 3.21: Effect of magnetic field on the rest potential during a linear sweep experiment in 0.75 M $CuSO_4$.*

# Chapter Four

## Magnetic field effects on the diffusion of $Cu^{2+}$

## 4.1 Impedance spectroscopy

Impedance spectroscopy is a powerful electrochemical technique which may be used to obtain quantitative information about processes of diffusion and electron transfer accompanying an electrode reaction. In contrast to linear sweep and potential step methods, where the system is perturbed far from equilibrium, a small a.c. perturbation is applied to the cell and the response is monitored as a function of the perturbation frequency. In particular, the measurement of the magnitude and phase of the impedance as a function of frequency may be readily analysed in terms of equivalent circuits. In this type of analysis, the cell response is modelled on that of an electrical circuit containing combinations of resistors and capacitors, each representing a particular physical or chemical process. In general, a resistor represents a conductive path, such as conduction by ions in solution or the charge transfer accompanying an electrode reaction. A capacitor represents a space charge layer, such as the electrical double layer at the electrode interface. The impedance spectrum of the redox couple of a metal atom and its cation (e.g. $Cu^{2+}/Cu$) may be modelled by the circuit shown in Figure 4.1.

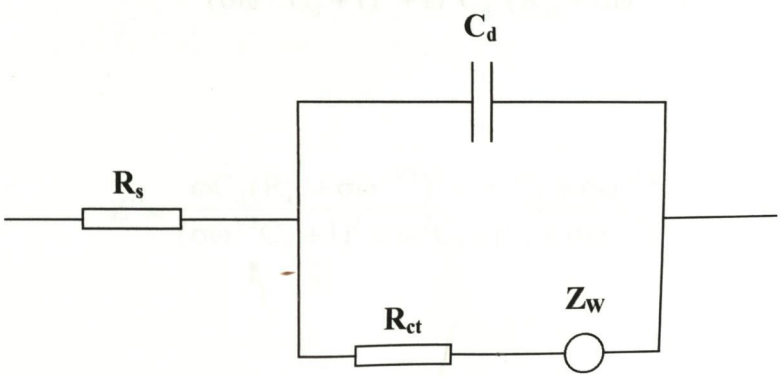


*Figure 4.1: Equivalent circuit used to model the electrochemical behaviour of the redox couple $Cu^{2+}/Cu$.*

The resistor $R_s$ represents the solution resistance between the working and reference electrodes, while the resistor $R_{ct}$ represents the charge transfer resistance at the electrode. The capacitor $C_d$ represents the double layer capacitance. Mass transport effects are included in the Warburg impedance, $Z_W$, which is a measure of the immobility of the electroactive species in solution. This particular equivalent circuit is often called a Randles circuit. The numerical value of each component in the circuit may be readily deduced from the impedance spectrum and related to a relevant electrochemical parameter. The determination of $R_{ct}$ gives the exchange current, $I_0$, while the variation of $Z_W$ with frequency yields the diffusion coefficient, D, of the ionic species in solution.

In an typical experiment, a small a.c. voltage (~ 10 mV) is applied at the electrode and the magnitudes of the in-phase (Z') and out-of-phase (Z'') components of the impedance are measured as a function of frequency, f. The perturbation may be supplied by a potentiostat and the response monitored using a lock-in amplifier. It can be shown that when a small sinusoidal perturbation of angular frequency, ω, is applied to a cell modelled on the Randles circuit:

$$Z' = R_s + \frac{R_{ct} + \sigma\omega^{1/2}}{(\sigma\omega^{1/2}C_d + 1)^2 + \omega^2 C_d{}^2 (R_{ct} + \sigma\omega^{-1/2})^2} \qquad (4.1a)$$

$$Z'' = \frac{\omega C_d (R_{ct} + \sigma\omega^{-1/2})^2 + \sigma^2 C_d + \sigma\omega^{-1/2}}{(\sigma\omega^{1/2}C_d + 1)^2 + \omega^2 C_d{}^2 (R_{ct} + \sigma\omega^{-1/2})^2} \qquad (4.1b)$$

$$\text{where } \sigma = \frac{RT}{n^2 F^2 A c_\infty \sqrt{2D}} \qquad (4.1c)$$

where A is the electrode area. A plot of -Z'' against Z' is known as a Nyquist plot, and has a form similar to the Argand representation of complex numbers. The Nyquist plot for the Randles circuit, from Eq. 4.1, is shown in Fig. 4.2.

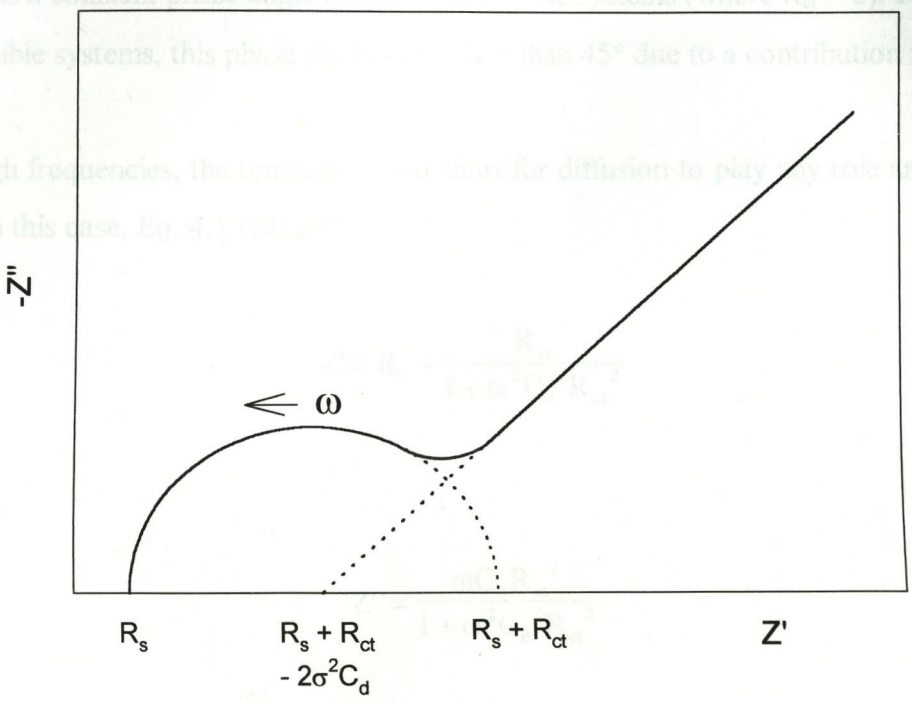


*Figure 4.2: Impedance spectrum for a Randles circuit (from Eq. 4.1).*

Two limiting cases may be identified. At low frequencies, Eq. 4.1 reduces to:

$$Z' = R_s + R_{ct} + \sigma\omega^{-1/2} \tag{4.2a}$$

$$Z'' = -\sigma\omega^{-1/2} - 2\sigma^2 C_d \tag{4.2b}$$

where the Warburg impedance is given by:

$$Z'_W = \sigma\omega^{-1/2} \tag{4.3}$$

The low frequency limit is the straight line of slope unity and intercept ($R_s + R_{ct} + 2\sigma^2 C_d$) shown in Fig. 4.2. This line is characteristic of a reaction controlled by diffusion and has a constant phase angle of 45° for reversible systems (where $R_{ct} \sim 0$). For quasi-reversible systems, this phase angle will be less than 45° due to a contribution from $R_{ct}$.

At high frequencies, the timescale is too short for diffusion to play any role and $R_{ct} >> Z_W$. In this case, Eq. 4.1 reduces to:

$$Z' = R_s + \frac{R_{ct}}{1 + \omega^2 C_d^{\,2} R_{ct}^{\,2}} \tag{4.4a}$$

$$Z'' = \frac{\omega C_d R_{ct}^{\,2}}{1 + \omega^2 C_d^{\,2} R_{ct}^{\,2}} \tag{4.4b}$$

Combining these two expressions we obtain:

$$\left(Z' - R_s - \frac{R_{ct}}{2}\right)^2 + (Z'')^2 = \left(\frac{R_{ct}}{2}\right)^2 \tag{4.5}$$

which is the equation of a circle of diameter $R_{ct}$ and intercepts on the Z' axis of $R_s$ and $(R_s + R_{ct})$, as shown in Fig. 4.2. The exchange current, $I_0$, is related to $R_{ct}$ by:

$$R_{ct} = \frac{RT}{nFI_0} \tag{4.6}$$

The variation of the magnitude of the impedance, | Z |, and the phase angle, | $\phi$ |, is often plotted as a function of frequency. Such a plot is known as a Bode plot. However, the Nyquist plot is more useful in determining electrochemical parameters. The power of impedance spectroscopy is that it is possible to determine both kinetic ($I_0$) and mass transport (D) parameters from the same spectrum. One disadvantage of this technique is that the impedance response is usually extremely sensitive to the condition of the electrode surface, which can lead to problems with reproducibility.

## 4.2 Magnetic field effects on the impedance response

The effect of a 0.5 T field on the Bode plot for a copper working electrode in 0.2 M $CuSO_4$ at pH 0 is shown in Figs. 4.3 and 4.4. The a.c. signal applied to the electrode was 5 mV in amplitude. The data were collected at the open circuit potential in the frequency range 0.1 Hz - 100 kHz.

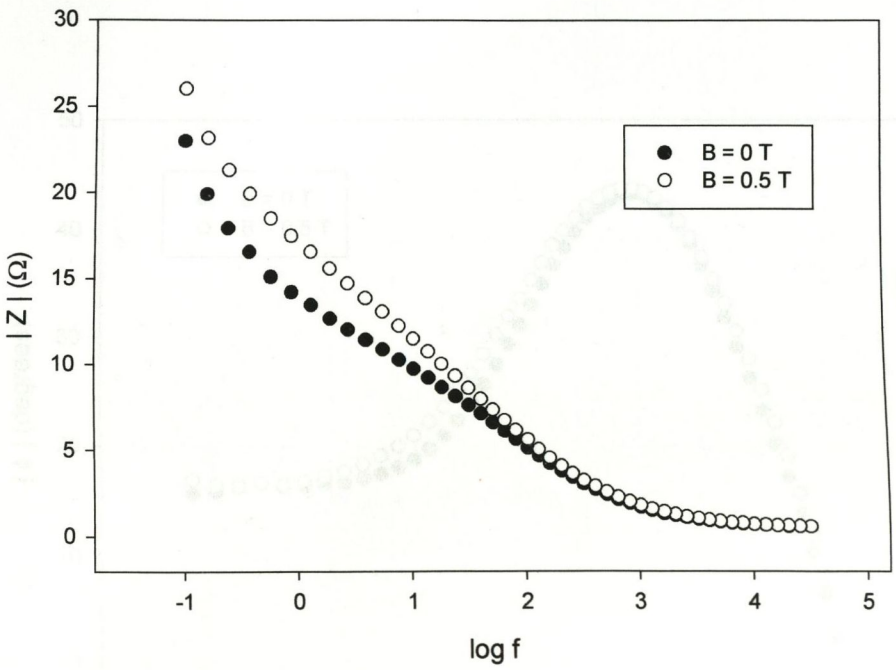


*Fig. 4.3: Effect of a 0.5 T field on the magnitude of the impedance as a function of frequency for a copper working electrode in 0.2 M $CuSO_4$ (pH = 0).*

At high frequencies the impedance response is purely resistive. Here Eqs. 4.4a and 4.4b may be reduced to:

$$Z' = R_s \tag{4.7a}$$

$$Z'' = 0 \tag{4.7b}$$

From Fig. 4.3, it is clear that the solution resistance is unaffected by the field. At low frequencies, the impedance response would level off at $(R_s + R_{ct})$ were it not for the contribution from the Warburg impedance. The Nyquist plot is more useful in this frequency range. In general, the magnitude of the impedance is greater in the presence of the field. This increase is more significant at low frequencies.

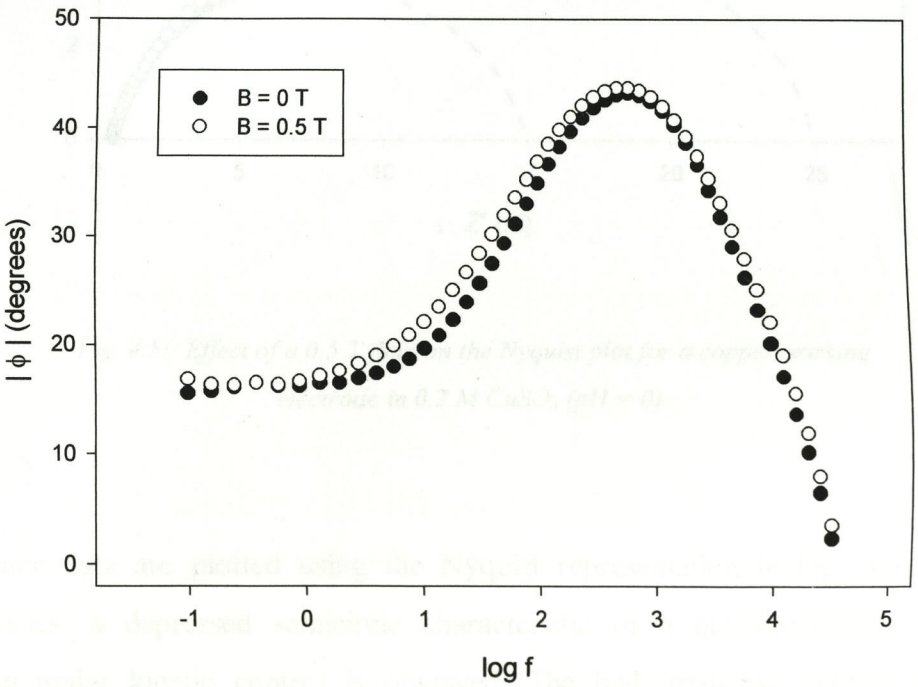


*Fig. 4.4: Effect of a 0.5 T field on the magnitude of the phase angle as a function of frequency for a copper working electrode in 0.2 M $CuSO_4$ (pH = 0).*

Fig. 4.4 shows that the effect of the field on the phase angle is not significant. At low frequencies, a constant phase angle of about 16° is observed in both field-on and field-off cases. This is lower than the value expected for a system under pure diffusion control (45°), and provides further evidence that the reaction is not completely reversible.

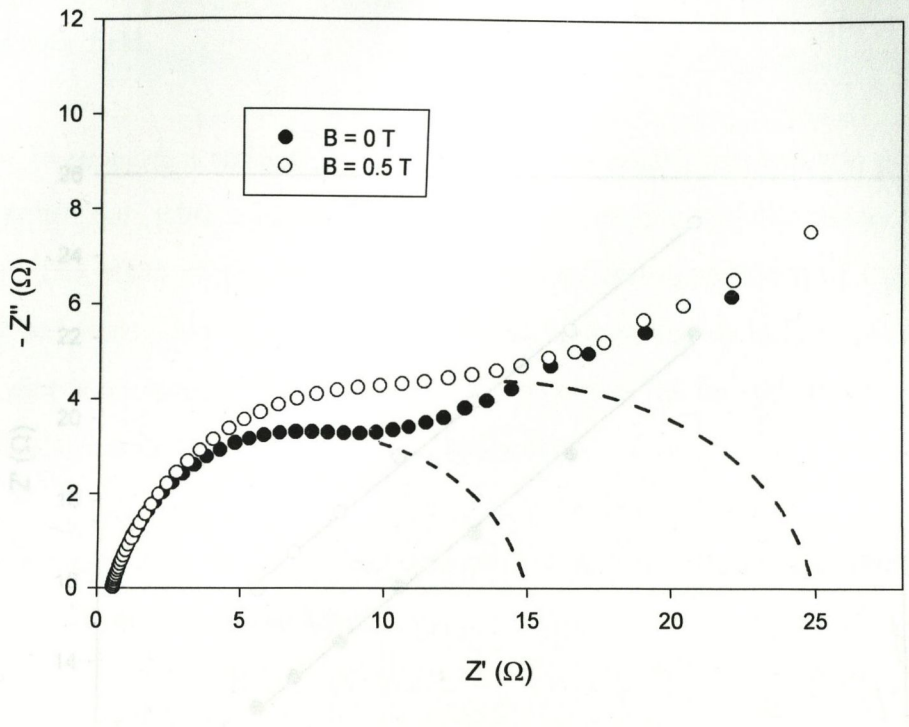


*Fig. 4.5: Effect of a 0.5 T field on the Nyquist plot for a copper working electrode in 0.2 M $CuSO_4$ (pH = 0).*

The same data are plotted using the Nyquist representation in Fig. 4.5. At high frequencies, a depressed semicircle characteristic of a quasi-reversible electrode reaction under kinetic control is observed. The high frequency intercept of this semicircle gives $R_s$ = 0.6 Ω, independent of field. The low frequency intercept is shifted from 15 Ω in zero field to 25 Ω in a field of 0.5 T, indicating that $R_{ct}$ is increased by the field. According to Eq. 4.6, this corresponds to a decrease in the exchange current density from 10 $A/m^2$ in zero field to 6 $A/m^2$ in a field of 0.5 T.

The double layer capacitance may be estimated from the position of the peak in the semicircle of the Nyquist plot using the equation:

$$C_d = \frac{1}{2\pi f_{max} R_{ct}} \tag{4.8}$$

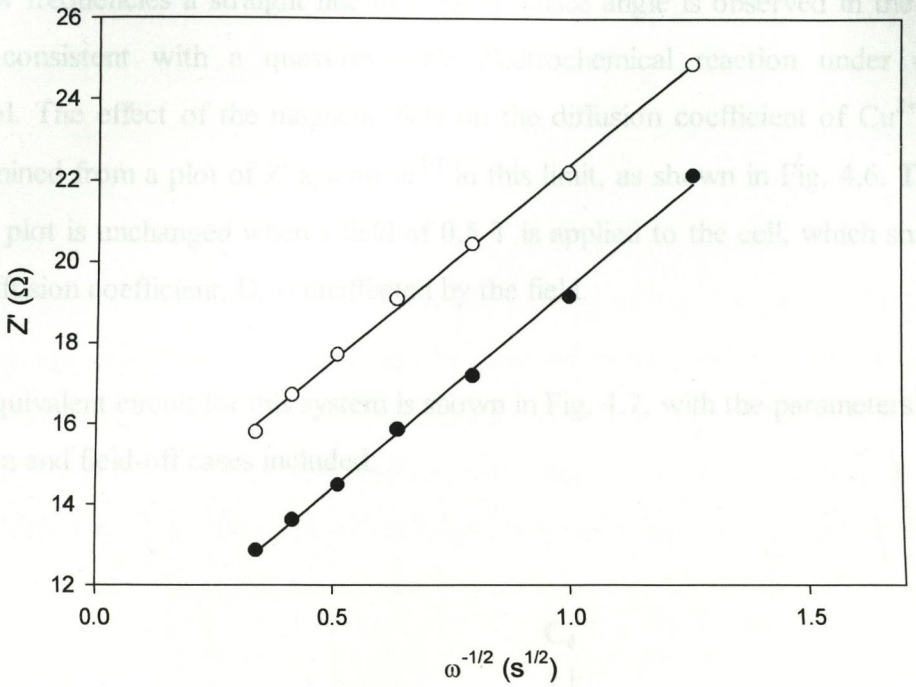


*Fig. 4.6: Effect of a 0.5 T field on the plot of Z' against $\omega^{-1/2}$ for a copper working electrode in 0.2 M $CuSO_4$ (pH = 0).*

From Fig. 4.5, $f_{max}$ changes from 26 Hz in zero field to 15 Hz in a field of 0.5 T. According to Eq. 4.8, the double layer capacitance is around 350 μF in both field-on and field-off cases. The double layer thickness, $x_d$, may then be estimated by using the parallel plate approximation:

$$C_d = \frac{\varepsilon\varepsilon_0 A}{x_d} \tag{4.9}$$

where $\varepsilon$ is the relative permittivity of the medium and $\varepsilon_0$ is the permittivity of free space. Taking $\varepsilon = 80$ for water and with $A = 8.5 \times 10^{-5}$ m$^2$, we obtain $x_d = 0.2$ nm, which is a reasonable value. The thickness of the electrical double layer is unaffected by magnetic field.

At low frequencies a straight line of constant phase angle is observed in the Nyquist plot, consistent with a quasi-reversible electrochemical reaction under diffusion control. The effect of the magnetic field on the diffusion coefficient of $Cu^{2+}$ may be determined from a plot of $Z'$ against $\omega^{-1/2}$ in this limit, as shown in Fig. 4.6. The slope of the plot is unchanged when a field of 0.5 T is applied to the cell, which shows that the diffusion coefficient, D, is unaffected by the field.

The equivalent circuit for this system is shown in Fig. 4.7, with the parameters for both field-on and field-off cases included.

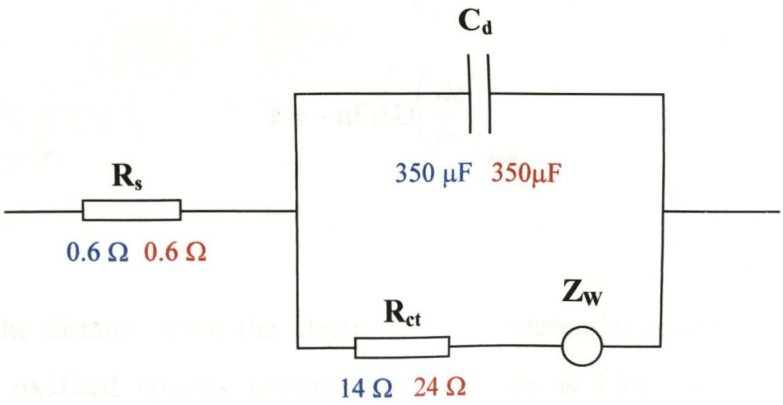


*Figure 4.7: Equivalent circuit used to model the electrochemical behaviour of the redox couple $Cu^{2+}/Cu$. The parameters shown are for B = 0 T (blue) and B= 0.5 T (red).*

## 4.3 Chronoamperometry

Chronoamperometry is a transient technique which is commonly used in electrochemical studies to measure diffusion coefficients of both neutral and ionic species. If the diffusion coefficient for a particular species is known, chronoamperometric measurements may be used to determine either the electrode area or the number of electrons transferred during an electrode reaction. A potential step is applied to an electrode, in a solution containing either oxidised or reduced species, from an initial value where no faradaic reaction occurs to a final value where all electroactive species that reach the electrode react instantaneously. This corresponds to a potential in the diffusion-limited current plateau of Fig. 3.1, where the electrode kinetics are significantly faster than the rate of mass transport. At a uniformly accessible planar electrode, these conditions are known as semi-infinite linear diffusion. In quiescent solution, the rate of reaction, and hence the measured current response, is solely determined by the rate of diffusion. For a reduction reaction, such as the electrodeposition of copper, the current is given by:

$$I = -nFAD\left(\frac{\partial c}{\partial y}\right)_{y=0} \tag{4.10}$$

where y is the distance from the electrode. The differential equation governing the diffusion of oxidised species towards the electrode is Fick's second law in one dimension:

$$\frac{\partial c}{\partial t} = D\frac{\partial^2 c}{\partial y^2} \tag{4.11}$$

for which the boundary conditions under conditions of semi-infinite linear diffusion are:

$$t = 0: \qquad c_0 = c_\infty \tag{4.12a}$$

$$t \geq 0: \qquad \lim_{y \to \infty} c = c_\infty \tag{4.12b}$$

$$t > 0: \qquad c_0 = 0 \text{ (at } y = 0) \tag{4.12c}$$

Eq. 4.12a expresses the equilibrium condition before any reaction takes place, Eq. 4.12b states that the concentration is always equal to that of the bulk solution at large distances from the electrode, and Eq. 4.12c allows for the removal of reactant species at the electrode surface. The solution to Eq. 4.11, using the Laplace transformation, leads to the following expression for the concentration as a function of y and t:

$$c = c_\infty \text{erf}\left(\frac{y}{2\sqrt{Dt}}\right) \tag{4.13}$$

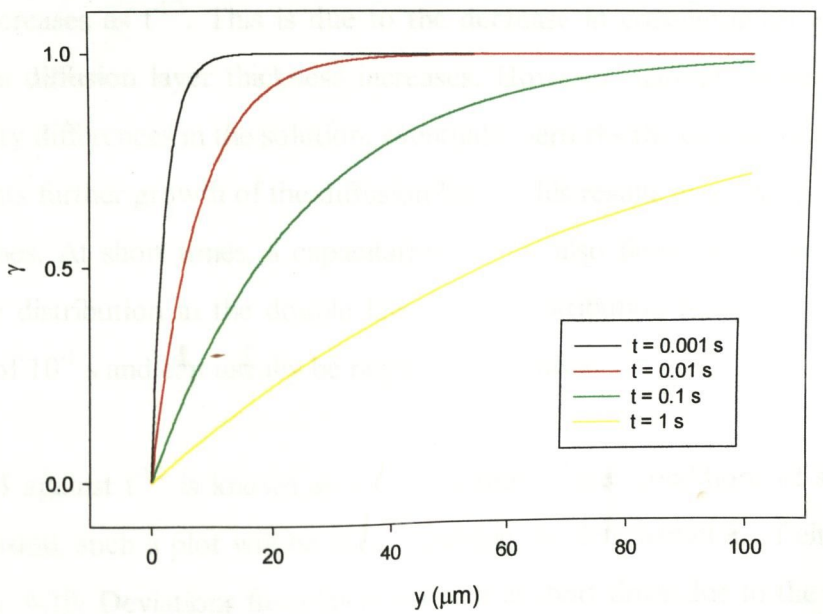


*Fig. 4.8: Variation of normalised concentration, $\gamma = c/c_\infty$, with distance and time under conditions of semi-infinite linear diffusion, according to Eq. 4.13 ($D = 10^{-9}$ m$^2$/s).*

where the error function erf(z) is defined as:

$$\mathrm{erf}(z) = \frac{2}{\sqrt{\pi}} \int_0^z \exp(-t^2)dt \tag{4.14}$$

As shown in Fig. 4.8, the concentration gradient decreases with time as reactant species are depleted from the region of solution close to the electrode. The diffusion layer thickness, $\delta$, introduced in Section 1.3, may be approximated by extrapolation of the concentration gradient at $y = 0$ to the distance at which $\gamma = 1$.

The current response due to a potential step may be obtained by differentiation of the concentration profile given by Eq. 4.13. When combined with Eq. 4.10 this yields:

$$I(t) = \frac{nFAD^{1/2}c_\infty}{(\pi t)^{1/2}} \tag{4.15}$$

This equation is known as the Cottrell equation and shows that the diffusion limited current decreases as $t^{-1/2}$. This is due to the decrease in concentration gradient with time as the diffusion layer thickness increases. However, natural convection, arising from density differences in the solution, eventually perturbs the concentration gradients and prevents further growth of the diffusion layer. This results in a steady-state current at long times. At short times, a capacitative current also flows due to re-ordering of the charge distribution in the double layer. This contribution is only important on a timescale of $10^{-1}$ s and can usually be neglected thereafter.

A plot of I against $t^{-1/2}$ is known as a Cottrell plot. Under conditions of semi-infinite linear diffusion, such a plot will be linear, enabling the determination of either n, A or D from Eq. 4.15. Deviations from linearity occur at short times due to the charging of the double layer and at long times due to natural convection.

## 4.4 Magnetic field effects on the chronoamperometric response

The effect of a magnetic field on the diffusion of $Cu^{2+}$ was investigated using chronoamperometry. A potential step of - 500 mV was applied to a copper working electrode in 0.05 M $CuSO_4$ (pH = 0.5) that was initially at the rest potential. The effect of a field of 0.5 T on the resulting current transient is shown in Fig. 4.9.

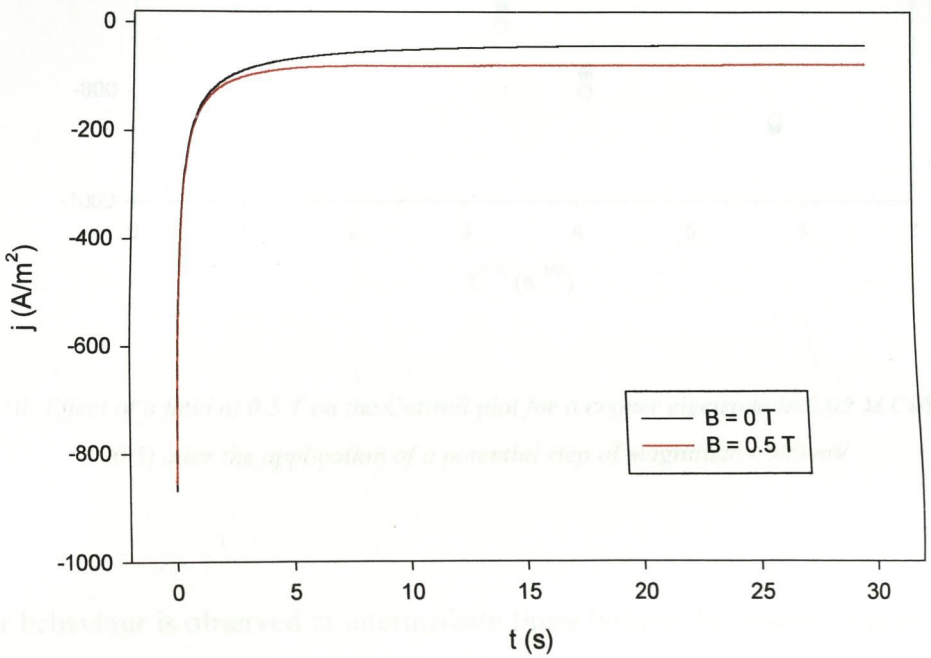


*Fig. 4.9: Effect of a field of 0.5 T on the chronoamperometric response of a copper electrode in 0.05 M $CuSO_4$ (pH = 0.5) after the application of a potential step of magnitude - 500 mV.*

The current density at long times is increased by 85 % in the field, from 43 $A/m^2$ in zero field to 79 $A/m^2$ in a field of 0.5 T. The Cottrell plot for this experiment is shown in Fig. 4.10.

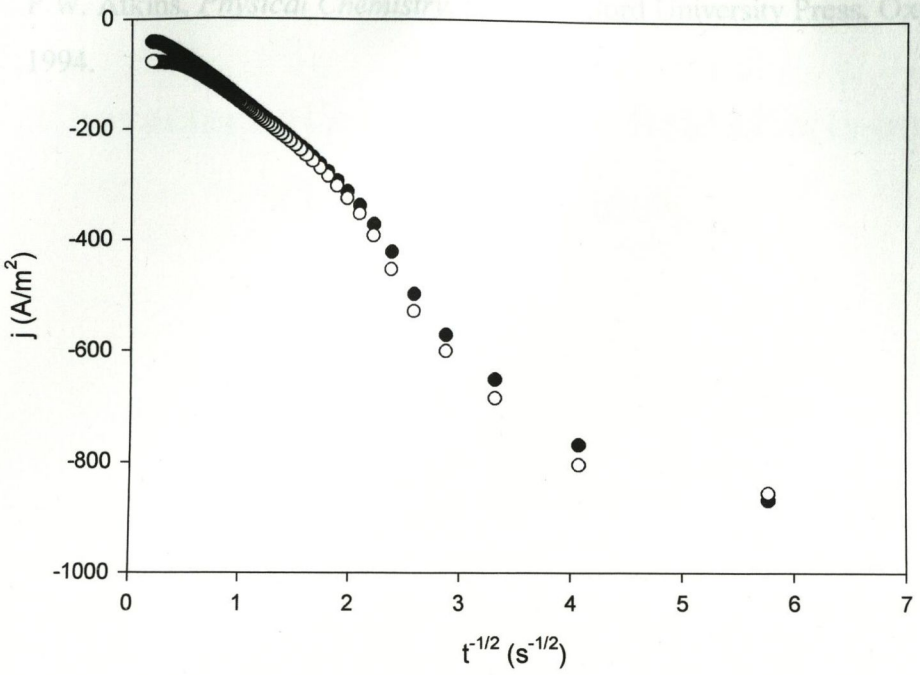


*Fig. 4.10: Effect of a field of 0.5 T on the Cottrell plot for a copper electrode in 0.05 M $CuSO_4$ (pH = 0.5) after the application of a potential step of magnitude - 500 mV.*

Linear behaviour is observed at intermediate times both in the absence and presence of the field. This part of the graph of the graph may be extrapolated to the origin, thereby demonstrating good Cottrell behaviour, and the slope yields a diffusion coefficient of 7 x $10^{-10}$ $m^2/s$, in good agreement with the literature[1]. The value of the diffusion coefficient is unchanged by the field. Deviations from linearity at short times are due to charge ordering in the double layer. Given that these deviations occur for $t^{-1/2} > 2$, we can conclude that the capacitative currents which interfere with the faradaic response are negligible after 250 ms. At long times, the Cottrell plot in a field of 0.5 T levels off before that in zero field. These deviations from linearity at long times are due to convective effects, which prevent further growth of the diffusion layer, so that Eq. 4.15 no longer holds.

## References


1 P.W. Atkins, *Physical Chemistry*, p. C28, Oxford University Press, Oxford, 1994.

# Chapter Five

# Characterisation of magnetic field effects on Cu electrodeposition

## 5.1 Scanning electron microscopy

Scanning electron microscopy (SEM) is a well established diagnostic technique used to examine surface morphology to almost atomic dimensions. The resolution of electron microscopy can be up to 10 nm and a higher depth of focus is achievable compared to optical microscopy. The technique consists of bombarding the sample with a beam of highly focused monochromatic electrons, as shown in Fig. 5.1. The secondary electrons emitted due to the interaction of the beam with the surface are detected as the beam is rastered across the surface. Non-conducting samples may be coated with a thin layer of gold by sputtering in order to prevent the build-up of charge on the surface.

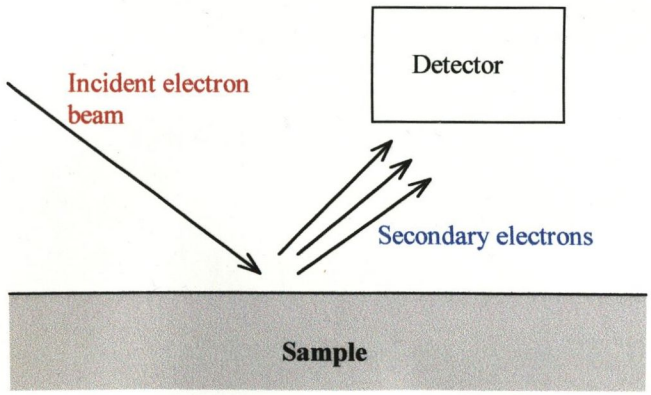


*Fig 5.1: Principle of scanning electron microscopy.*

In addition to providing information about the morphology of the surface, detection of other products of the interaction between the beam and the surface may be used to identify the chemical species present. The detection of back scattered electrons provides information about the atomic mass distribution at the surface. Heavier atoms produce more back scattering leading to brighter areas on the image, while lighter atoms show up as darker areas. The energy spectrum of emitted X-rays may also be measured and the peaks assigned to particular elements. Resolution of 1 μm is

obtainable by this method. The area under the peaks gives an estimate of the percentage composition of the surface. By fixing the energy corresponding to a particular element, it is then possible to produce a map of the surface showing the local distribution of that element.

## 5.2 X-ray diffraction spectroscopy

X-ray diffraction spectroscopy is a powerful tool for the characterisation of crystalline materials. It is a direct probe of the size and structure of the crystal lattice. Diffraction of electromagnetic radiation occurs when the wavelength of the incident radiation is comparable to the interatomic spacing. This condition is satisfied by X-rays, whose wavelength is of order 0.1 nm. The principle of X-ray diffraction spectroscopy is illustrated in Fig. 5.2. X-rays are specularly reflected from successive parallel planes of atoms in the crystal, with each plane reflecting only a tiny fraction of the incident radiation. Diffracted beams may be detected at certain angles where the reflected beams interfere constructively. The position and intensity of these diffracted beams are unique to each crystalline material, which allows for relatively straightforward identification.

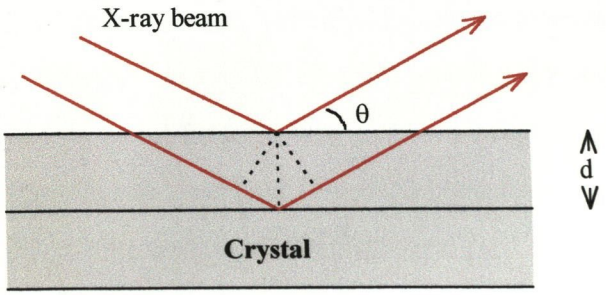


*Fig. 5.2: Principle of X-ray diffraction spectroscopy.*

The Bragg condition expresses the relationship between the interatomic spacing, d, and the diffraction angle, θ. Bragg reflection can only occur for wavelengths of order 2d or less.

$$2d \sin\theta = m\lambda \tag{5.1}$$

In an X-ray diffraction experiment, a monochromatic beam of X-rays is directed at the sample and the intensity of the diffracted radiation is measured as a function of $\theta$. In practice, the position of the X-ray beam usually remains fixed while the sample and detector are rotated. The peaks in the X-ray spectrum obtained may be assigned to different lattice spacings in the crystal.

## 5.3 Analysis of electrodeposited copper

No difference in the appearance of the electrodeposited copper due to the presence of a magnetic field during electrodeposition was observed with the naked eye. In general, dull brown layers of copper were observed at higher pH values and low concentrations, while bright shiny copper layers were obtained at low pH and high concentrations. The dull or shiny deposits are related to the rough and smooth reflectivity on the scale of the wavelength of light (~ 0.5 μm). Glassy carbon working electrodes were used in the analysis of the electrodeposited copper, as the layers could be easily removed, either with double-sided sellotape or with a razor blade.

The effect of the magnetic field on the surface morphology of electrodeposited copper was examined using scanning electron microscopy. Copper films of micron thickness were deposited on a glassy carbon working electrode (diameter 3 mm) from unstirred solutions of 0.75 M $CuSO_4$ at pH 0.5 both in the absence and presence of the field. A standard three-electrode cell was used, with the deposition potential held at - 500 mV until a fixed amount of charge had passed. The films were removed using a razor blade and coated in gold for imaging by scanning electron microscopy. The surface of a representative film deposited in zero field (Fig. 5.3) is compared to that deposited in a field of 0.5 T (Fig. 5.4). The surface of the film deposited in the field is considerably rougher than that deposited in zero field. The surface of a copper film deposited on a glassy carbon rotating disk electrode at 10 rpm is shown in Fig. 5.5 for comparison.

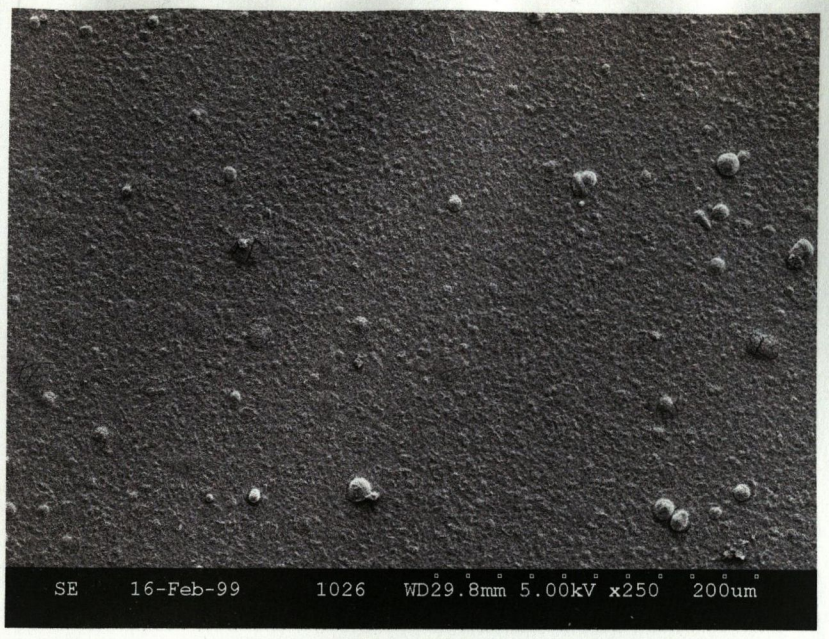


*Fig. 5.3: Scanning electron micrograph of electrodeposited copper from 0.75 M $CuSO_4$ (pH = 0.5) in zero applied field.*

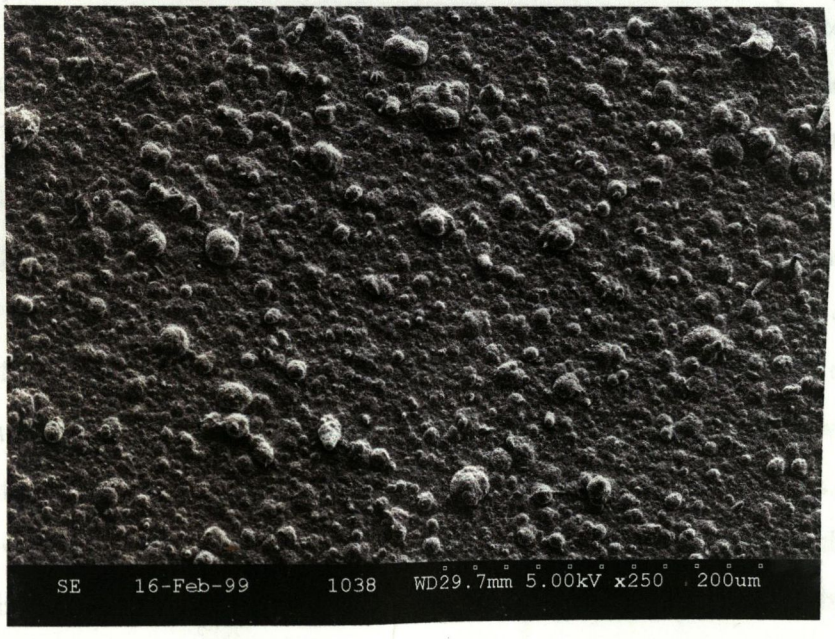


*Fig. 5.4: Scanning electron micrograph of electrodeposited copper from 0.75 M $CuSO_4$ (pH = 0.5) in a field of 0.5 T.*

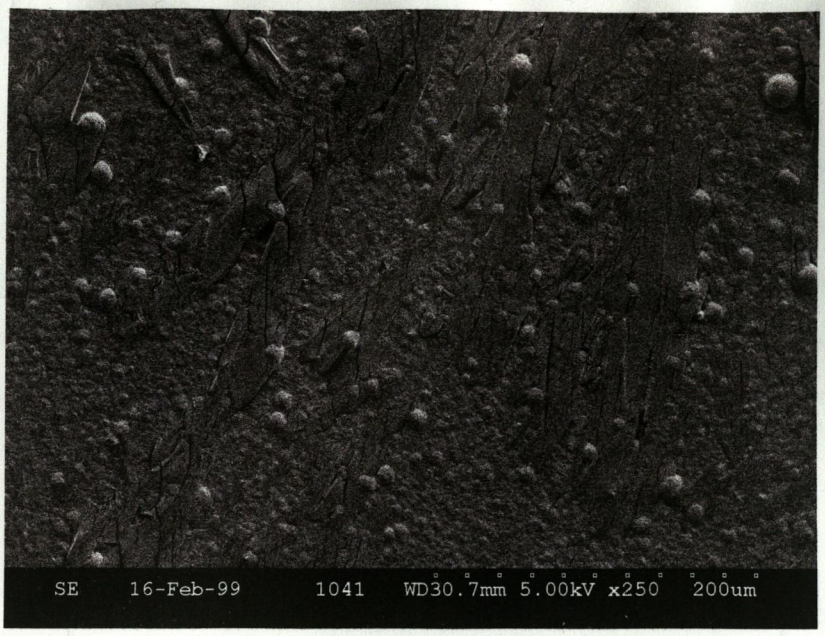


*Fig. 5.5: Scanning electron micrograph of electrodeposited copper from 0.75 M $CuSO_4$ (pH = 0.5) at a rotating disk electrode (10 rpm).*

The effect of the field on the crystal structure of the electrodeposited copper was investigated using X-ray diffraction spectroscopy. A larger glassy carbon electrode, of diameter 7 mm, was used to deposit the copper films, in order to increase the amount of material deposited. The copper was deposited from unstirred solutions of 0.2 M $CuSO_4$ at pH 0.5 at a fixed potential of - 500 mV. In each case the charge passed during this electrodeposition was 4 C, giving an estimated layer thickness of 3.8 μm. The rate of growth of the films was accelerated by the field. Under these conditions, the growth of a 3.8 μm layer of copper in zero field took around 240 s, while in the presence of a field of 0.5 T, the layer had reached this thickness after 180 s. The films were removed using double-sided sellotape, and attached to a microscope slide for X-ray analysis. The X-ray spectra of copper films deposited both in the absence and presence of a field of 0.5 T are shown in Figs. 5.6 and 5.7 respectively. The peaks in both figures are characteristic of fcc copper with a lattice parameter of 0.3615 nm. No significant effect of the field was observed on either the crystalline structure or the texture of the electrodeposited copper.

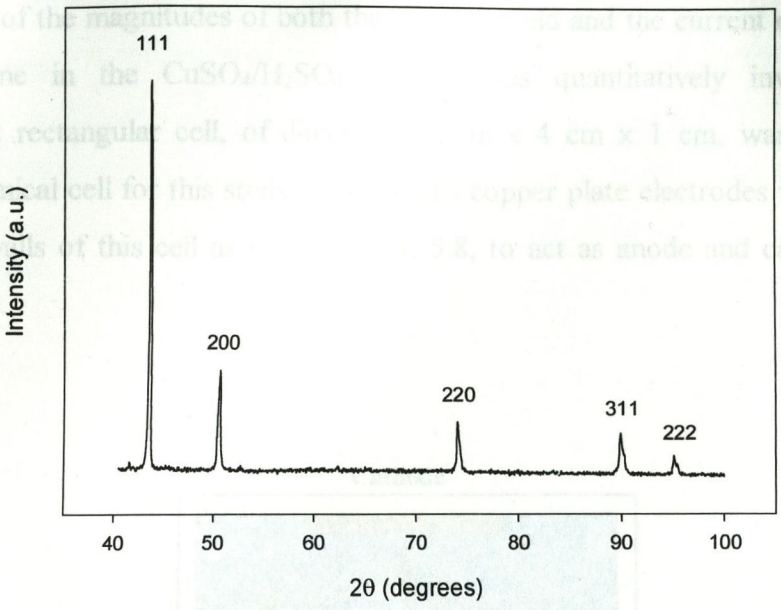


*Figure 5.6: X-ray spectrum of electrodeposited copper from 0.2 M $CuSO_4$ (pH = 0.5) in the absence of an applied field.*

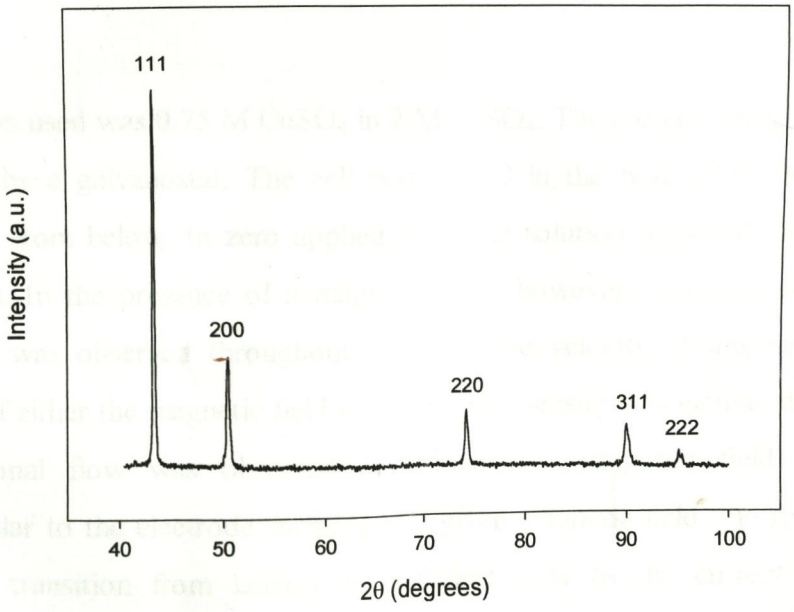


*Figure 5.7: X-ray spectrum of electrodeposited copper from 0.2 M $CuSO_4$ (pH = 0.5) in a field of 0.5 T.*

## 5.4 Characterisation of the flow regime

The effect of the magnitudes of both the magnetic field and the current density on the flow regime in the $CuSO_4/H_2SO_4$ solution was quantitatively investigated. A transparent rectangular cell, of dimensions 4 cm x 4 cm x 1 cm, was used as the electrochemical cell for this study. Two parallel copper plate electrodes were glued to opposite walls of this cell as shown in Fig. 5.8, to act as anode and cathode during electrolysis.

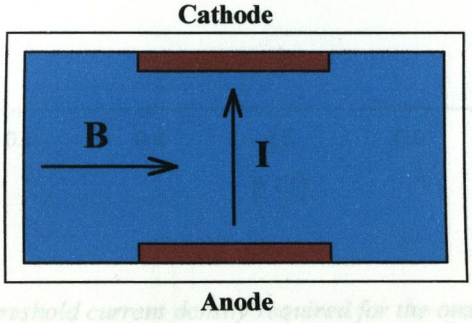


*Fig. 5.8: Rectangular cell used to study the flow regime.*

The solution used was 0.75 M $CuSO_4$ in 2 M $H_2SO_4$. The current through the cell was controlled by a galvanostat. The cell was placed in the bore of the Multimag and illuminated from below. In zero applied field, the solution remained stagnant during electrolysis. In the presence of a magnetic field, however, a rotational flow of the electrolyte was observed throughout the cell. The velocity of this rotational flow increased if either the magnetic field or the current density was increased. In addition, the rotational flow was observed even when the magnetic field was applied perpendicular to the electrode surface. At a given magnetic field, the rotational flow showed a transition from laminar to turbulent flow as the current density was increased. The threshold current density, $j_t$, required to induce the onset of turbulence in the solution was identified visually at several different values of magnetic field. The results are shown in Fig. 5.9.

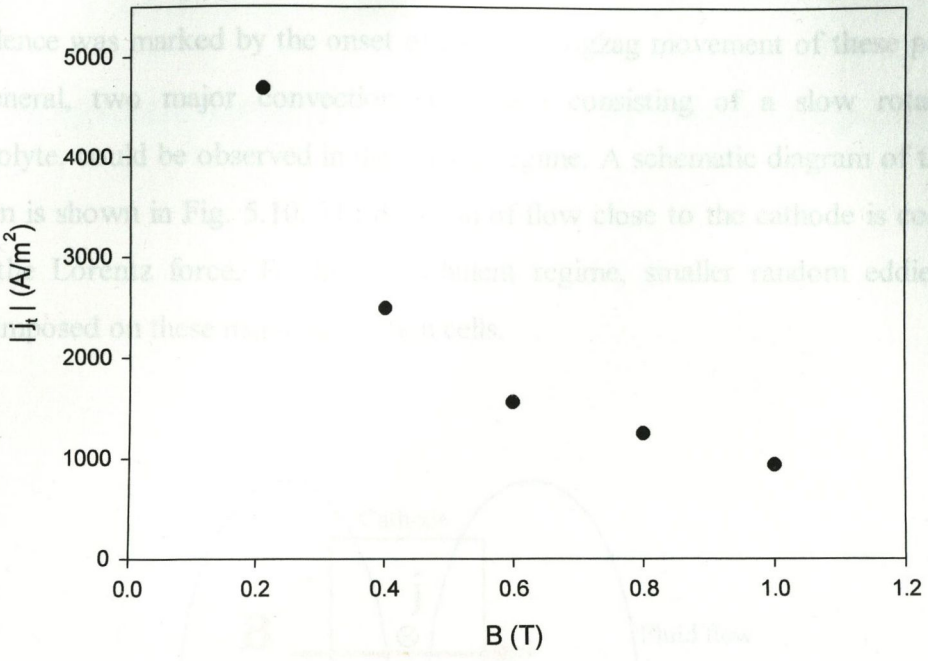


*Figure 5.9: Threshold current density required for the onset of turbulence as a function of magnetic field.*

The threshold current density decreases significantly with increasing magnetic field, from 4700 A/m$^2$ in a field of 0.2 T to 950 A/m$^2$ in 1 T. It was noted that the product $j_tB$ remains practically constant as the field is increased, as shown in Table 5.1.

*Table 5.1: Effect of magnetic field on the product $j_tB$*

| B (T) | $j_t$ (A/m$^2$) | $j_tB$ (N/m$^3$) |
|---|---|---|
| 0.2 | 4700 | 940 |
| 0.4 | 2400 | 960 |
| 0.6 | 1600 | 960 |
| 0.8 | 1200 | 960 |
| 1.0 | 950 | 950 |

The rotational flow in the presence of the field took place throughout the whole cell. The observation of the flow pattern was aided by debris from copper electrodeposits that had been swept off the cathode by the flow of solution. The transition to turbulence was marked by the onset of a random zigzag movement of these particles. In general, two major convection cells, each consisting of a slow rotation of electrolyte, could be observed in the laminar regime. A schematic diagram of the flow pattern is shown in Fig. 5.10. The direction of flow close to the cathode is consistent with the Lorentz force, $F_L$. In the turbulent regime, smaller random eddies were superimposed on these major convection cells.

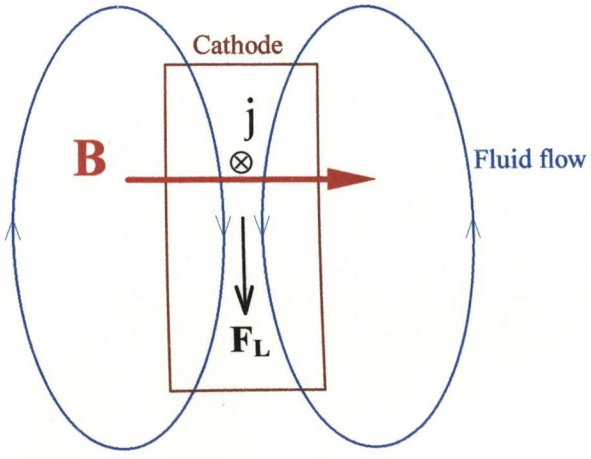


*Fig. 5.10: Relationship between the flow pattern in the cell and the Lorentz force.*

# Chapter Six

# Magnetic field effects on fractal electrodeposits

## 6.1 Fractal geometry

The study of non-Euclidean boundaries is called fractal geometry. It was devised in 1975 by Benoit Mandelbrot[1], who noted that although the coastline of Britain encloses a finite area, it has an infinite perimeter with decreasing length scales. Fractal patterns are common in nature - they are self-similar over a range of length scales, e.g. fern leaves, tree roots and the structure of lungs and clouds. The concept of self-similarity is illustrated in Fig. 6.1. Four stages of the recursive construction of a chequered pattern are shown. At each iteration, the length scale is divided by 2, and each square is replaced by four smaller ones.

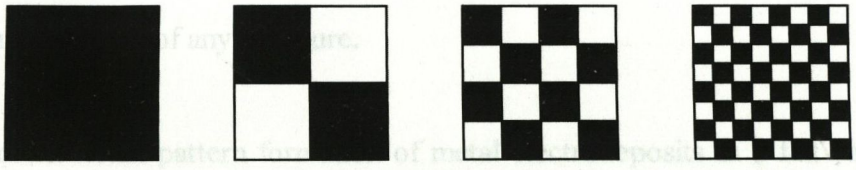

*Fig. 6.1: The concept of invariance under scale transformation.*

The pattern is thus reproduced over an infinite range of length scales and it is impossible to distinguish between different levels of magnification. However, a quantitative measure of this self-similarity may be obtained by considering the scaling of number density with length in such patterns. If we examine the pattern in Fig. 6.1, we find that the number of squares, N, increases as the scale, S, decreases according to:

$$N = S^d \tag{6.1}$$

where d is known as the dimensionality of the structure. For the chequered pattern, d = 2, and for a line, d = 1. These are examples of the familiar Euclidean dimensions.

However, physical systems do not normally display such rigid order, and in general the exponent d is a non-integer. This non-integer exponent is called the fractal dimensionality, $d_f$, and is characteristic of randomness in a structure. The box counting method is the most practical and widely used method of determining the fractal dimensionality. In this method a regular grid, of mesh size s, is superimposed on the structure. The number of boxes, N(s), containing at least part of the structure is determined for a range of different mesh sizes. The fractal dimensionality is then defined by:

$$d_f = \frac{\log N(s)}{\log(1/s)} \tag{6.2}$$

Hence a plot of log N(s) against log (1/s) for meshes of different sizes will yield the fractal dimensionality of any structure.

The two-dimensional pattern formation of metal electrodeposits in a flat circular cell often shows this characteristic fractal form. Although in general the electrodeposition mechanism is complex and may involve several factors, if the reaction is largely diffusion controlled the random nature of the diffusion process leads to aggregates exhibiting fractal geometry. The fractal dimensionality of such deposits is a measure of the ruggedness of their fine structure. The fractal dimensionality of the observed electrodeposits usually varies between 1.5 and 2. A system under pure diffusion control will yield a structure with $d_f = 1.66$[2]. Such a process is known as diffusion limited aggregation (DLA). DLA structures are frequently observed in nature, e.g. the electric discharge during dielectric breakdown, the aggregation of soot particles in the atmosphere, and the phenomenon of viscous fingering, which occurs when a high viscosity fluid is displaced by a lower viscosity fluid in a porous medium. The fractal patterns formed by electrodeposition are sensitive to the electrolyte concentration and applied voltage[3,4] and may be influenced by a magnetic field[5,6].

## 6.2 Magnetic field effects on fractal electrodeposits

Copper electrodeposits were grown from unacidified solutions of 0.2 M $CuSO_4$ in a flat circular cell, shown schematically in Fig. 6.2. The copper ring (inner diameter 22 mm) was set into a Perspex plate with 0.2 mm exposed above the surface. The solution could then be contained in a 0.2 mm film by the addition of an upper Perspex plate, which was held firmly in place by M3 nylon bolts. The central graphite cathode (pencil lead, diameter 0.9 mm) was introduced through a hole in the upper plate. In a typical experiment, a voltage of 6 V was applied between the graphite cathode and the copper anode for 300 s. The resulting electrodeposits were photographed using a digital camera. The cell could be mounted either horizontally or vertically and a Multimag system was used to apply a variable magnetic field in the range 0 - 1 T either parallel or perpendicular to the plane of the cell.

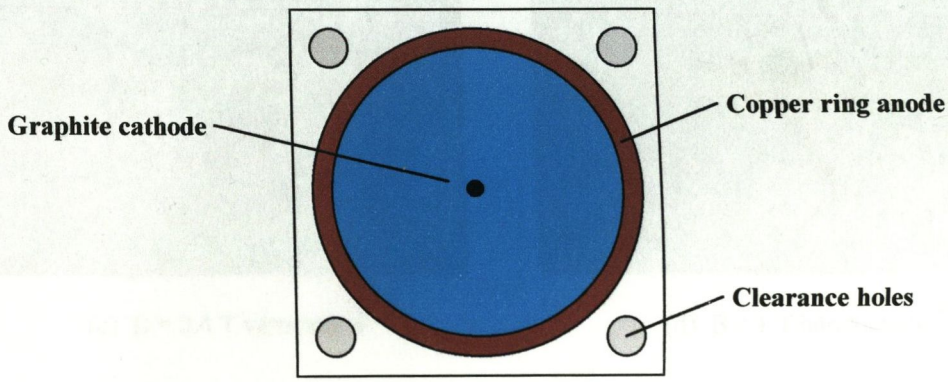


*Fig. 6.2: Flat circular cell used to grow fractal electrodeposits.*

Some typical fractal electrodeposits grown in this cell are shown in Figs. 6.3 and 6.4. With the cell horizontal, dense radial growth is observed in zero field (Fig. 6.3a), but when the field is applied perpendicular to the plane of the cell a branching spiral pattern forms instead (Fig. 6.3b). If the direction of the field is inverted, the chirality of the spiral is reversed (Fig. 6.3c). When the magnetic field is applied parallel to the plane of the cell, a stringy deposit appears (Fig. 6.3d). It was noted that growth of the

stringy deposit predominated in one specific direction perpendicular to the field. Repeated measurements showed that this direction is the one in which the gravitational force and the Lorentz force are acting in unison.

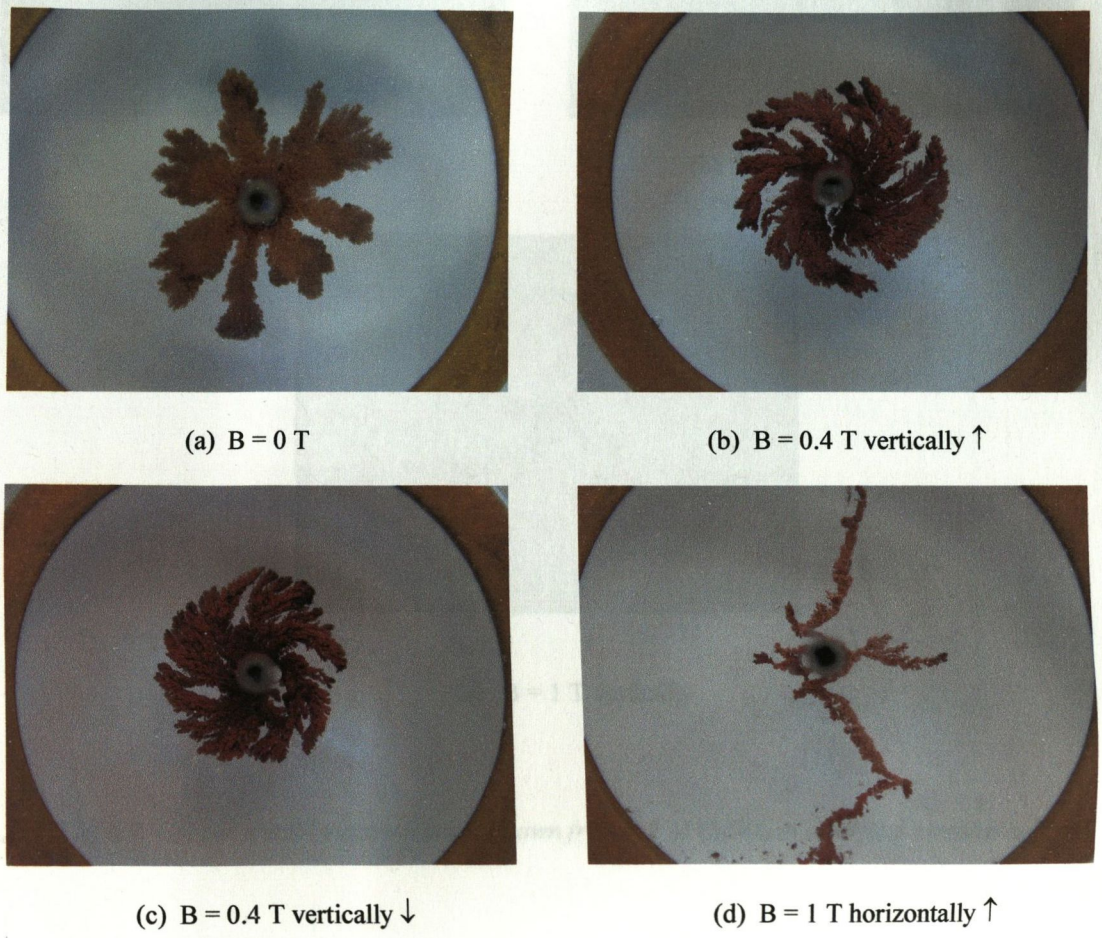

(a) B = 0 T

(b) B = 0.4 T vertically ↑

(c) B = 0.4 T vertically ↓

(d) B = 1 T horizontally ↑

*Fig. 6.3: Copper fractal electrodeposits grown from 0.2 M $CuSO_4$ in a horizontal circular cell.*

With the cell vertical, a dense deposit grows upwards from the electrode in zero field (Fig. 6.4a), but turns into a branching spiral when the field is perpendicular to the plane (Fig. 6.4b). When the field is applied horizontally in the plane of the cell, a stringy pattern is formed with growth again predominating normal to the field direction (Fig. 6.4c). These results are summarized in Table 6.1.

(a) B = 0 T

(b) B = 0.4 T horizontally

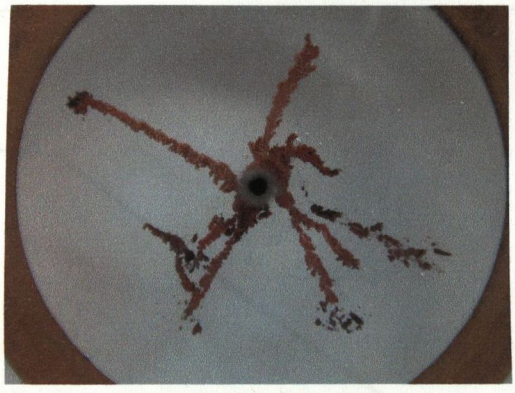

(c) B = 1 T vertically

*Fig. 6.4: Copper fractal electrodeposits grown from 0.2 M $CuSO_4$ in a vertical circular cell.*

*Table 6.1: Summary of different fractal patterns observed in the circular cell.*

| Cell | B = 0 | B = 1 T (vertical) | B = 1 T (horizontal) |
|---|---|---|---|
| Horizontal | dense radial | branched chiral | stringy unidirectional |
| Vertical | dense unidirectional | stringy unidirectional | branched chiral |

The fractal dimensionality of each deposit was determined using the box counting method. Each pixel in the digital image of the structure was converted into either a black or a white pixel according to its contrast level. Then a computer program was used to calculate the number of black pixels, N(s), over a range of different mesh sizes, s. A schematic plot of log N(s) against log (1/s) is shown in Fig. 6.5. The fractal dimensionality is equal to the magnitude of the slope of the linear section of the plot.

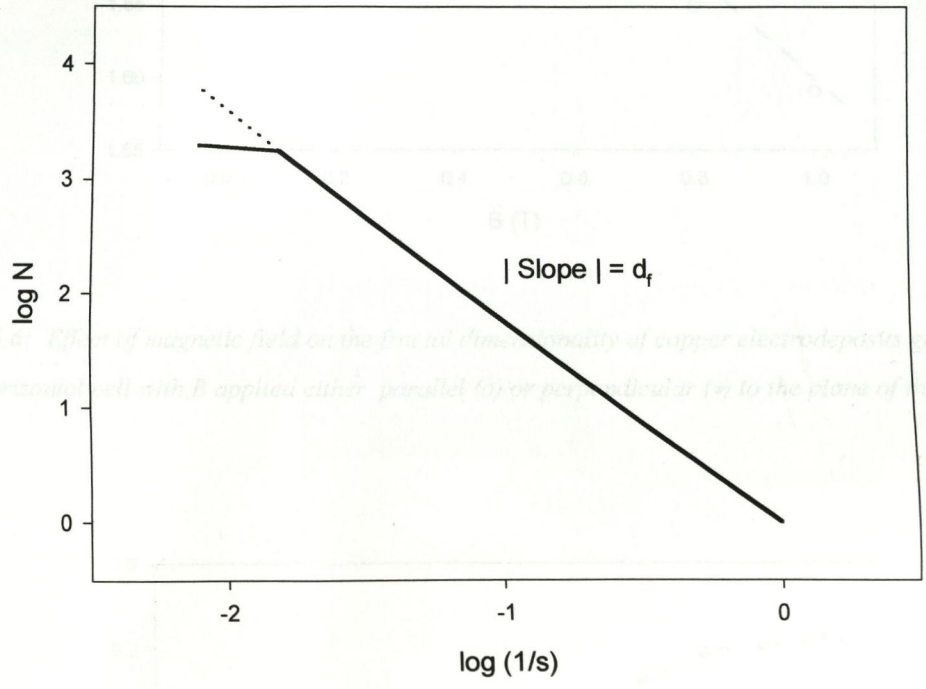


*Fig. 6.5: Schematic plot of log N against log (1/s) for electrodeposited structure.*

The effect of the magnitude of the field on the fractal dimensionality of deposits grown in the horizontal cell is shown in Fig. 6.6. There is a broad increase in fractal dimensionality in a perpendicular field, but a clear decrease, from 1.8 to 1.6, when the field is applied in-plane, corresponding to the increasingly stringy nature of the deposit.

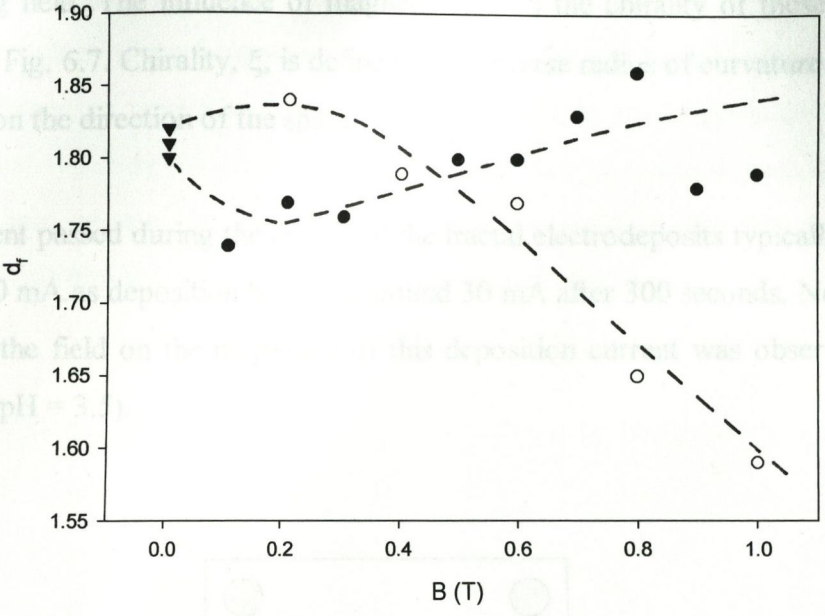


*Fig. 6.6: Effect of magnetic field on the fractal dimensionality of copper electrodeposits grown in a horizontal cell with B applied either parallel (o) or perpendicular (•) to the plane of the cell.*

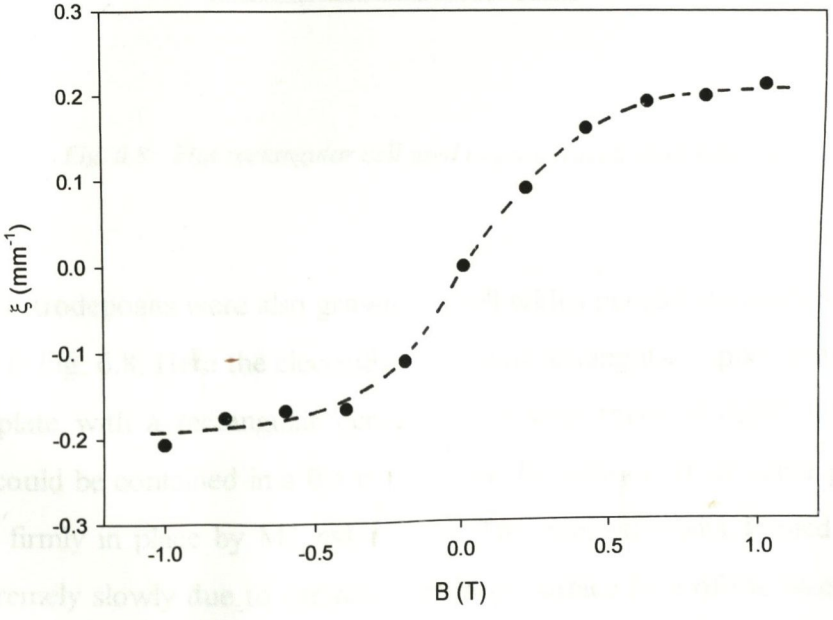


*Fig. 6.7: Effect of magnetic field on chirality of copper electrodeposits grown in a horizontal cell with the field applied vertically.*

The radius of curvature of the main branches of the fractal electrodeposits formed when a field is applied perpendicular to the plane of a horizontal cell decreases with increasing field. The influence of magnetic field on the chirality of these deposits is shown in Fig. 6.7. Chirality, $\xi$, is defined as the inverse radius of curvature and its sign depends on the direction of the spiral.

The current passed during the growth of the fractal electrodeposits typically rises from around 10 mA as deposition begins to around 30 mA after 300 seconds. No significant effect of the field on the magnitude of this deposition current was observed for this solution (pH = 3.5).

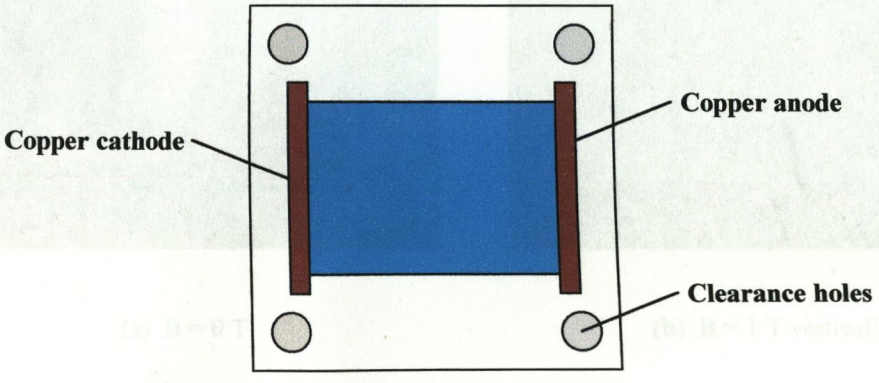


*Fig. 6.8: Flat rectangular cell used to grow fractal electrodeposits.*

Copper electrodeposits were also grown in a cell with a parallel electrode arrangement, as shown in Fig. 6.8. Here the electrodes were two rectangular copper plates set into a Perspex plate with a rectangular depression between them of depth 0.5 mm. The solution could be contained in a 0.5 mm film by the addition of an upper plate, which was held firmly in place by M3 nylon bolts. The electrodeposits formed in this cell grew extremely slowly due to the relatively large surface area of the electrodes. In a typical experiment, a voltage of 12 V was applied between cathode and anode for 45 min.

Some typical electrodeposits grown in the parallel electrode cell are shown in Fig. 6.9. Initially a thin dendritic layer forms over the entire surface of the cathode. Eventually, one or two dendrites extend into the solution and form branching structures. No significant effect of the field was observed on these electrodeposits, although the main dendrite branches tended to become slightly less dense in the presence of the field. The current typically varied from 25 mA at the onset of electrodeposition to 50 mA after 45 min. Again, no significant effect of the field on the magnitude of this deposition current was observed for this solution (pH = 3.5).

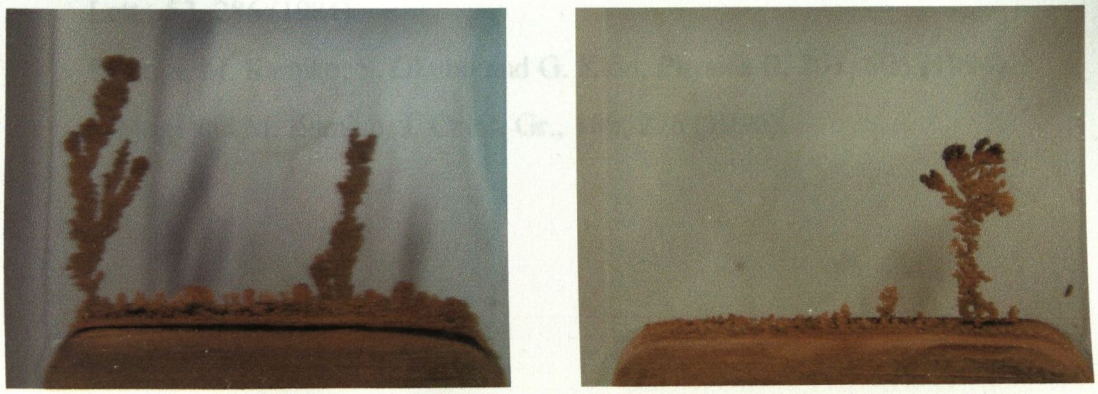

(a) B = 0 T

(b) B = 1 T vertically

*Fig. 6.9: Copper fractal electrodeposits grown from 0.2 M $CuSO_4$ in a horizontal rectangular cell.*

## References


1 B.B. Mandelbrot, *The Fractal Geometry of Nature*, Freeman, New York, 1982.

2 P. Meakin, *Fractals, scaling and growth far from equilibrium*, Cambridge University Press, Cambridge, 1998.

3 D. Grier, E. Ben-Jacob, R. Clarke and L.M. Sander, Phys. Rev. Lett., **56**, 1264 (1986).

4 M. Matsushita, M. Sano, Y. Hayakawa, H. Honjo and Y. Sawada, Phys. Rev. Lett., **53**, 286 (1984).

5 I. Mogi, M. Kamiko, S. Okubo and G. Kido, Physica B, **201**, 606 (1994).

6 I. Mogi and M. Kamiko, J. Cryst. Gr., **166**, 276 (1996).

# Chapter Seven

# Discussion and Future Work

## 7.1 Discussion

A summary of the magnetic field effects observed on copper electrodeposition and electrodissolution in this work is provided in Table 7.1.

*Table 7.1: Summary of magnetic field effects in this work.*

| Property | Measured parameter | Technique | Field effect |
|---|---|---|---|
| Free energy of reaction | Rest potential, $V_{eq}$ | Open circuit | No |
| Electron transfer kinetics | Exchange current density, $j_0$ | LSV | No |
| | Charge transfer coefficients, $\alpha_{a,c}$ | LSV | No |
| | Double layer capacitance | IS | No |
| Mass transport | Limiting current density, $j_L$ | LSV | Yes |
| | Diffusion coefficient, D | IS, CA | No |
| Morphology | Fractal dimensionality, $d_f$ | Box counting | Yes |
| | Chirality, $\xi$ | Ruler | Yes |
| | Surface roughness | SEM | Yes |
| Crystal structure | Lattice parameter, $a_0$ | XRD | No |
| Hydrogen evolution | Current density, j | LSV | Yes |

*(LSV = Linear Sweep Voltammetry, IS = Impedance Spectroscopy, CA = Chronoamperometry, SEM = Scanning electron microscopy, XRD = X-ray diffraction)*

Upon examination of the data presented in this work, the most striking effects of the field are the significant increase in the limiting current and the dramatic change in morphology of the fractal electrodeposits. Since both effects are manifested in mass transport controlled regimes, it is reasonable to assume that the primary affect of the field is to increase the rate of transport of electroactive species to or from the electrode. The enhancement of mass transfer in the field must be due to some force of magnetic origin. There are four possible forces which could be responsible for the observed effects. Two of these are due to the interaction of the field with the magnetic properties of the electrolyte. One is the paramagnetic gradient force, $F_P$:

$$F_P = \frac{B^2 \chi_m \nabla c}{2\mu_0} \tag{7.1}$$

which arises from the variation in the paramagnetic susceptibility of the diffusion layer due to the concentration gradient of $Cu^{2+}$ ions. Here $\chi_m$ is the molar susceptibility of $Cu^{2+}$. The second force is the field gradient force, $F_B$:

$$F_B = \frac{Bc\chi_m \nabla B}{\mu_0} \tag{7.2}$$

which is the force due to the field gradient in the solution, i.e. when the field is non-uniform. $F_P$ and $F_B$ are thus driving forces due to a magnetic energy gradient.

The other two forces - the Lorentz force and the electrokinetic force - are due to the interaction of the field with the electric field or current. The Lorentz force, $F_L$:

$$F_L = q\vec{v} \times \vec{B} \tag{7.3}$$

arises from the motion of charge across lines of magnetic flux, while the electrokinetic force, $F_E$:

$$F_E = \sigma_d E_{\parallel} \tag{7.4}$$

is the force on the charge carriers in the diffuse double layer under the influence of an electric field, $E_{\parallel}$, parallel to the electrode surface. This electric field is created by the interaction of the electric field across the double layer with a magnetic field applied parallel to the electrode surface.

It is difficult to see how a field of the order of 1 T could have a direct effect on the diffusion of $Cu^{2+}$. The instantaneous velocity of $Cu^{2+}$ in aqueous solution is of the order 400 m/s, giving a Lorentz force, $F_L \sim 1.3 \times 10^{-16}$ N. Estimating the time between collisions, $\tau \sim 1$ ps, and using $\Delta v_\perp = F_L \tau / m$, where m is the mass of the $Cu^{2+}$ ion ($1.06 \times 10^{-25}$ kg), we obtain the change in transverse velocity $\Delta v_\perp \sim 10^{-3}$ m/s, which is five orders of magnitude lower than v. The direct influence of the Lorentz force on the diffusive movement of ions in solution is therefore completely negligible. The same order of magnitude argument applies to both the electrokinetic force and the field gradient force. The effect of the paramagnetic force here is also negligible. The driving force for diffusion is:

$$F_D = RT\nabla c \tag{7.5}$$

Both $F_D$ and $F_P$ act along the same line and depend linearly on the concentration gradient. For a field of 1 T, the ratio $F_P/F_D$ is $10^{-6}$ at room temperature. In any case, the enhancement in mass transport is also observed for diamagnetic cations such as $Zn^{2+}$, for which $F_P$ has the opposite sign.

The negligible effect of the field on the diffusion coefficient is confirmed by the impedance data in Fig. 4.6 and by the chronoamperometric data in Fig. 4.10. The slope of the Cottrell plot is unchanged by the application of a 0.5 T field and yields $D = 7 \times 10^{-10}$ $m^2/s$, in good agreement with the literature[1]. However, we have seen that the field does have a dramatic effect on the diffusion limited current density, given by:

$$j_L = nFD\nabla c \tag{7.6}$$

If the diffusion coefficient remains constant, then the concentration gradient, $\nabla c$, must increase in the field. Using the linear approximation, $\nabla c = c_\infty / \delta$ (Fig. 1.2), it is possible to quantify the effect of the field on the thickness of the diffusion layer. From the data

in Fig. 3.4, the diffusion layer thickness as a function of field may be calculated. The results are shown in Fig. 7.1.

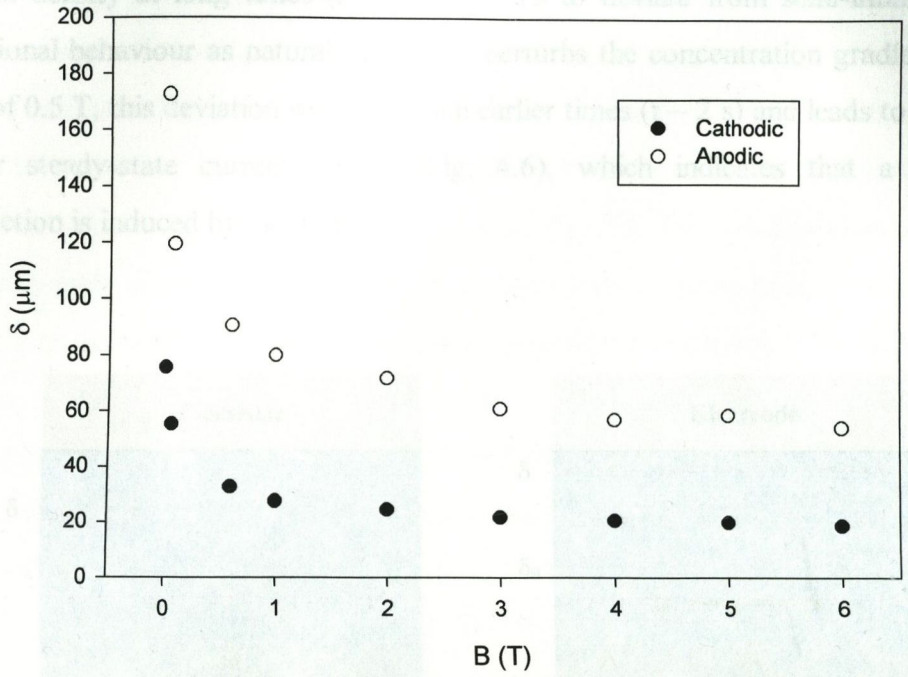


*Fig. 7.1: Effect of magnetic field on the diffusion layer thickness.*

The diffusion layer thickness decreases with increasing field as expected. The greatest decrease occurs in the low field region. Here, the diffusion layer thickness at the cathode decreases from 76 μm in zero field to 28 μm in a field of 1 T, while that at the anode decreases from 173 μm in zero field to 80 μm in 1 T. This narrowing of the region over which the majority of the concentration gradient occurs causes an increase in the diffusional flux to the electrode (cathode) or away from the electrode (anode).

Convection is usually responsible for such a reduction in the diffusion layer thickness. At a given potential, the diffusion layer thickness grows as $t^{1/2}$. Natural convection, arising from density differences in the solution, eventually prevents the diffusion layer from extending any further into the bulk solution and a steady-state concentration gradient results. Forced convection, such as that provided by stirring the solution, may

be used to control the thickness of the diffusion layer. The equivalence of the effect of a 0.5 T field with that of rotating the electrode at 10 rpm (Fig. 3.19) supports the idea that the field acts to induce convection in the solution. Further evidence is provided by the steady-state behaviour observed in the Cottrell plot of Fig. 4.7. In zero field, the current density at long times ($t > 20$ s) begins to deviate from semi-infinite linear diffusional behaviour as natural convection perturbs the concentration gradients. In a field of 0.5 T, this deviation sets in at much earlier times ($t \sim 2$ s) and leads to an 85 % higher steady-state current density (Fig. 4.6), which indicates that a stronger convection is induced by the field.

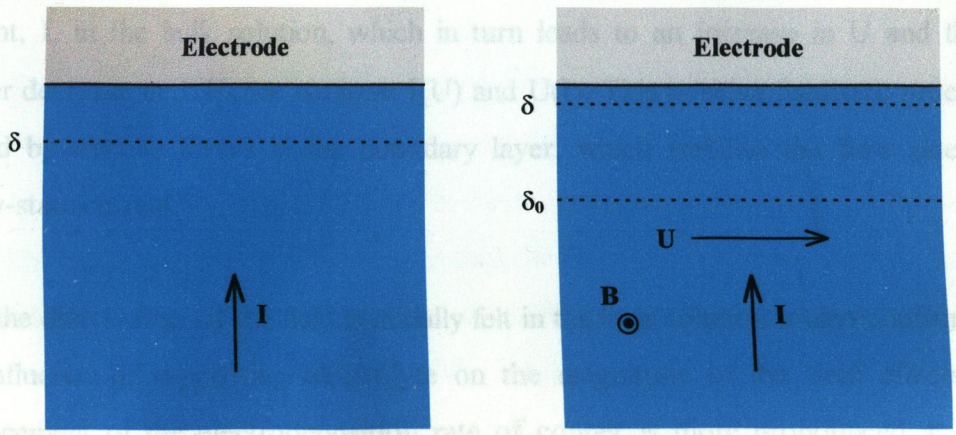


*Fig. 7.2: Effect of Lorentz force on the diffusion layer thickness, δ, during electrodeposition. $\delta_0$ is the boundary layer thickness.*

The direct effect of the field on the convective flow should take place outside the diffusion layer, i.e. in the bulk solution. This is because within the diffusion layer, transport by convection is negligible since $D\nabla c >> v\nabla v$. This is supported by the observations in Section 5.4, which show that rotative convection occurs throughout the cell. We have seen in Section 1.4 how a tangential velocity, U, of electroactive species can bring about a significant increase in the concentration gradient in the diffusion layer. It is clear that this velocity has its origins in the entrainment of $Cu^{2+}$ in the convective flow of the solvent. Since the flow of current is normal to the electrode

surface, a tangential flow could be induced by the Lorentz force. A schematic view of this process for the electrodeposition of copper is shown in Fig. 7.2.

In the absence of an applied field the diffusion layer thickness is a function of concentration, potential and time. Holding these constant we observe a steady diffusion layer thickness, $\delta$, as shown on the left hand panel of Fig. 7.2. If we then apply a magnetic field, the Lorentz force induces a tangential velocity component, U, in the bulk solution. This leads to the formation of a hydrodynamic boundary layer of thickness $\delta_0$, as shown in the right hand panel of Fig. 7.2. The velocity gradients in the boundary layer create mixing in the diffusion layer thus reducing its thickness. The net result is an increase in the rate of diffusion towards the electrode. This increases the current, I, in the bulk solution, which in turn leads to an increase in U and thus a further decrease in $\delta$. Hence we have I(U) and U(I). This positive feedback process is limited by viscous forces in the boundary layer, which stabilise the flow rate at a steady-state current.

That the direct effect of the field is initially felt in the bulk solution is also confirmed by the influence of supporting electrolyte on the magnitude of the field effects. The enhancement of the electrodeposition rate of copper is more pronounced at higher concentrations of supporting electrolyte (low pH). This effect is also observed if $Na_2SO_4$ is used as the supporting electrolyte (Fig. 3.9). In quiescent solution, transport in the bulk solution occurs primarily through migration. In acidified copper sulphate solution, this migrational transport is mainly due to the supporting electrolyte. The relative contributions of each ion in solution to the overall conductivity may be estimated from the transport number, $t_i$, defined by:

$$t_i = \frac{|z_i| c_i \mu_i}{\sum |z_j| c_j \mu_j} \qquad (7.7)$$

where $z_i$ is the charge on the ion, and $\mu_i$ is the ionic mobility. The transport number of an ion in a given solution is thus the ratio of its own conductivity to the total

conductivity of the solution. The mobilities of $H^+$, $SO_4^{2-}$ and $Cu^{2+}$ in aqueous solution are shown in Table 7.2.

*Table 7.2: Mobilities of ions in aqueous solution at 25 ℃.*

| Ion | $\mu$ (x $10^{-8}$ $m^2s^{-1}V^{-1}$) |
|---|---|
| $H^+$ | 36.2 |
| $SO_4^{2-}$ | 8.3 |
| $Cu^{2+}$ | 5.6 |

From Eq. 7.7, the transport numbers of the ions in 0.75 M $CuSO_4$ at pH 0.5 are calculated to be 0.46 ($H^+$), 0.37 ($SO_4^{2-}$) and 0.17 ($Cu^{2+}$). This demonstrates that only 17 % of the current is carried by $Cu^{2+}$ in the bulk solution. The effect of the field on the migration of supporting electrolyte is thus the main cause of convection in the cell. In the absence of supporting electrolyte, the effect of the field is reduced due to the lower conductivity of the bulk solution (Fig. 3.8). Of course, within the diffusion layer, the entire current is due to diffusion of $Cu^{2+}$, except when the hydrogen evolution reaction is taking place.

It has been noted in recent literature[2] that the rate of transport of electrically neutral species, such as nitrobenzene, can also be significantly enhanced by an external static magnetic field. Since the Lorentz force acting on a neutral species is zero, the enhancement in mass transport must occur through the convective effect of the field on the supporting electrolyte. The Lorentz force may thus be represented as a magnetic body force acting on a fluid element through which a distributed and continuous current passes, rather than in terms of the direct influence of the field on the random motion of individual ionic species. The magnetic body force per unit volume is given by:

$$F_L = \vec{j} \times \vec{B} \tag{7.8}$$

The tangential velocity may be related to this body force through the Navier-Stokes equation (Eq. 1.31) to obtain:

$$\tfrac{1}{2}\rho U^2 = jBL \tag{7.9}$$

when the field is applied at right angles to the flow of current. Here L is the length of the electrode. Taking a typical value for j ($10^3$ A/m$^2$), it follows from Eq. 7.9 that the tangential velocity induced by the field at an electrode with dimensions of 1 cm should be of order 0.1 m/s. This is in agreement with the experimentally observed flow rates in Section 5.4. The relationship between the diffusion layer thickness and the tangential velocity derived in Section 1.4 was:

$$\delta \approx D^{1/3}\nu^{1/6}\sqrt{\frac{x}{U}} \tag{7.10}$$

Taking x ~ 1 cm, $\nu \sim 10^{-6}$ m$^2$/s and U ~ 0.1 m/s, we obtain $\delta \sim 28$ μm in a field of 1 T, in excellent agreement with the experimental data in Fig. 7.1.

The reduction in the magnitude of the magnetic field effects under various conditions adds further weight to the notion that field induced convection in the bulk solution is the dominant effect. The current enhancement at a rotating disk electrode, where forced convection due to the rotation of the electrode is far stronger than the field induced convection, is reduced to only 2 or 3 % (Fig. 3.18). A similar reduction in current enhancement is observed at microelectrodes, under conditions of enhanced diffusion (Fig. 3.20). Most convincing though, is the effect of adding glycerol to the solution. A gradual reduction in the effect of the field on the limiting current as a function of glycerol concentration is observed (Fig. 3.16). This is because as the

glycerol concentration is increased, the viscosity of the solution increases, leading to damping of the field induced convection.

Experiments in both high and low fields show that the limiting current at low pH during both electrodeposition and electrodissolution varies approximately as $B^{1/3}$, in agreement with other reports in the literature[3-5]. The scale of the magnetic effect is comparable in both processes. The fact that the exponent $m << 1$ means that a large part of the effect of the field on mass transport is achieved in relatively low fields, ~ 1 T (Fig. 3.4). The data are in particularly good agreement with experiments carried out by Aogaki et al[3], who derived the $B^{1/3}$ dependence by incorporating the effect of the Lorentz force on the current flow into the Navier-Stokes equation. However, their derivation is applicable only the orthogonal geometry of their channel electrode cell and does not explain the independence of the magnetic field effects observed here on field direction and electrode orientation.

The limiting current was found to vary linearly with concentration in zero field and approximately as $c_\infty^{4/3}$ in a field of 0.5 T at constant pH. Similar power dependencies have been observed by Aogaki et al[3] with copper sulphate and by Leventis et al[5] with various electroactive organic compounds.

The transition from laminar to turbulent flow as the current density is increased at constant magnetic field provides further evidence that the field effects scale with the Lorentz force. The bulk flow velocity, U, is given by rearrangement of equation 7.9:

$$U = \sqrt{\frac{2jBL}{\rho}} \tag{7.11}$$

When this velocity is substituted into the equation for the Reynolds number (Eq. 1.33), we obtain the magnetic Reynolds number, $Re_m$:

$$Re_m = \sqrt{\frac{2jB}{\rho}} \frac{L^{3/2}}{\nu} \qquad (7.12)$$

The observation that the transition to turbulence occurs at a constant value of the product $j_tB$ (Table 5.1) provides qualitative support for this form of $Re_m$. Taking $j_tB \sim 950$ N/m$^3$, $L \sim 1$ cm, $\rho \sim 1000$ kg/m$^3$ and $\nu \sim 10^{-6}$ m$^2$/s, yields $Re_m \sim 1400$, which compares favourably to the Reynolds number for a flat plate, $Re \sim 1500$. Further work is required to determine whether the transition to turbulence depends on L and $\nu$ as predicted by Eq. 7.12.

The effect of the field on the kinetics of the electrode reaction has been the subject of much debate in the literature. Tafel plots were taken in a regime of strong forced convection, in order to eliminate any mass transport field effects on the electrode process. The exchange current density for $Cu^{2+}/Cu$ was determined to be 10 A/m$^2$ from both the impedance data (Fig. 4.5) and from the Tafel plots (Fig. 3.17). This is an intermediate value, which suggests that the reaction may be considered quasi-reversible. The well defined Tafel behaviour and the depressed semicircle in the Nyquist plot strongly support this hypothesis. According to the Tafel plots, no change in any of the kinetic parameters was observed in a field of 0.5 T. However, the impedance data indicate that the exchange current density decreases to 6 A/m$^2$ in 0.5 T. The discrepancy between the two experiments may be related to the fact that the Tafel plots were carried out in a regime of forced convection, while the impedance data were collected in stagnant conditions. The decrease in exchange current density in the field according to the impedance experiments may then be ascribed to an indirect mass transport effect, rather than a direct effect on the electron transfer kinetics. The field-induced convection may decrease the number of active sites leading to a lower exchange current density. The kinetic data from the Tafel plots should be more reliable since the very strong forced convection prevents any mass transport effects from interfering with the electrode kinetics. The conclusion that the field has no effect on the kinetics is in agreement with Chopart et al[4] and Devos et al[6].

From the Tafel plots, the cathodic transfer coefficient was found to be 0.45, which is consistent with a rate determining step involving a one electron transfer. The values for $j_0$ and $\alpha_c$ are in good agreement with the values established in the classic paper by Mattsson and Bockris[7]. However, the anodic Tafel slope was found to be exactly half that of the cathodic branch, rather than one third as observed by Mattsson and Bockris, yielding $\alpha_a = 0.9$. The reason for this difference is not clear. In any case, the behaviour is unchanged in the presence of the field. From the value of the cathodic transfer coefficient, we can conclude that during electrodeposition the electron transfer proceeds in two steps:

$$Cu^{2+}_{aq} + e^- \xrightarrow{\text{slow}} Cu^{+}_{aq}$$

$$Cu^{+}_{aq} + e^- \xrightarrow{\text{fast}} Cu$$

The first step is rate determining. It is possible in principle that a magnetic field could effect the rate of such a reaction. There have been many studies of magnetic field effects on the rates of chemical reactions, but to date the only well established effects have been those on the recombination of radical pairs[8,9]. Applied magnetic fields either enhance or impede the coherent oscillation of the radical pair between its singlet and triplet states thereby modifying the rate of recombination. However, it is unlikely that a magnetic field could influence the rate of a heterogeneous reaction, since the magnetic energy is negligible compared to both the thermal energy and the electrostatic potential energy.

The fact that no field effect is observed on the rest potential should not be surprising either. The rest potential is determined by the chemical equilibrium between aqueous $Cu^{2+}$ and metallic Cu and is therefore entirely governed by thermodynamic parameters. Even in a field of 6 T, the magnetic energy in a paramagnetic system is still several orders of magnitude lower than the activation energy or the thermal energy. The ratio of the magnetic energy, $E_M$, to the thermal energy, $E_T$, is given by:

$$\frac{E_M}{E_T} = \frac{B^2 \chi_m}{2\mu_0 RT} \qquad (7.13)$$

For a paramagnetic system, $\chi_m \sim 10^{-8}$ $m^3/mol^{-1}$, and this ratio is $10^{-6}$ in a field of 1 T at room temperature. However, for a ferromagnetic material the magnetic energy is $BMV_m$, where M is the magnetisation of the material and $V_m$ is the molar volume (~ $10^{-5}$ $m^3$), which does become only an order of magnitude smaller than the thermal energy in high fields (B ~ 10 T). Application of a magnetic field to a ferromagnetic system causes the chemical equilibrium to shift to the side which has the greater magnetisation, in order to minimise the magnetic energy. Such an effect was reported by Yamamoto et al[10] on the equilibrium between the ferromagnetic hydride $LaCo_5H_x$ and hydrogen, in fields in the range 2 - 14 T. A general thermodynamic theory of magnetic field effects on chemical equilibria has been published by Yamaguchi et al[11]. Waskaas and Kharkats[12] have reported shifts of the order of tens of millivolts in the rest potentials of Fe, Ni and Co electrodes in paramagnetic solutions of their ions, in fields of up to 0.8 T. These effects are inexplicably large, since the energy shifts due to the ferromagnetic magnetisation in 0.8 T are 0.11, 0.03 and 0.08 mV respectively. However, no such effect is seen with copper. The decrease in rest potential in the field observed after a potential sweep from + 2 V, shown in Fig. 3.21, may be ascribed to concentration polarisation of the working electrode due to the higher currents flowing as a function of field. This is an example of a mass transport effect manifesting itself in the activation regime.

Mass transport is also the rate-limiting factor during the growth of the fractal electrodeposits. It is well known that the pattern formation of such deposits is very sensitive to the growth conditions. The fractal dimensionality of zinc deposits has been shown to increase with both electrolyte concentration and voltage as their form changes from diffusion limited aggregation (DLA) to dendritic[13,14]. The deposits we observe are characterized as intermediate between DLA and dendritic in form. The broad increase in fractal dimensionality as a function of B, when the field is perpendicular to the plane of the horizontal cell, is related to the more compact spirals

formed as the field is increased. The increasingly stringy nature of the deposits grown when the field is parallel to the plane of this cell is reflected in the sharp decrease in $d_f$ with field for this orientation. The deposits grown in the horizontal cell with a vertical magnetic field are similar in nature to those reported by Mogi et al[15,16].

The results with the vertical cell establish unambiguously that convection of the solvent near the cathode is important for mass transport. The competition between the Lorentz force and natural convection has a direct bearing on the observed pattern formation. Evidence that the magnetic body force is significant is seen in the unidirectional nature of the stringy deposits whenever B is applied in-plane, and particularly the fact that these strings tend to grow in the sense where the gravitational force and the Lorentz force add (Figure 6.3d). Further evidence is the change from unidirectional to branched when the cell is vertical and the field is applied perpendicular to the cell. (Fig. 6.4b). The relevant quantity here is the dimensionless ratio:

$$R_g = \frac{jB}{\Delta\rho g} \tag{7.14}$$

where $\Delta\rho$ is the density difference between the copper-rich and copper-depleted electrolyte. $R_g$ will be 1 when the Lorentz and gravitational body forces are equal in magnitude. For the fractal electrodeposits, $j \sim 2 \times 10^5$ A/m$^2$ at the beginning of the experiment and $\Delta\rho \sim 100$ kg/m$^3$ so $R_g \sim 1$ when $B = 5$ mT. This argument demonstrates that even relatively low fields can produce large effects. Experimentally, the chiral behaviour exhibited by the deposits shown in Figs. 6.3b and 6.3c was observed in fields as low as 5 mT. This chiral behaviour may be modelled by superimposing a field dependent probability of moving in a particular direction on random walkers on a square lattice[17].

The most notable feature of the field effects on fractal growth is the marked dependence of the pattern formation of the copper electrodeposits on the relative orientations of cell and magnetic field. This is in contrast to the independence of the

magnetic field effects on electrode orientation and field direction for the electrochemical measurements described in Chapters 3 and 4. This difference may be ascribed to the effect of the constrained geometry of the fractal cell on the convection cells in the solution. Since the field effects scale with current density, they should be most pronounced where the deposition occurs at points, such as those at the end of fractal branches or at rough electrode surfaces.

The chirality of the fractal electrodeposits grown in the horizontal cell with the field applied vertically may be accounted for by the asymmetry of the Lorentz force. Data from the electrochemical experiments suggest that the force is exerted on the ionic current in the bulk solution. An alternative theory is that the chirality is due to the Hall effect on the flow of electronic current within the copper fractal branches themselves. This idea is illustrated in Fig. 7.3.

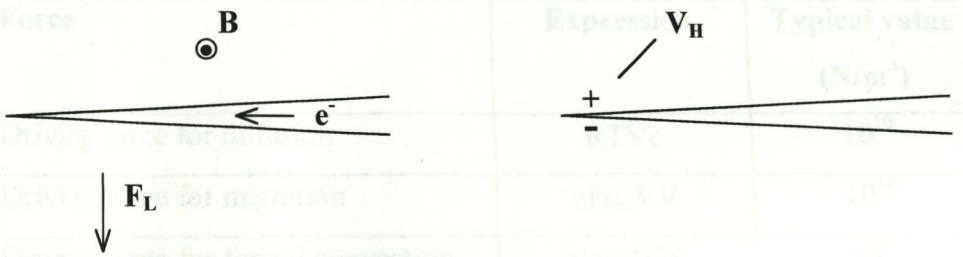


*Fig. 7.3: Hall effect on chirality of fractal electrodeposits.*

In this model, the action of the Lorentz force on the motion of electrons in the already deposited copper fractal branches leads to a Hall voltage, $V_H$, across the branch. If the Hall voltage is significant, there will be a difference in potential on either side of the tip, as shown in the right hand panel of Fig. 7.3. Since most of the growth occurs at the tip, deposition should occur preferentially on the more negative side of the tip, causing the fractal branch to spiral anticlockwise, as observed experimentally (Fig. 6.3b). The Hall electric field at the tip is given by:

$$E_H = jBR_H \tag{7.15}$$

where the Hall coefficient for copper, $R_H = -5.5 \times 10^{-11}$ $m^3/C$. The current density at the tip may be high enough for this electric field to influence the preferential deposition of copper on one side of the tip. However, this theory predicts that the direction of spiral for zinc should be opposite to that of copper, since $R_H$ is of opposite sign. This is not observed experimentally. The absence of any magnetic field effects on the electrode kinetics (Fig. 3.17) added to the fact that the deposits are grown under mass transport control therefore lead us to conclude that the observed effects originate entirely in the bulk solution.

*Table 7.3: Typical forces acting in aqueous copper sulphate solution*

| **Force** | **Expression** | **Typical value ($N/m^3$)** |
|---|---|---|
| Driving force for diffusion | $RT\nabla c$ | $10^{10}$ |
| Driving force for migration | $zFc_\infty \nabla V$ | $10^{10}$ |
| Driving force for forced convection | $\rho(r\omega)^2/2\delta_0$ | $10^5$ |
| Driving force for natural convection | $\Delta\rho g$ | $10^3$ |
| Viscous drag | $\eta\nabla^2 v$ | $10^2$ |
| Paramagnetic force | $B^2\chi_m\nabla c/2\mu_0$ | $10^4$ |
| Field gradient force | $Bc_\infty\chi_m\nabla B/\mu_0$ | $10^1$ |
| Lorentz force | $\vec{j} \times \vec{B}$ | $10^3$ |
| Electrokinetic force | $\sigma_d E_\parallel/\delta_0$ | $10^3$ |
| Magnetic damping force | $\sigma\vec{v} \times \vec{B} \times \vec{B}$ | $10^1$ |

*($T = 298$ K, $c_\infty = 10^3$ mol/m$^3$, $\delta = 10^{-4}$ m, $z = 2$, $V = 1$ V, $\rho = 10^3$ kg/m$^3$, $d = 10^{-2}$ m, $\omega = 10^2$ rad/s, $\delta_0 = 10^{-3}$ m, $\Delta\rho = 10^2$ kg/m$^3$, , $\eta = 10^{-3}$ Ns/m$^2$, $v = 10^{-1}$ m/s, $B = 1$ T, $\chi_m = 10^{-8}$ m$^3$/mol, $\nabla B = 1$ T/m, $j = 10^3$ A/m$^2$, $\sigma_d = 10^{-1}$ C/m$^2$, $E_\parallel = 10$ V/m, $\sigma = 10^2$ $(\Omega m)^{-1}$).*

A summary of the main forces acting in copper sulphate solution is given in Table 7.3. The three dominant forces in the absence of an applied field are the driving forces due to diffusion, migration and forced convection (for the case of a rotating disk electrode). Their relative magnitudes may be somewhat misleading for several reasons. Firstly, the quoted driving force for diffusion applies only in the diffusion layer; in the bulk solution this force is negligible. Secondly, although the driving force for migration is significantly larger than that for forced convection, its effect in terms of material flux is many orders of magnitude smaller. One reason for this is the microscopic scale of the interaction (the drift velocity, $v_d \sim 5.6 \times 10^{-6}$ m/s for $Cu^{2+}$), the other is that the electric field tends to be screened out by the presence of the other charged species in solution. In quiescent solution, the net rate of migration in the bulk solution is essentially controlled by the rate of diffusion in the diffusion layer. The migrational current flows through the bulk solution to compensate for the charge imbalance at each electrode, thus preserving electroneutrality. In stirred solutions, however, the flux of material occurs on a macroscopic scale and convection is the dominant transport mechanism.

Of the five magnetic forces listed in Table 7.3, we have already seen that the Lorentz force has a significant effect on the diffusion limited current during an electrode process. The asymmetry of the fractal electrodeposits provides clear evidence that the Lorentz force is at least comparable to that driving natural convection. Could any of the other forces exert a comparable influence on the convection? In recent years, several papers have been published[18-20] claiming that the paramagnetic gradient force is responsible for current enhancements at microdisk electrodes. However, it is not clear how such a force could have any effect on the rate of transport of electroactive species. Unlike the Lorentz force, which as we have shown acts in the bulk solution, the paramagnetic force only becomes significant in the diffusion layer. It arises from the gradient in paramagnetic susceptibility due to the concentration gradient of paramagnetic $Cu^{2+}$ ions in this region. However, since it acts along the same line as the thermodynamic driving force for diffusion, it would have to be comparable in magnitude to this force to have any significant effect. The ratio of these two forces is:

$$\frac{F_P}{F_D} = \frac{B^2 \chi_m}{2\mu_0 RT} \tag{7.16}$$

This ratio is equal to the ratio of magnetic energy to thermal energy, given by Eq. 7.13, which is of order $10^{-6}$ at room temperature. Therefore, we expect this force to have a negligible effect on mass transport. As mentioned previously, the only scenario in which it is envisaged that the magnetic energy might play a role in a uniform field is in the determination of chemical equilibria for ferromagnetic systems in high fields.

The magnetic energy gradient does become significant in non-uniform fields. In the permanent magnet flux sources used in this work, the field gradient force is of order 10 $N/m^2$ (1% of the Lorentz force). The interference of this force with the effect of the Lorentz force may explain the independence of the field effects on the orientation of the field. This force becomes dominant as the field gradient increases ($\nabla B >> 1$ T/m).

Recent work by Olivier et al[21] has shown that the effect of a magnetic field on the limiting current is equivalent to that produced by the application of a tangential electric field close to the electrode surface. Such an electric field may be created by the use of a non-equipotential working electrode or by the application of a magnetic field parallel to the electrode surface. The electrokinetic force, $F_E$, on the charge density, $\sigma_d$ ($C/m^2$), in the diffuse double layer induces a tangential convection which is transmitted to the bulk solution via viscous forces. This force per unit area, given by Eq. 7.3, acts on the scale of a few nanometers from the electrode surface and may be compared to the other body forces in Table 7.3 by dividing by a characteristic length, x, and then scaling with the dimensions of the hydrodynamic boundary layer, $\delta_0$. Taking $x \sim 1$ nm gives $F_E \sim 10^9$ $N/m^3$, which when scaled by a factor $x/\delta_0$ yields $F_E \sim 10^3$ $N/m^3$, which is comparable in magnitude to the Lorentz force. Both forces are similar in origin; the main difference between them is the scale on which they operate. The question remains as to whether the flow on a microscopic scale drives the macroscopic flow or vice

versa. Since both forces are comparable in magnitude it is likely that both play some role in the interplay between the two scales of flow.

The magnetic damping force listed in Table 7.3 is negligible in aqueous solution, where the conductivity is relatively low $\sigma \sim 10^2$ $(\Omega m)^{-1}$. In conducting melts such as those used in metal and semiconductor processing, $\sigma \sim 10^6$ $(\Omega m)^{-1}$ and this force becomes significant. The extensive use of static magnetic fields to control convection during growth of crystals such as silicon from conducting melts[22] depends on this damping force. The argument is that longitudinal flow in the direction of B is unimpeded, but transverse flow with velocity v is damped because it is opposed by a force[23]:

$$F = \sigma \vec{v} \times \vec{B} \times \vec{B} \tag{7.17}$$

where $\vec{v} \times \vec{B}$ is the non-electrostatic field due to the applied magnetic field. In such conditions, the magnetic damping force is of order $10^4$ in a field of 1 T.

Given the asymmetric nature of the both the Lorentz force and the electrokinetic force, the independence of the diffusion limited current on the orientation of the applied magnetic field is somewhat surprising. However, the rotational flow observed in the cell when the field is applied perpendicular to the electrode surface is further proof that convection is induced here too. The explanation may be related the migrational current distribution in the bulk solution, shown schematically in Fig. 7.4, although the field gradient force may also have some influence here, as the cell occupies a greater volume of the magnet bore and $\nabla B$ is larger over these dimensions.

Since the migrational current density distribution is hemispherical rather than planar, the application of a magnetic field in any of the three orthogonal directions will have the same effect on the convection. In each case a rotational flow will be induced around the axis of the applied field, leading to a tangential fluid velocity at the electrode surface.

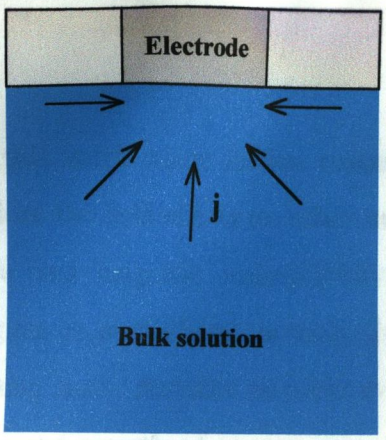


*Fig. 7.4: Distribution of migrational current density near electrode.*

In conclusion, the magnetic field effects on copper electrodeposition and electrodissolution may be entirely explained by field-induced convection. The tangential fluid velocity induced by the field results in the formation of a hydrodynamic boundary layer at the electrode surface, which decreases the diffusion layer thickness and thus increases the rate of mass transport. This is manifested experimentally in the higher currents observed in the field when the electrode process is under diffusion control. The effect of the field on the morphology of the deposited copper may then be directly related to the modified mass transport rate. It is still not clear, however, on which scale the induced convection originates. Equivalent effects would be observed whether the induced convection originated in the bulk solution by the action of the Lorentz force or on a nanometer scale in the diffuse layer due to the electrokinetic force. The magnitudes of the magnetic body forces involved ($F_L$, $F_E$, $F_B$) may be comparable in magnitude, depending on the experimental conditions. It is therefore likely that all three play some role in inducing convection.

## 7.2 Future Work

There are several areas of this work where further research could prove fruitful. It would be interesting to explore the field effects on other metals, in particular those on cations of differing charge and magnetic susceptibility. The effect of the field magnitude on the flow regime in electrolytes, notably the transition to turbulence, would also make an interesting study. Another possible avenue is the investigation of the field effect on nucleation and growth of copper using microelectrode techniques. The scope of the magnetic field effects is not limited to electrochemistry. Various related effects on crystal growth[23] and magnetic water treatment[24] have been described in the literature. There are also many dubious and conflicting reports of magnetic field effects on biological systems, a subject which is of topical interest due to the controversy over the effects of increased mobile phone usage on human health.

Technological applications of the field effect on industrial scale copper plating are unlikely. This is because the convection employed in the industrial plating process, using either a paddle cell or impinging jet electrodes, is many orders of magnitude greater than that induced by the field. One possible technological application, however, is the application of a magnetic field during the electroplating of copper interconnects on semiconductor wafers. In this process, copper is electrodeposited from highly acidic solution onto a thin sputtered copper seed layer on a silicon wafer. The aim is to obtain defect free deposits in micron scale vias etched into the surface of the wafer, which act as microwires, carrying current between the various components in a chip. The problem is that plating occurs preferentially at corners where the current density is highest (Fig. 7.5a), sealing the vias and leading to voids (Fig. 7.5b) which have an adverse effect on the conductivity. Various organic inhibitors are used to prevent this preferential deposition. These inhibitors are adsorbed onto the surface due to the strong electric field at the corners and prevent copper from depositing there (Fig. 7.5c). The result is a perfectly formed interconnect (Fig. 7.5d). The surface layer of copper is then removed by polishing to leave the isolated interconnect. It is conceivable that the convection induced by a magnetic field could enhance the motion

of copper ions on this scale, leading to a more uniform deposition within the vias. A preliminary study has already been carried out with this objective in mind.

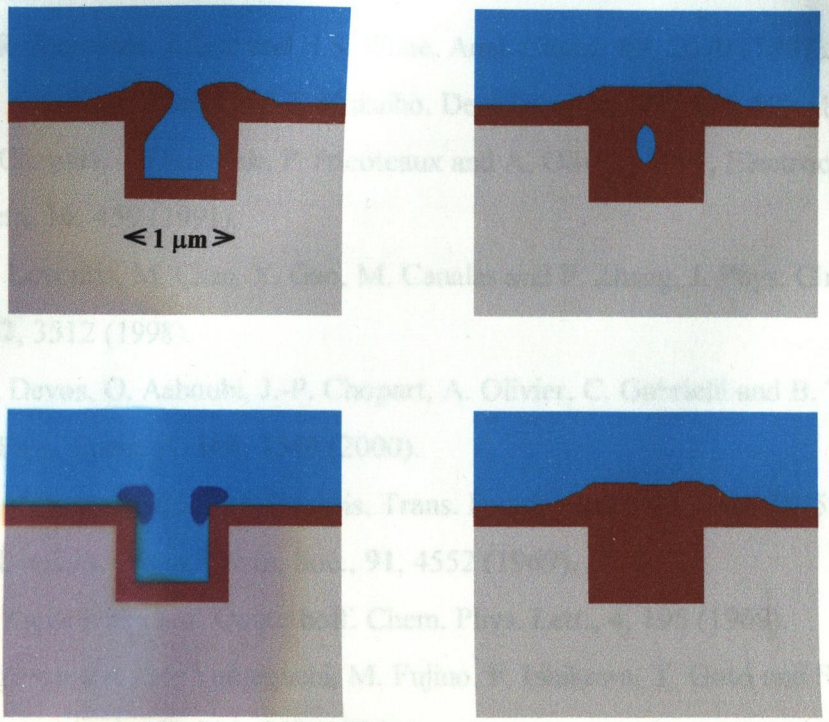


*Fig. 7.5: Electroplating of micron scale vias on silicon wafers. (a) Preferential deposition at corners (b) Void (c) Effect of organic inhibitors (d) Perfectly formed interconnect.*

Another possible application is the effect of a field on the electrodeposition of magnetic alloys. In recent years, it has been reported that soft magnetic alloys of Fe-Ni-Co, produced by electrodeposition, have exhibited anomalously high saturation polarisation ($J_s \sim 2.1$ T)[25]. The application of a magnetic field during the electrodeposition process could be used to tailor the anisotropy profile of such films. Read heads in hard disks require soft magnetic films with high saturation polarisation such as these.

## References


1 P.W. Atkins, *Physical Chemistry*, p. C28Oxford University Press, Oxford, 1994.

2 S.R. Ragsdale, J. Lee and H.S. White, Anal. Chem., **69**, 2070 (1997).

3 R. Aogaki, K, Fueki and T. Mukaibo, Denki Kagaku, **43**, 504; 509 (1975).

4 J. Chopart, J. Dougdale, P. Fricoteaux and A. Olivier, 1991, Electrochim. Acta, **36**, 459 (1991).

5 N. Leventis, M. Chen, X. Gao, M. Canalas and P. Zhang, J. Phys. Chem. B, **102**, 3512 (1998).

6 O. Devos, O. Aaboubi, J.-P. Chopart, A. Olivier, C. Gabrielli and B. Tribollet, J. Phys. Chem. A, **104**, 1544 (2000).

7 E. Mattsson and J.O'M. Bockris, Trans. Faraday Soc., **55**, 1586 (1959).

8 G.L. Closs, J. Am. Chem. Soc., **91**, 4552 (1969).

9 R. Kaptein and L.J. Oosterhoff, Chem. Phys. Lett., **4**, 195 (1969).

10 I. Yamamoto, M. Yamaguchi, M. Fujino, F. Ishikawa, T. Goto and S. Miura, Physica B, **216**, 399 (1996).

11 M. Yamaguchi, I. Yamamoto, F. Ishikawa, T. Goto and S. Miura, J. All. Comp., **253-254**, 191 (1997).

12 M. Waskaas and Y.I. Kharkats, J. Phys. Chem. B, **103**, 4876 (1999).

13 D. Grier, E. Ben-Jacob, R. Clarke and L.M. Sander, Phys. Rev. Lett., **56**, 1264 (1986).

14 M. Matsushita, M. Sano, Y. Hayakawa, H. Honjo and Y. Sawada, Phys. Rev. Lett., **53**, 286 (1984).

15 I. Mogi, M. Kamiko, S. Okubo and G. Kido, Physica B, **201**, 606 (1994).

16 I. Mogi and M. Kamiko, J. Cryst. Gr., **166**, 276 (1996).

17 H. Mizuseki, K. Tanaka, K. Kikuchi, K. Ohno and Y. Kawazoe, Comp. Mat. Sci., **10**, 46 (1998).

18 R.N. O'Brien and K.S.V. Santhanam, J. Appl. Electrochem., **27**, 573 (1997).

19 S.R. Ragsdale, K.M. Grant and H.S. White, J. Am. Chem. Soc., **120**, 13461 (1998).

20 K.M. Grant, J.W. Hemmert and H.S. White, Electrochem. Comm., **1**, 319

(1999).

[21] A. Olivier, J.-P. Chopart, J. Amblard, E. Merienne and O. Aaboubi, Models in Chemistry, **137**, 213 (2000).

[22] G.M. Opeper and J. Szekely, J. Cryst. Growth, **64**, 505 (1983).

[23] D.T.J. Hurle and R.W. Series, Handbook of Crystal Growth, vol. 2A, Chapter 5, North Holland, Amsterdam, 1994.

[24] H.E. Lundager Madsen, J. Cryst. Growth, **152**, 94 (1995).

[25] J.M.D. Coey and S. Cass, J. Magn. Magn. Mater., **209**, 374 (2000).

[26] T. Osaka, M. Takai, K. Hayashi, K. Ohashi, M. Saito and K. Yamada, Nature, **392**, 796 (1998).